# Benchmarking Noisy Quantum Computation through Quasiprobability Methods

SHIGEO HAKKAKU

MARCH, 2022

# Benchmarking Noisy Quantum Computation through Quasiprobability Methods

A dissertation submitted to
THE GRADUATE SCHOOL OF ENGINEERING SCIENCE
OSAKA UNIVERSITY
in partial fulfillment of the requirements for the degree of
DOCTOR OF PHILOSOPHY IN ENGINEERING

BY

SHIGEO HAKKAKU

MARCH, 2022

# Abstract

Quantum computers are expected to provide an exponential speedup compared to classical computers for specific problems, including factoring and quantum simulations. These facts have motivated us to develop quantum computers. Google Quantum AI team has demonstrated that their quantum processor with 53 qubits can perform a specific task in about 200 seconds, although their tensor-network-based simulator on a state-of-the-art supercomputer at that time would take 10000 years to complete. (After this experiment, better tensor-network-based methods have been developed, and the current best record of the classical simulation has reduced to 304 seconds.) The quantum supremacy experiment has shown that current or near-future quantum computers may solve certain problems faster than classical computers. However, current or near-term quantum computers suffer from noise. Thus, they cannot run complicated algorithms such as Shor's algorithm. To run complicated algorithms, we need a full-fledged fault-tolerant quantum computer with quantum error correction (QEC). However, decades may be necessary to implement enough qubits for it.

Instead of waiting for the realization of large-scale fault-tolerant quantum computers, many researchers have been trying to use existing quantum computing devices without QEC, namely, noisy intermediate-scale quantum (NISQ) devices, for practical purposes. One of the most promising algorithms is the variational quantum algorithms (VQAs). Many VQAs have been proposed for practical applications, including machine learning, quantum chemistry, and quantum simulation. However, it is still not clear what kind of quantum circuits under how low error rates can demonstrate quantum advantages. A sufficient condition for a quantum advantage is hard to identify since it depends on the choice of the classical best counterpart. Still, we can quantify a quantumness in the sense that how a given quantum algorithm or quantum circuit itself is hard to be simulated classically, which is a necessary condition for a quantum advantage.

On the other hand, in the context of the realization of a fault-tolerant quantum computer, an experimental demonstration of QEC is a near-term milestone in the NISQ era. The surface code is a promising candidate for the implementation of QEC. Numerical calculations exploiting the classical simulatability of Clifford circuits showed that the threshold error rate of the surface codes is high, around 1%, by assuming stochastic Pauli noise. However, in practice, quantum devices suffer from more general noise, such as an over-rotation error,

which cannot be described by Clifford operations. As an opposite demand to the quantum advantage mentioned above, we need an efficient classical simulation method that can take such coherent noise into consideration to analyze the performance of QEC in a realistic situation.

In this thesis, we address these two opposing issues: (i) how to quantify the difficulty of the classical simulation of a NISQ-oriented algorithm possessing a quantum advantage and (ii) how to simulate QEC under a realistic noise efficiently. These issues are addressed by providing quasiprobability-sampling-based simulators and quantifying their simulation costs. Here, the quasiprobability method is a Monte-Carlo method that samples a classically simulatable class of quantum computations, including negative coefficients. More precisely, by choosing a set of states or operations in a classically simulatable class such that they span an overcomplete basis, any quantum operation can be simulated. Of course, it is not possible to simulate an arbitrary quantum computation efficiently. The sampling cost diverges exponentially as it deviates from a classically simulatable one. Therefore, the sampling cost allows us to evaluate the hardness of a classical simulation.

Regarding (i), we extend a quasiprobability-based simulation method based on the classical simulatability of Clifford circuits to noisy quantum circuits by actively using noise to reduce simulation costs. We estimate the classical sampling costs of noisy quantum circuits and compare the costs with those of an existing quasiprobability-based simulator. Studying the sampling cost of a noisy rotation gate found that a quantum circuit composed of many small rotation gates can be made classically simulatable by a small amount of noise. We also find that, at a low error rate, our extended algorithm is more efficient than the existing quasiprobability-based simulator for noisy quantum circuits. We believe that these methods and results help to narrow down the candidates for a quantum advantage.

Regarding (ii), we apply the proposed quasiprobability-based algorithm to simulate QEC with the planar surface codes under a realistic noise model, including coherent and Pauli noise. We perform a numerical calculation with 81 qubits, whose dimension of the state vector is enormous, and a full state-vector simulation never works. In our estimation, our method can cope with the surface code with $\mathcal{O}(1000)$ qubits under such noise with an experimentally motivated noise parameter. We believe that this work helps to analyze the performance of near-term and small-scale QEC codes.

The simulation of fermionic systems with NISQ devices is one of the most promising applications to demonstrate a quantum advantage. Thus, it is also important to quantify the classical simulation costs of such quantum circuits. However, the above methods are unsuitable to do so because the quantum circuits for simulation of fermionic systems have many rotation gates, which increases the classical simulation costs if we employ the classical simulatability of the Clifford circuits. Thus, we need a more efficient quasiprobability-based algorithm to simulate noisy quantum circuits for fermionic systems. In order to analyze quantum algorithms for fermionic systems regarding (i), we further construct another quasiprobability-based simulation method based on the classical

simulatability of free fermionic dynamics. We investigate the sampling cost of a chemically inspired ansatz circuit for VQAs under stochastic noise to assess a potential quantum advantage there, and the result suggests that one should choose Hamiltonians of strongly correlated materials to demonstrate quantum advantages; otherwise, a small amount of noise makes the quantum circuits classically efficiently simulable, and hence one fails to demonstrate quantum advantages with the quantum circuits.

The proposed method for simulating noisy quantum circuits is helpful as a Monte-Carlo type simulation that successfully benchmarks a large system with reasonable overhead. It is expected that more and more research on the application of quantum devices will be carried out in the future, and we expect that the simulation methods we have developed will be useful. On the other hand, as for the classical simulation cost as an indicator for a possible quantum advantage, we found that if the fermionic nonlinearity in ansatz is small, the classical simulation is tractable in the presence of noise. It is important to choose the target systems so that they essentially require a high fermionic nonlinearity in order to achieve a quantum advantage. Furthermore, the quasi-probability method has also been applied for a Monte-Carlo method using actual quantum devices, such as an error mitigation method. It will be interesting to see future development by combining our methods with sampling on actual quantum devices.

# Contents

# Chapter 1

# Introduction

## 1.1 Goal of Quantum Computers

Academia, industry, and government are actively developing quantum computers because quantum computers are theoretically guaranteed to execute specific problems exponentially faster than classical (conventional) computers, such as supercomputers. Problems suited to quantum computers are roughly divided into two types:

(i) Problems contain a "good" linear algebraic structure.

(ii) Problems are to simulate quantum phenomena.

Shor's algorithm [1, 2] is a typical example of (i). It can solve the factoring problem exponentially faster than the best classical algorithm. Additionally, the Harrow-Hassidim-Loyd (HHL) algorithm is an exponentially faster quantum algorithm for linear systems of equations [3]. As for (ii), Ref. [4] originally proposed a simulation of the dynamics of a quantum system on a quantum computer. The required memory of a classical computer increases exponentially as a function of the size of a target quantum system if all entries of a quantum state vector are stored. However, quantum computers can only use a polynomial number of qubits. This quantum algorithm has the potential to solve the problems of quantum many-body systems and quantum chemistry intractable for classical computers. Consequently, quantum computers should impact many fields, including security, machine learning, quantum physics, and quantum chemistry. This is our motivation to build quantum computers.

To execute the above quantum algorithms, the quantum error correction (QEC) is essential because quantum information is vulnerable to environmental noise. QEC prevents noise by encoding quantum information into the subspace of a collection of qubits, allowing computations to be performed with arbitrary precision [5, 6]. Although QEC is a necessary ingredient for a scalable fault-tolerant quantum computer, a massive amount of qubits have to be prepared when the above algorithms are executed under QEC. For instance, the authors

of Ref. [7] showed that $\mathcal{O}(10^7)$ physical qubits would be required to factor a 2048-bit number into its primes. Considering that the number of qubits of the current quantum computers is from $\mathcal{O}(10)$ to $\mathcal{O}(100)$, it will take decades to run these quantum algorithms with theoretically proven speedup with QEC codes.

## 1.2 Near-term Quantum Computations

Although we are short of sufficient qubits to perform error-corrected quantum algorithms, current quantum computers might solve the problems intractable for classical computers. John Preskill coined two terminologies [8]: *Noisy Intermediate-Scale Quantum* (NISQ) devices, which stands for quantum computers that consist of about 50 to several hundred qubits and that are limited performance due to the intrinsic noise, and *quantum supremacy*, which stands for the demonstration that quantum computers can perform an intractable task for classical computers. In 2019, the Google Quantum AI team announced that their quantum processor demonstrated quantum supremacy by performing a classically intractable task that would take 10,000 years even with a state-of-the-art supercomputer [9]. Although the task does not aim to solve a practical problem, this experiment has shown that NISQ devices have the potential to tackle applied problems. After this experiment, better tensor-network-based methods have been developed, and the current best record of the classical simulation has reduced to 304 seconds [10]. However, it will not be able to classically simulate the experiment when the number of qubits increases and the gate fidelity improves. Toward the demonstration of quantum supremacy with practical problems, i.e., quantum advantage, many NISQ algorithms have been proposed. Examples include quantum chemistry [11] and quantum machine learning [12]. However, it is still unclear what kind of quantum circuits under how low error rates can demonstrate quantum advantages. Although it is important to figure out such a sufficient condition of a quantum advantage, such a kind of approach is hard to solve in general. On the other hand, one can consider, as a necessary condition of a quantum advantage, the classical simulation cost of a given quantum circuit, and it is helpful to design quantum circuits that have the potential to demonstrate quantum advantages.

Along with the development of NISQ algorithms, we should also continue to study QEC toward the realization of fault-tolerant quantum computers. The surface code is one of the most promising candidates for the implementation of the QEC code in NISQ devices due to the high threshold error rate and easiness of physical implementation [13]. Numerical calculations reveal that the threshold error rate under the Pauli noise is around 1%, which is almost approaching the gate and measurement error rate of state-of-the-art NISQ devices [14, 15]. Moreover, the $d = 5$ rotated surface code requires 49 qubits, which is also almost the same as the number of the qubits achieved with NISQ devices. These facts have motivated us to implement a small-scale surface code as a testbed for large-scale QEC circuits in the future, resulting in massive experimental efforts devoted in recent years [16–18]. Although the numerical simulations exploited

the efficient simulability of Pauli noise, NISQ devices suffer from more general noise, such as an over-rotation noise [19], which cannot be described by Clifford operations. Some numerical calculations have considered such noise [20–23]. However, these methods fail to simulate the QEC code suitable to NISQ devices, such as a surface code, with faulty syndrome measurements. Therefore, we need a classical simulation method that can simulate QEC codes under coherent noise to implement and benchmark small-scale fault-tolerant quantum computers.

## 1.3 Overview of this thesis

Based on the above discussion, at least the quantum circuits that have the potential quantum advantages should be difficult to simulate classically. Thus, we need to (i) clarify and extend the classical simulatable regime, thereby narrowing down the candidates for quantum advantages. As for QEC, it is essential to (ii) benchmark the performance of QEC codes under more realistic noise. This is because most numerical studies on QEC exploited the efficient classical simulability of stochastic Pauli noise, although quantum devices suffer from more realistic noise, including an over-rotation noise, which cannot be represented by Clifford operations. In this thesis, we address these two problems using quasiprobability-based sampling algorithms, which is one of the classical simulation algorithms. In the quasiprobability-based simulation, a quantum channel $\mathcal{E}$ is decomposed over a discrete set of classically tractable channels $\{\mathcal{S}_i\}$ i.e., $\mathcal{E} = \sum_i q_i \mathcal{S}_i$. Because the coefficients $\{q_i\}$ is not always positive, they are called quasiprobability. A classically tractable channel $\mathcal{S}_i$ is sampled and executed instead of $\mathcal{E}$ with probability $|q_i|/\sum_i |q_i|$. As explained later, the L1 norm of the quasiprobability $\sum_i |q_i|$ determines the sampling cost of the simulation. We extend an existing quasiprobability simulation algorithm to noisy quantum circuits, thereby quantifying and estimating the classical simulation costs of noisy quantum circuits in terms of sampling costs. As a practical application of the extended quasiprobability simulation algorithm, we propose a sampling-based simulation for fault-tolerant QEC under coherent noise. We provide a quasiprobability-based simulation algorithm tailored to variational quantum algorithms (VQAs) for fermionic Hamiltonians and the corresponding quantifier, i.e., the measure for the simulation cost for the quasiprobability-based simulation algorithm.

As summarized in Fig. 1.1, the rest of this thesis is organized as follows:

**Chapter 2: Preliminaries**
We introduce the basis of quantum computations relevant to our work and the notion of the quasiprobability simulation algorithm, which plays a central role in this thesis.

**Chapter 3: Comparative Study of Sampling-Based Simulation Costs of Noisy Quantum Circuits**

We extend an existing quasiprobability simulation algorithm to noisy quantum circuits and estimate the classical sampling costs of noisy random quantum circuits. In addition, we compare the sampling costs with those for another quasiprobability simulation algorithm. We find that, at a low error rate, our extended algorithm surpasses the compared one. Moreover, we showed that a small amount of stochastic Pauli noise makes quantum circuits composed of many small-angle rotation gates classically simulable. Since some VQE ansatze are such quantum circuits, one should carefully design quantum circuits for demonstrating quantum advantages. This chapter is based on [Hakkaku and Fujii, Phys. Rev. Applied **15**, 064027 (2021)] with slight modifications to fit in the context.

**Chapter 4: Sampling-Based Quasiprobability Simulation for Fault-tolerant Quantum Error Correction on the Surface Codes under Coherent Noise**
We propose a sampling-based simulation for fault-tolerant QEC under coherent noise as a practical application of the extended quasiprobability simulation algorithm introduced in the previous chapter. Using our proposed method, we simulate the planar surface code with 81 qubits under coherent noise within a reasonable computational time. We find that the coherent noise increases the logical error rate. Furthermore, we estimate the size of the classically simulable planar surface code with the use of a high-performance parallel computer of $10^6$ CPU cores and find that the surface code with over 1000 qubits at a specific realistic parameter set can be simulable by our proposed method. We believe that our proposed method is useful to analyze the implementation of a QEC code by NISQ devices. This chapter is based on [Hakkaku, Mitarai, and Fujii, Phys. Rev. Research, **3**, 043130 (2021)] with slight modifications to fit in the context.

**Chapter 5: Quantifying Fermionic Nonlinearity of Fermionic Quantum Circuits**
We provide a quasiprobability-based simulation algorithm tailored to VQAs for fermionic Hamiltonians and the corresponding quantifier. With the quantifier, we estimate the classical sampling cost of an ansatz quantum circuit for preparing the ground state of fermionic Hamiltonians and find that strongly-correlated materials are suitable for demonstrating quantum advantages. Although we estimate the classical simulation cost of such an ansatz in this chapter, classical simulation costs of quantum circuits for the dynamics of fermionic Hamiltonians can also be estimated through our method. This chapter is based on [Hakkaku, Tashima, Mitarai, Mizukami, and Fujii, arXiv:2111.14599].

**Chapter 6: Conclusion**
We summarize the thesis and state future directions.

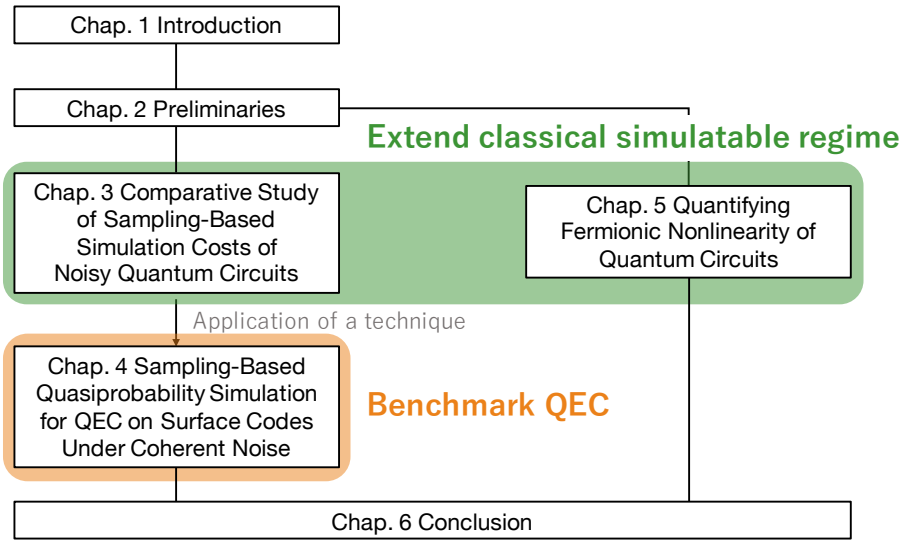


Figure 1.1: Structure of this thesis.

# Chapter 2

# Preliminary

This chapter summarizes the basics of quantum computation. We define a quantum state and review the description of the dynamics of a quantum state, including quantum measurement. First, we introduce gate teleportation [24]. The gate teleportation replaces a quantum gate with a preparation of a resource state and plays a central role in a quasiprobability-based algorithm, as we will see later. Then, we review two existing efficient simulatable quantum circuits: Clifford circuits and fermionic linear optics. Finally, existing quasiprobability-based algorithms are reviewed.

## 2.1 Quantum State

In classical information theory, the elementary unit of information is a bit. The state of a bit can be represented by 0 or 1. In contrast, the elementary unit of information in the quantum world is a qubit, whose state can be represented by a superposition of $|0\rangle$ and $|1\rangle$. The state of a single qubit system is represented by a unit vector in two-dimensional complex vector space $\mathbb{C}^2$. For example, the state vector of a single-qubit can be given by

$$|\psi\rangle = \alpha\,|0\rangle + \beta\,|1\rangle\,,$$

where $\alpha, \beta \in \mathbb{C}$ and $|\alpha|^2 + |\beta|^2 = 1$. The state of an $n$-qubit system is described by a tensor product space of $n$ vector spaces $\mathbb{C}^{2n}$:

$$|\psi\rangle = \sum_{i_0,\ldots,i_n=0,1} x_{i_0,\ldots i_n}\,|i_0,\ldots,i_n\rangle\,,$$

where $\sum_{i_0,\ldots,i_n=0,1} |x_{i_0,\ldots,i_n}|^2 = 1$ and $|\psi\phi\rangle \coloneqq |\psi\rangle \otimes |\phi\rangle$.

A more convenient way to describe a quantum state is to use a density operator. A density operator can represent an ensemble of state vectors. A density operator is defined as

$$\rho = \sum_i p_i\,|\psi_i\rangle\langle\psi_i|\,, \quad \sum_i p_i = 1.$$

The density operator satisfies the following properties:

$$\rho \geq 0, \quad \mathrm{Tr}(\rho) = 1,$$

where $\rho \geq 0$ means $\langle\psi|\rho|\psi\rangle \geq 0$ for all $|\psi\rangle$. Note that an operator $A$ satisfying $A \geq 0$ is referred to as a positive operator. We say that a quantum state is a pure state if $\rho^2 = \rho$, and hence can be written as $\rho = |\psi\rangle\langle\psi|$.

## 2.2 Quantum Gate

Quantum circuits consist of input states, unitary gates, and measurements. Here, we describe the various unitary gates and give their definitions. Later, we will see the quantum measurements and quantum noise which are parts of quantum dynamics but nonunitary processes.

We introduce the most important quantum gates, single-qubit Pauli gates: $I$, $X$, $Y$, and $Z$:

$$I = \begin{bmatrix} 1 & 0 \\ 0 & 1 \end{bmatrix}, \quad X = \begin{bmatrix} 0 & 1 \\ 1 & 0 \end{bmatrix}, \quad Y = \begin{bmatrix} 0 & -i \\ i & 0 \end{bmatrix}, \quad Z = \begin{bmatrix} 1 & 0 \\ 0 & -1 \end{bmatrix},$$

The computational states $\{|0\rangle, |1\rangle\}$ are defined as the eigenstates of the $Z$ gate. The $X$ gate flips the computational states:

$$X|0\rangle = |1\rangle, \quad X|1\rangle = |0\rangle.$$

We call $U_{\mathrm{Cl}}$ a Clifford gate iff $U_{\mathrm{Cl}}^\dagger P U_{\mathrm{Cl}} \in P'$ , where $P$ and $P'$ are $n$-qubit Pauli operators, elements of $\{\pm 1, \pm i\} \times \{I, X, Y, Z\}^{\otimes n}$. Single-qubit Pauli gates mentioned above are elements of Clifford gates. Important single-qubit Clifford gates, Hadamard gate $H$ and phase gate $S$, are defined as follows:

$$H = \begin{bmatrix} 1 & 1 \\ 1 & -1 \end{bmatrix}, \quad S = \begin{bmatrix} 1 & 0 \\ 0 & i \end{bmatrix}.$$

The actions of the Hadamard gate $H$ and the phase gate $S$ by conjugation on single-qubit Pauli gates are given by

$$HZH^\dagger = X, \quad SXS^\dagger = Y.$$

To simulate any quantum phenomena, quantum computers should implement arbitrary unitary operators, i.e., universal quantum computation. However, Clifford and Pauli gates cannot even make an arbitrary single-qubit gate. To do so, we need a single-qubit non-Clifford gate [25]. The $T$ gate is a typical example of a non-Clifford gate and is defined as

$$T = \begin{bmatrix} 1 & 0 \\ 0 & e^{i\frac{\pi}{4}} \end{bmatrix}.$$

One can create an arbitrary single-qubit unitary operator if we have the gate set $\{H, T\}$ by the Solovay-Kitaev theorem [26]. To create an $n$-qubit unitary operator, we also need a CNOT gate, which is a two-qubit Clifford gate and is helpful to create an entangled state. A CNOT gate $\Lambda_{c,t}(X)$ is given by

$$\Lambda_{c,t}(X) \coloneqq |0\rangle\langle 0|_c I_t + |1\rangle\langle 1|_c X_t,$$

where $A_t$ indicates that $A$ acts on qubit $t$. The gate set $\{H, T, \mathrm{CNOT}\}$ forms a universal set of gates and can perform universal quantum computation.

## 2.3 Quantum dynamics

The dynamics of the density operator $\rho$ under a unitary gate $U$ are described as a super-operator $\Lambda$, which maps a density operator to another:

$$\Lambda : \rho \to U\rho U^\dagger.$$

Any quantum dynamics can be described as a unitary process if the whole system including a system of interest and its environment is considered. However, it is sometimes difficult to describe the whole quantum system including the environmental systems. In such a case, a non-unitary operation is useful to describe the target system considering the environmental effect. In general, a physical quantum operation $\Lambda$ is described as the Kraus representation:

$$\Lambda(\rho) = \sum_i V_i \rho V_i^\dagger, \quad \sum_i V_i^\dagger V_i = I,$$

where $V_i$ is called the Kraus operator. A quantum operation is also called a quantum channel. A quantum operation $\mathcal{E}$ has the following properties:

- $\Lambda$ preserves the trace of the input operator $A$ i.e., $\mathrm{Tr}(\Lambda(A)) = \mathrm{Tr}(A)$. Thus, $\mathcal{E}$ is a *trace-preserving* map.
- $\mathcal{E}(A) \geq 0$ for any positive operator $A$. Thus, $\mathcal{E}$ is a *positive* map.
- Let $\mathcal{E}$ be defined in the Hilbert space $\mathcal{H}_{\mathrm{target}}$, and let $I$ be the identity channel in the Hilbert space $\mathcal{H}_{\mathrm{ancilla}}$. Suppose $A$ is defined in $\mathcal{H}_{\mathrm{target}} \otimes \mathcal{H}_{\mathrm{ancilla}}$, $(\mathcal{E} \otimes I)(A) \geq 0$ for any positive operator $A$. Thus, $\mathcal{E}$ is a *completely positive* map.

Therefore, a quantum operation is a completely positive trace-preserving (CPTP) map. The next section provides non-unitary processes.

### 2.3.1 Quantum Noise

A target quantum system often interacts with an environmental system unexpectedly. The quantum operation in a system of interest caused by such an interaction is called quantum noise. Quantum noise leaks the quantum information of the state into the environmental system and causes the error of quantum

computation. The quantum noise often decoheres the quantum state, i.e., maps the pure states to mixed states and is modeled by simple stochastic Pauli operations. Here we give examples of the quantum noise models causing quantum decoherence.

The bit-flip noise is given by

$$\mathcal{E}_{\text{bit-flip}}(\rho) \coloneqq (1-p)\rho + pX\rho X.$$

This noise flips $|0\rangle$ to $|1\rangle$ and vice versa. Another example is the depolarizing noise. The depolarizing noise for a single-qubit gate is given by

$$\mathcal{E}_{\text{depolarizing}}(\rho) \coloneqq (1-p)\rho + p\frac{I}{2}. \tag{2.1}$$

This noise replaces a given state $\rho$ with the completely mixed state $I/2$ with probability $p$. The form in Eq. (2.1) can be rewritten as the following form in the operator-sum representation as

$$\mathcal{E}_{\text{depolarizing}}(\rho) \coloneqq \left(1 - \frac{3}{4}p\right)\rho + \frac{p}{4}(X\rho X + Y\rho Y + Z\rho Z).$$

The above quantum noise models are called incoherent or stochastic Pauli noise since Pauli operators are applied with a certain probability.

On the other hand, quantum devices suffer from noise which cannot be described by the incoherent noise. The over-rotation noise is a typical example. A faulty calibration causes the over-rotation noise, which rotates a quantum state unexpectedly when one acts a rotation gate to the quantum state. The rotation gate about the $Z$ axis being subject to over-rotation noise about the $Z$ axis is modeled by

$$\mathcal{E}_{\text{over-rotation}} \circ \left[e^{-i\frac{\theta}{2}Z}\right] = \left[e^{-i\frac{\epsilon}{2}Z}\right] \circ \left[e^{-i\frac{\theta}{2}Z}\right],$$

where $[A]\rho = A\rho A^\dagger$, and we use the notation $\mathcal{E} \circ \mathcal{N}$ to denote the composition of $\mathcal{E}$ with $\mathcal{N}$, defined by $(\mathcal{E} \circ \mathcal{N})(\rho) \coloneqq \mathcal{E}(\mathcal{N}(\rho))$. $\mathcal{E}_{\text{over-rotation}}$ rotates the given quantum state $\epsilon$ more than a desired rotation angle $\theta$.

## 2.4 Quantum Measurement

We obtain classical information from a quantum state by performing a quantum measurement. The measurement is performed by measurement operators $\{V_m\}$, which satisfies $\sum_m V_m^\dagger V_m = I$. Here, $m$ indicates a label of each measurement outcome. Given a state $\rho$, the probability of obtaining outcome $m$ is calculated as

$$p_m = \text{Tr}\big(V_m \rho V_m^\dagger\big).$$

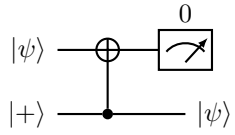


Figure 2.1: One-bit teleportation.

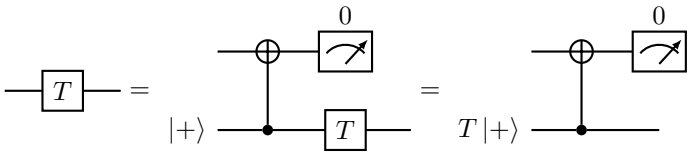


Figure 2.2: $T$ gate teleportation.

The post-measurement state is given by

$$\frac{V_m \rho V_m^\dagger}{\mathrm{Tr}\left(V_m \rho V_m^\dagger\right)}.$$

In particular, if the measurement operators are projection operators $\{P_m\}$ (i.e., $P_m P'_m = \delta_{m,m'} P_m$ and $\sum_m P_m = I$), then the post-measurement state is given by

$$\frac{P_m \rho P_m}{\mathrm{Tr}(P_m \rho)}$$

with probability

$$p_m = \mathrm{Tr}\,(P_m \rho),$$

where we used $P_m = P_m^\dagger = P_m^2$. Such a measurement is called a projective measurement.

## 2.5 Gate Teleportation

Here, we introduce gate teleportation [24]. Quantum teleportation is a quantum communication protocol, where one can send a quantum state to another by sharing a maximally entangled state firstly and communicating classically. In this protocol, one can teleport a quantum gate by preparing an appropriate entangled state instead of the maximally entangled state, which is the gate teleportation. Expanding on this notion, it turns out that universal quantum computation can be performed by first preparing a large entangled state, called a cluster state, and then measuring it adaptively. The scheme of universal quantum computation is called measurement-based quantum computation (MBQC) [27]. Note that the gate teleportation technique is useful not only for MBQC

but also for the implementation of a non-Clifford gate in topological QEC codes [15].

We briefly explain how a quantum gate can be transformed into a resource state. The quantum circuit shown in Fig. 2.1 depicts the one-bit teleportation, which is the building block of the gate teleportation. The quantum state $|\psi\rangle$ in qubit 1 is teleported to qubit 2 by the preparation of $|+\rangle$ with the Clifford circuit and the Pauli $Z$ measurement. Using this technique, the $T$ gate can be implemented by preparing the corresponding resource state $T|+\rangle$and a Clifford circuit shown in Fig. 2.2. In the middle quantum circuit, the $T$ gate in the lower wire can be moved backward because the $T$ gate commutes with $|0\rangle\langle 0|$ or $|1\rangle\langle 1|$.

The gate teleportation also plays a vital role in a classical simulation. By using the gate teleportation, an arbitrary quantum circuit can be transformed into a Clifford circuit with the preparation of a resource state of non-Clifford gates. It is known that a Clifford circuit with a stabilizer state can be classically efficiently simulatable, as will be discussed in the next section. Thus, the non-Clifford resource state stands for the difficulty of a classical simulation. In Section 2.7, we will show that a quantum circuit composed of a Clifford circuit with a non-Clifford resource state can be classically simulated by repeatedly sampling a stabilizer state and setting it to the Clifford circuit. Furthermore, we will explain that the classical simulation cost of a quantum circuit is quantified by the non-Clifford resource state.

## 2.6 Efficiently simulatable quantum circuits

It is known that certain restricted states and their dynamics can be simulated efficiently (polynomial time) in the number of qubits. Here, we explain two such classes of classically and efficiently tractable quantum circuits: Clifford circuits and fermionic linear optics (FLO).

### 2.6.1 Stabilizer Formalism and Classical Simulation of Clifford Circuits

Stabilizer formalism [28] provides us to write a restricted type of entangled states efficiently. It is used for many applications, including QEC and a quasiprobability-based classical simulation. Here we review stabilizer formalism and stabilizer code, which is a class of QEC codes.

#### Stabilizer State

The $n$-qubit Pauli group $\mathcal{P}_n$ is defined as follow:

$$\mathcal{P}_n \coloneqq \{\pm 1, \pm i\} \times \{I, X, Y, Z\}^{\otimes n}.$$

The $n$-qubit stabilizer group $S_n = \{s_i\}$ is a subgroup of $\mathcal{P}_n$ and satisfies the following properties:

$$s_i \in P_n, \quad \forall_{ij}[s_i, s_j] = 0, \quad s_i \neq -I.$$

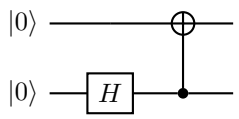


Figure 2.3: Quantum circuit to create the Bell state.

The condition $s_i \neq -I$ makes every $s_i$ hermitian, resulting that the eigenvalue of $s_i$ is either 1 or $-1$. We say that $G = \{g_1, \dots g_n\}$ are the stabilizer generators of a stabilizer group $S_n$ if an arbitrary element of $S_n$ can be written by a product of elements in $G$ and an arbitrary element of G cannot be written by a product of other elements in $G$. The stabilizer group $S_n$ is said to be generated by $\{g_1, \dots, g_n\}$ and is sometimes denoted by $S_n = \langle g_1, \dots, g_n \rangle$. A stabilizer state is defined as the simultaneous eigenstate of all elements of $S_n$ with the eigenstate 1 and is given as

$$\forall_{s_i \in S_k} \quad s_i \left|\psi\right\rangle_{\text{stab}} = \left|\psi\right\rangle_{\text{stab}}.$$

Let $k$ be the number of the stabilizer generators in $G$. If the system is composed of $n$ qubits, $k$ is at most $n$. This is because stabilizer operators commute with each other, and $k$ stabilizer generators divide the Hilbert space of an $n$-qubit system by $2^k$ orthogonal subspaces. Thus, the dimension of the space spanned by the stabilizer states is $2^{n-k}$, and, when $n = k$, the stabilizer state is uniquely determined. For example, consider a two-qubit stabilizer group $S_{\text{Bell}} = \{XX, ZZ, -YY, II\} = \langle XX, ZZ \rangle$. The stabilizer state is given by

$$\left|\psi\right\rangle_{\text{Bell}} = \sqrt{2}\frac{II + XX}{2}\frac{II + ZZ}{2}\left|00\right\rangle = \frac{\left|00\right\rangle + \left|11\right\rangle}{\sqrt{2}}.$$

**Clifford gate**

Here, we explain how to describe the action of the Clifford gates on a stabilizer state. A Clifford gate is an operation that maps a Pauli operator to another Pauli operator by conjugation. Consider a Clifford gate $U$ and a stabilizer state $\left|\psi\right\rangle$ stabilized by $S = \langle g_1, \dots, g_n \rangle$. The stabilizer state after applying $U$ can be written as

$$U\left|\psi\right\rangle = Ug_i\left|\psi\right\rangle = Ug_iU^\dagger U\left|\psi\right\rangle = g_i' U\left|\psi\right\rangle, \tag{2.2}$$

where $g_i' = Ug_iU^\dagger$. From Eq. (2.2), we observe that $U\left|\psi\right\rangle$ can be stabilized by $\langle g_1', \dots g_n' \rangle$. Therefore, the action of a Clifford gate on a stabilizer state can be described by the transformation of stabilizer generators of $S$ under conjugation of Clifford gates. In the stabilizer formalism, we only need to keep track of the dynamics of $n$ operators to calculate the output state after a sequence of Clifford gates, while the full-vector simulation stores exponential entries of a vector. To be more concrete, let us consider the transformation of Pauli operators under

some Clifford gates, a Hadamard gate, and a CNOT gate. The Hadamard gate $H$ acts on single-qubit Pauli operators, $X$, $Y$, and $Z$ by conjugation as follows:

$$HXH = Z, \quad HZH = X. \tag{2.3}$$

As for the CNOT gate, the Pauli operators transform under conjugation as follows:

$$\begin{aligned} &[\Lambda_{1,2}(X)]X_1 = X_1X_2, \quad [\Lambda_{1,2}(X)]Z_1 = Z_1, \\ &[\Lambda_{1,2}(X)]X_2 = X_2, \quad [\Lambda_{1,2}(X)]Z_2 = Z_1Z_2, \end{aligned} \tag{2.4}$$

where $A_1B_2 \coloneqq A \otimes B$ and the indices 1 and 2 label the qubits to be acted. Using Eqs. (2.3) and (2.4), let us consider the output state of the quantum circuit shown in Fig. 2.3. The output state of the quantum circuit is the Bell state, $|\psi\rangle_{\text{Bell}}$. Let us see this in the stabilizer formalism. The initial state is stabilized by $\langle Z_1, Z_2\rangle$. $Z_1$ is transformed through the quantum circuit $Z_1 \to Z_1Z_2$, and $Z_2$ is transformed $Z_2 \to X_2 \to X_1X_2$. Thus, the output state has a stabilizer $\langle Z_1Z_2, X_1X_2\rangle$, whose stabilizer state is $|\psi\rangle_{\text{Bell}}$.

### Pauli measurement

A quantum measurement can also be described within the stabilizer formalism if the measurement is done in the Pauli basis. Here, consider how stabilizer generators transform due to a quantum measurement. Let $\langle g_1, \ldots, g_n\rangle$ be the stabilizer group of the output state of a Clifford circuit. We measure a Pauli operator $P \in \mathcal{P}_n$ as an observable on the stabilizer state. There are two possibilities for the transformation of the generators:

1. $P$ commutes with all the stabilizer generators in $\langle g_1, \ldots, g_n\rangle$. In this case, $P$ or $-P$ is in $\langle g_1, \ldots, g_n\rangle$. If $P$ is included in $\langle g_1, \ldots, g_n\rangle$, the measurement output is 0 with probability 1, where the measurement outcomes of 0 and 1 correspond to the eigenvalues of $P$, $+1$ and $-1$, respectively. The stabilizer generators remain after the measurement.

2. $P$ anticommutes with at least one stabilizer generator, say $g_1$. In such a case, we can redefine the generators so that only $g_1$ anticommutes with $P$, and all others $\{g_2, \ldots, g_n\}$ commute with $P$. In this case, the measurement outcome $m$ is 0 or 1 with probability 1/2. After the measurement, $g_1$ is replaced with $(-1)^m P$. Thus, the post-measurement state is stabilized by $\langle P, g_2, \ldots, g_n\rangle$.

### Gottesman-Knill theorem

Stabilizer formalism can represent the restricted dynamics of the specific states without storing exponential entries of a vector. The authors of Refs. [29, 30] go much further. They show that classical computers can simulate a Clifford circuit with the preparation of a stabilizer state:

**Theorem 2.1.** A Clifford circuit with the preparation of the stabilizer state followed by the measurement with a Pauli operator $P$ can be classically efficiently simulatable in the *strong* sense.

Here, a *strong* simulation of a quantum circuit is a classical computation that can calculate both the output probability $p(x)$ for a given bitstring $x$ and all its marginal probabilities [31]. This theorem is referred to as the Gottesman-Knill theorem.

*Proof.* Without loss of generality, we can assume that the initial state is $|0^n\rangle$, whose stabilizer is $\langle Z_0, \ldots, Z_{n-1}\rangle$, and every qubit is measured in the computational basis. We denote the stabilizer of the output state before the measurements $S^{(0)} = \langle g_1, \ldots, g_n\rangle$ and denote measurement outcomes $\{x_i = 0, 1\}$. Let $p_n$ be the probability of obtaining measurement outcomes $\{x_i\}$ and set $p_0 = 1$. Then $p_n$ can be calculated as follows:

1. For $k = 0, \ldots, n-1$, repeat the following procedures.
   (a) If $(-1)^{x_k} Z_k \in S^{(k)}$, the measurement outcome $x_k$ is obtained with probability 1. Thus, set $p^{(k+1)} = p^{(k)}$ and $S^{(k+1)} = S^{(k)}$.
   (b) If $(-1)^{x_k \oplus 1} \in S^{(k)}$, the measurement outcome $x_k$ is never obtained. Thus, set $p^{(k+1)} = 0$.
   (c) If $Z_k$ anticommutes with at least one stabilizer generator of $S^{(k)}$, say $g_1$, we can redefine the stabilizer generators so that only $g_1$ anticommutes with $Z_k$, and all the others $\{g_2, \ldots g_n\}$ commute with $Z_k$. The measurement outcome $x_k$ is obtained with probability $1/2$. Set $S^{(k+1)}$ by removing $g_1$ and adding $(-1)^{x_k} Z_k$ instead. In addition, set $p^{(k+1)} = p^{(k)}/2$.
2. Return $p^{(n)}$.

□

A Clifford circuit with the preparation of a stabilizer state can also be efficiently simulated in the weak sense. Here, the weak simulation of a quantum circuit is a classical computation that samples an outcome $x$ from a probability distribution $p(x)$.

**Theorem 2.2.** A Clifford circuit with the preparation of the stabilizer state followed by the measurement with a Pauli operator $P$ can be classically efficiently simulatable in the *weak* sense.

*Proof.* We assume that the initial state is $|0^n\rangle$, whose stabilizer is $\langle Z_0, \ldots, Z_{n-1}\rangle$, and every qubit is measured in the computational basis. We denote the stabilizer of the output state before the measurements $S^{(0)} = \langle g_1, \ldots, g_n\rangle$ and denote measurement outcomes $\{x_i = 0, 1\}$. The measurement outcomes $\{x_i\}$ can be sampled as follows:

1. For $k = 0, \ldots, n-1$, repeat the following procedures.

(a) If $(-1)^{x_k} Z_k \in S^{(k)}$, the measurement outcome $x_k$ is obtained deterministically.

(b) If $Z_k$ anticommutes with at least one stabilizer generator of $S^{(k)}$, say $g_1$, we can redefine the stabilizer generators so that only $g_1$ anticommutes with $Z_k$, and all the others $\{g_2, \ldots, g_n\}$ commute with $Z_k$. Sample $x_k = 0, 1$ with probability $1/2$. Set $S^{(k+1)}$ by removing $g_1$ and adding $(-1)^{x_k} Z_k$ instead.

2. Return $x_0, \ldots, x_{n-1}$.

□

The stabilizer generators $\{g_1, \ldots g_n\}$ can be written by an $n \times 2n$ binary matrix whose rows correspond to the stabilizer generators $g_1$ through $g_n$. If $g_i$ contains an $I$ on the qubit $j$ then the $j$th and $n+j$th column elements are 0; if it contains an $X$ on the qubit $j$ then the $j$th column element is a 1 and the $n+j$th column element is a 0; if it contains a $Z$ on the qubit $j$ then the $j$th column element is 0 and the $n+j$ column element is 1. Combining this representation with the Gottesman-Knill theorem, the overhead of updating the stabilizer generators for each gate is $\mathcal{O}(n)$ (where $n$ is the number of qubits). A measurement is performed in $\mathcal{O}(n^3)$ steps when one uses the Gaussian elimination or $\mathcal{O}(n^2)$ steps when one uses the CNOT-Hadamard-phase (CHP) simulator proposed in Ref. [30].

**Quantum Error Correction**

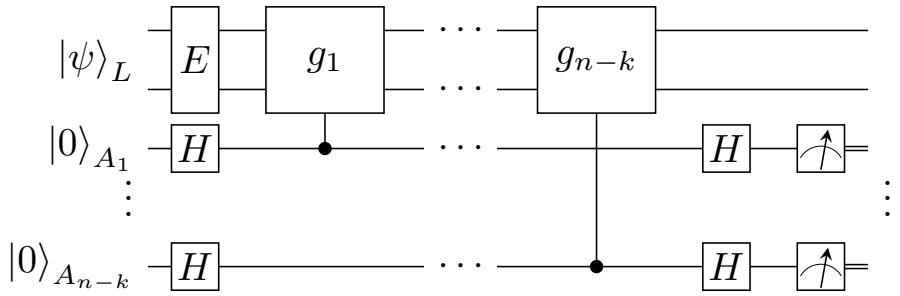


Figure 2.4: Syndrome measurement circuit of an $[[n, k]]$ stabilizer code.

One of the most important applications of the stabilizer formalism is quantum error correction (QEC). QEC is a scheme to protect qubits from environmental noise and is a necessary ingredient for fault-tolerant quantum computers. Here, we briefly review the stabilizer code, which is a class of QEC codes. Let us consider an $[[n, k]]$ stabilizer code composed of $n-k$ stabilizer generators, where $n$ is the number of qubits, and $k < n$. The dimension of the subspace spanned by the stabilizer states is $2^n/2^{n-k} = 2^k$. Thus the subspace can be regarded as a

logical $k$-qubit system. To execute quantum information processing in this logical qubit system, we introduce $2k$ logical Pauli operators $\{L_{X_i}, L_{Z_i}\}_{i=1}^{k}$. These logical operators commute with all of the generators $g_1, \ldots, g_n$ and anticommute with each other:

$$L_{X_i} L_{Z_j} = (-1)^{\delta_{ij}} L_{Z_j} L_{X_i}.$$

$L_{X_i}$ and $L_{Z_i}$ behave like Pauli operators in the $i$th logical qubit. Let $m_i$ be a binary value, 0 or 1, the computational basis states of the code space $|m_1, \ldots, m_k\rangle_L$ is defined by the stabilizer $\langle g_1, \ldots, g_{n-k}, (-1)^{m_1} L_{Z_1}, \ldots, (-1)^{m_k} L_{Z_k}\rangle$.

One can check whether the logical state has been deteriorated by Pauli error $E \in \mathcal{P}_n$ by performing projective measurements of $g_k$ using $n-k$ ancilla qubits as shown in Fig. 2.4. We call the projective measurement of a stabilizer generator *syndrome measurement*. If $g_i$ anticommutes with $E$, $E|\psi\rangle_L$ is the eigenstate of $g_i$ with eigenvalue $-1$. Thus, the measurement outcome of the ancilla qubit $A_i$ is 1, and one can detect the error from the outcome. The outcome is referred to as a *syndrome*.

With the collection of the outcomes of stabilizer measurements, one can determine the recovery operation $\mathcal{R}$ to minimize the logical error. One way to estimate which qubits are subject to errors is to estimate the most likely error pattern being subject to the syndrome condition. It is known that this problem can be solved by minimum-weight perfect matching (MWPM) algorithm. From the result by MWPM algorithm, one can determine the recovery operation $\mathcal{R}$. This error correction step is referred to as a decoding step. See [32, 33] for the details of the construction of the recovery operation.

In order to specify QEC capability, there is a metric called a code distance $d$, which is defined as follows. We introduce the weight $wt(P)$ of a Pauli string $P$, which is the number of single-qubit Pauli operators in $P$. For example, $wt(XIY) = 2$. The code distance $d$ is then defined as follows

$$d \coloneqq \min_{L\text{: Logical operators}} wt(L).$$

The code distance measures the "distance" between two different states in the code space in a sense that the code distance represents the minimum number of single-qubit Pauli operators to map a code state to a different code state. If less than $\lfloor (d-1)/2 \rfloor$ single-qubit Pauli errors act on the logical state, one can find a unique recovery operation that maps the erroneous state into the code space. Therefore, the number of correctable errors $t$ is defined by

$$t = \left\lfloor \frac{d-1}{2} \right\rfloor.$$

### 2.6.2 Fermiunic Linear Optics

We briefly review efficient simulatability of fermionic linear optics (FLO), which represents the dynamics of free fermions, based on Refs. [34, 35]. We define

$\{\hat{c}_i\}_{i=1}^{2n}$ as the Majorana fermion operators that satisfy

$$\begin{aligned}\{\hat{c}_i, \hat{c}_j\} &= 2\delta_{ij},\\ \hat{c}_i^\dagger &= \hat{c}_i,\\ \hat{c}_i^2 &= I,\end{aligned}$$

where $\{\hat{a}, \hat{b}\}$ denotes the anticommutator i.e., $\{\hat{a}, \hat{b}\} \coloneqq \hat{a}\hat{b} + \hat{b}\hat{a}$. The fermionic covariance matrix of a pure state is defined as

$$M_{ij} = \frac{-i \langle\psi|[\hat{c}_i, \hat{c}_j]|\psi\rangle}{2\langle\psi|\psi\rangle},$$

where $[\hat{a}, \hat{b}]$ denotes the commutator i.e., $[\hat{a}, \hat{b}] \coloneqq \hat{a}\hat{b} - \hat{b}\hat{a}$. We call $|\psi\rangle$ a fermionic Gaussian state (FGS) iff its covariance matrix $M$ satisfies $MM^T = I$. The important property of an FGS is the fact that the dynamics of the FGS are fully described by its covariance matrix $M$ and norm $\Gamma = \||\psi\rangle\|^2$. An operator $G$ is called a fermionic Gaussian operator iff it maps one FGS to another FGS, and an arbitrary FGO is written as $\exp\left\{\sum_{i<j} g_{ij}\hat{c}_i\hat{c}_j\right\}$. Note that FGOs are not always unitary. Consider an FGO $G$ and how it maps FGS $|\psi\rangle$ characterized by $(M, \Gamma)$. Let $|\psi_M\rangle$ be the fermionic maximally entangled state, and it is characterized by

$$\begin{aligned}M_M &= \begin{pmatrix} & I\\ -I & \end{pmatrix},\\ \Gamma_M &= 1,\end{aligned}$$

where $M_M$ is a $4n \times 4n$ covariance matrix. By calculating the Choi state of the FGO $G \otimes I\,|\psi_M\rangle$, the corresponding $4n \times 4n$ covariance matrix $M_G$ and norm $\Gamma_G$ are given by

$$\begin{aligned}M_G &= \begin{pmatrix} A & B\\ -B^T & D\end{pmatrix},\\ \Gamma_G &= \|G \otimes I\,|\psi_M\rangle\|^2,\end{aligned}$$

where $A$, $B$, and $D$ are $2n \times 2n$ submatrices. Using these submatrices, the resultant FGS $G\,|\psi\rangle$ is specified by

$$\begin{aligned}M' &= A - B(M - D)^{-1}B^T,\\ \Gamma' &= \Gamma\Gamma_G\sqrt{\det(M - D)}.\end{aligned}$$

We call this formalism fermionic linear optics (FLO). The computational complexity of the matrix multiplication is $\mathcal{O}(n^3)$. The computational complexity of the determinant operation is also $\mathcal{O}(n^3)$ by the LU decomposition. Therefore, we can efficiently update $(M, \Gamma)$ to $(M', \Gamma')$ by $G$.

FLO has been applied to quantum information processing, including QEC [21, 23, 35] and the calibration of the quantum operations [36]. In Ref. [21], the

efficient simulation method of the 1D repetition code under over-rotation noise has been proposed. The authors of Ref. [23] simulated the surface code under coherent noise with ideal syndrome measurements. Furthermore, FLO can be used for the decoder of the surface code [35]. Besides QEC, FLO is also used for a randomized benchmarking method of continuously parametrized gate sets [36].

## 2.7 Quasiprobability-based Simulation

In this section, we briefly review the central idea of quasiprobability-based simulation algorithms for quantum computations [37–41]. Quasiprobability-based methods have a long history in quantum optics [42]. A well-known example is the Wigner function. It maps a given quantum state to a real phase-space function, and it takes some negative values when the quantum state has no classical model. Recently, the ideas of quasiprobability-based methods have been imported into quantum computation [37, 38], and many such algorithms have been proposed [39–41]. These methods can simulate the quantum circuits which the Gottesman-Knill theorem fails to simulate with an additional sampling cost.

Let $\{\mathcal{B}_i\}$ be a set of classically simulatable operations such as Clifford gates or FLOs, and let $\mathcal{E}$ be an arbitrary target operation, which is not necessarily in $\{\mathcal{B}_i\}$. Let $\rho$ be an initial state that is a classical tractable state. The task we would like to do here is to simulate

$$\langle A \rangle = \mathrm{Tr}\left[A\mathcal{E}(\rho)\right]$$

by sampling $\mathcal{B}_i$ with an appropriate post-processing. To this end, we decompose $\mathcal{E}$ over $\mathcal{B}_i$ as follows:

$$\mathcal{E} = \sum_i q_i \mathcal{B}_i, \quad \sum_i q_i = 1,$$

where $q_i$ is real. The coefficients of the decomposition $\{q_i\}$ are called "quasiprobability distribution", which is not a probability distribution because $q_i$ can be negative. Using this decomposition, $\langle A \rangle$ can be rewritten as

$$\begin{aligned} \langle A \rangle &= \sum_i q_i \,\mathrm{Tr}\left(A\mathcal{B}_i(\rho)\right) \\ &= \sum_i \frac{|q_i|}{\|q\|_1} \mathrm{sign}(q_i) \|q\|_1 \,\mathrm{Tr}\left(A\mathcal{B}_i(\rho)\right), \end{aligned} \tag{2.5}$$

where $\|q\|_1 \coloneqq \sum_i |q_i|$. Suppose that $\mathrm{Tr}\left[A\mathcal{B}_i(\rho)\right]$ can be classically efficiently calculated. From Eq. (2.5), we can calculate calculate the desired quantity $\mathrm{Tr}(A\mathcal{E}(\rho))$ by sampling an index $i$ with probability $|q_i|/\|q\|_1$ and calculating $\|q\|_1 \mathrm{sign}(q_i)\,\mathrm{Tr}(A\mathcal{B}_i(\rho))$. Thus, $\|q\|_1 \mathrm{sign}(q_i)\,\mathrm{Tr}(A\mathcal{B}_i(\rho))$ is an unbiased estimator of $\mathrm{Tr}(A\mathcal{E}(\rho))$. Let $C$ be $\max_i |\mathrm{Tr}\left(A\mathcal{B}_i\right)|$, the unbiased estimator is bounded in the interval $[-\|q\|_1 C, \|q\|_1 C]$, and thus the Hoeffding inequality [43] shows that

to estimate $\mathrm{Tr}(A\mathcal{E}(\rho))$ within additive error at most $\epsilon$ with probability at least $1-\delta$, we must set the number of samples $N$ such that

$$N \geq 2\|q\|_1^2 C^2 \frac{1}{\epsilon^2} \ln \frac{2}{\delta}.$$

Thus, $\|q\|_1$ quantifies the sampling cost of a quasiprobability-based simulation algorithm. Let us see the state version of the quasiprobability-based simulation algorithm. The value we would like to estimate is again

$$\langle A \rangle = \mathrm{Tr}(A\mathcal{E}(\rho)).$$

Now $\mathcal{E}$ is supposed to be a classically simulatable operation, but $\rho$ is not the case. In such a case, a set of classically simulatable state $\{\sigma_i\}$ is defined, and $\rho$ is decomposed into a linear combination of them:

$$\rho = \sum_i q_i \sigma_i.$$

With a similar argument, $\langle A \rangle$ can be simulated by sampling an index $i$ with probability $|q_i|/\|q\|_1$ and calculating $\mathrm{sign}(q_i)\|q\|_1 \mathrm{Tr}(A\mathcal{E}(\sigma_i))$.

Let us see a concrete example, where $\{\mathcal{B}_i\}$ is chosen to be over completely stabilizer preserving (CSP) channels [39]. Roughly speaking, CSP channels are quantum channels that map a stabilizer state to another stabilizer state. To define CSP channels precisely, we introduce $\mathrm{STAB}_n$ to be the set of $n$-qubit stabilizer states and $\mathrm{SP}_{n,m}$ to be the set of $n$-qubit operations $\mathcal{E}$ such that $\mathcal{E} \otimes I_m \sigma \in \mathrm{STAB}_{n+m}$ for all $\sigma \in \mathrm{STAB}_{n+m}$. A quantum channel $\mathcal{E}$ is completely stabilizer-preserving channel if $\mathcal{E} \in \mathrm{SP}_{n,m}$ for all $m$. Moreover, the authors of Ref. [39] shows the following relation:

$$\begin{aligned}
\mathcal{E} \text{ is an } n\text{-qubit CSP channel.} &\iff \forall_m; \mathcal{E} \otimes I_m \in \mathrm{STAB}_{n,m} \\
&\iff \mathcal{E} \in \mathrm{STAB}_{n,n} \\
&\iff \text{The Choi state of } \mathcal{E} \text{ is a stabilizer state.}
\end{aligned}$$

Combining this relation with single-qubit stabilizer states, one can find that the Clifford gates, $[I]$, $[Z]$, $[S]$, and $[SZ]$ are enough single-qubit CSP channels to decompose a single-qubit diagonal channel. Thus, $\mathcal{E}$ can be decomposed over the four Clifford gates as follows:

$$\mathcal{E} = \sum_i q_i [U_{\mathrm{Cl}\ i}], \quad \{U_{\mathrm{Cl}\ i}\}_i \coloneqq \{I, Z, S, SZ\}.$$

Similarly, one can confirm that single-qubit CSP channels for decomposing a non-diagonal single-qubit quantum channel are Clifford operations. Note that $n$-qubit CSP channels for $n \geq 2$ do not coincide Clifford operations [44].

Let us consider the task to estimate the expectation value of a Pauli operator $\mathrm{Tr}(P\mathcal{E}(\sigma))$, where $\mathcal{E}$ is a single-qubit quantum channel, $\sigma$ is a stabilizer state, and $P$ is a Pauli operator. The expectation value can be written as

$$\mathrm{Tr}(P\mathcal{E}(\sigma)) = \sum_i \frac{|q_i|}{\|q\|_1} \|q\|_1 \mathrm{sign}(q_i) \mathrm{Tr}(P[U_{\mathrm{Cl}\ i}]\sigma), \tag{2.6}$$

where $\|q\|_1 \coloneqq \sum_i |q_i|$. From Eq. (2.6), we can calculate calculate the desired quantity $\mathrm{Tr}(P\mathcal{E}(\sigma))$ by sampling an index $i$ with probability $|q_i|/\|q\|_1$ and calculating $\|q\|_1 \mathrm{sign}(q_i)\,\mathrm{Tr}(P[U_{\mathrm{Cl}i}]\sigma)$. Thus, $\|q\|_1 \mathrm{sign}(q_i)\,\mathrm{Tr}(P[U_{\mathrm{Cl}\ i}]\sigma)$ is an unbiased estimator of $\mathrm{Tr}(P\mathcal{E}(\sigma))$. The unbiased estimator is bounded in the interval $[-\|q\|_1, \|q\|_1]$, and thus the Hoeffding inequality [43] shows that to estimate $\mathrm{Tr}(P\mathcal{E}(\sigma))$ within additive error at most $\epsilon$ with probability at least $1-\delta$, we must set the number of samples $N$ such that

$$N \geq 2\|q\|_1^2 \frac{1}{\epsilon^2} \ln \frac{2}{\delta}.$$

With the use of the minimization of all possible single-qubit CSP channels, the channel robustness of a single-qubit quantum channel $\mathcal{E}$ is defined as follows:

$$R(\mathcal{E}) = \min_{\{q_i\}} \left\{ \|q\|_1 ; \mathcal{E} = \sum_i [U_{\mathrm{Cl}\ i}] \right\}.$$

The channel robustness satisfies the submultiplicativity under composition:

$$R(\mathcal{E} \circ \mathcal{N}) \leq R(\mathcal{E}) R(\mathcal{N}).$$

In the following, we give other examples of the quasiprobability methods. First, we review the stabilizer-state sampling. In contrast to the previous quasiprobability-based simulation algorithm using CSP channels, $\mathcal{E}$ is converted into a resource state by the gate teleportation. Then the resource state is decomposed over stabilizer states, and one of the stabilizer states is to be sampled. Next, we review the Heisenberg propagation, which decomposes an observable to be measured over Pauli operators.

### 2.7.1 Stabilizer-state sampling

Here, we explain stabilizer-state sampling based on Ref. [38]. In general, a quantum circuit can be decomposed into Clifford gates and non-Clifford gates. Clifford gates can be simulated efficiently by the Gottesman-Knill theorem [30], whereas non-Clifford gates, such as the $T$ gate cannot. To handle this situation, we use gate teleportation [24], which replaces a quantum gate with a Clifford circuit and the preparation of a resource state. More concretely, a single-qubit rotation through angle $\theta$ around the $z$ axis

$$U(\theta) = |0\rangle\langle 0| + e^{i\theta} |1\rangle\langle 1| \tag{2.7}$$

can be replaced with the preparation of the resource state

$$|U(\theta)\rangle \coloneqq U(\theta) |+\rangle , \tag{2.8}$$

where

$$|+\rangle \coloneqq \frac{1}{\sqrt{2}}(|0\rangle + |1\rangle),$$

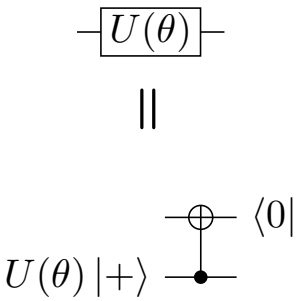


Figure 2.5: Top: Single-qubit rotation gate about the $z$ axis, $U(\theta)$. Bottom: Gate teleportation of $U(\theta)$ composed of a CNOT gate and measurement in the $Z$ basis with the nonstabilizer resource state $U(\theta)\,|+\rangle$. The state is postselected on the measurement outcome 0. This is justified because we are using teleportation just to translate a quantum circuit for classical simulation. In the following figures, projections to $|0\rangle$ are made in the same way.

via gate teleportation as shown in Fig. 2.5. The gate teleportation consists of a CNOT gate, measurement in the $Z$ basis, and the preparation of the resource state $|U(\theta)\rangle$. On the measurement, the state is projected to $|0\rangle$ so that there is no by-product. This is justified because the teleportation is used just to translate a quantum circuit for a classical simulation. In the following figures, projections to $|0\rangle$ are made in the same way. When $\theta = \pi/4$, $U(\pi/4)$ is specifically called the "$T$ gate," and its corresponding resource state is

$$|T\rangle \coloneqq U(\pi/4)\,|+\rangle\,.$$

This is called the "magic state" [25]. Because the resource state is not a stabilizer state, it cannot be simulated efficiently. To handle this, we decompose the resource state into a linear combination of stabilizer states by using the fact that stabilizer states form an overcomplete basis on the operator space. In the case of the magic state, we have

$$|T\rangle\langle T| = \frac{1+\sqrt{2}}{4}\left(\frac{I+X}{2}+\frac{I+Y}{2}\right)+\frac{1-\sqrt{2}}{4}\left(\frac{I-X}{2}+\frac{I-Y}{2}\right),$$

where each term of the right-hand side is a stabilizer state. Note that the coefficients are no longer positive and form a quasiprobability distribution.

Consider an arbitrary $n$-qubit universal quantum circuit $U$, where we want to calculate the expectation value of a Pauli operator $A \in \mathcal{P}_n \coloneqq \{I, X, Y, Z\}^{\otimes n}$:

$$\langle A\rangle = \langle 0|^{\otimes n} U^\dagger A U\,|0\rangle^{\otimes n}\,.$$

By decomposing the quantum circuit $U$ into Clifford and $T$ gates, we can rewrite the expectation value $\langle A\rangle$ as

$$\langle A\rangle = 2^t \mathrm{Tr}\left[\left(A\otimes|0\rangle\langle 0|^{\otimes t}\right)U_{\mathrm{Cl}}\left(|0\rangle\langle 0|^{\otimes n}\,|T\rangle\langle T|^{\otimes t}\right)U_{\mathrm{Cl}}^\dagger\right]$$

where $t$ is the number of $T$ gates and $U_{\mathrm{Cl}}$ is a Clifford circuit (we assume that there is a local description of $U$ so that we can efficiently decompose $U$ into Clifford and $T$ gates.). The projector $|0\rangle\langle 0|^{\otimes t}$ is used for the gate teleportation, and $2^t$ is due to its normalization. Although we decompose the given quantum circuit into Clifford and $T$ gates for simplicity, any diagonal non-Clifford gate, $e^{-i\theta/2Z}$, can be used straightforwardly instead of using $T$ gates.

A classical simulation based on stabilizer-state sampling runs as follows:

1. Let $\{\sigma_i\}$ be a set of pure $t$-qubit stabilizer states. The product of the magic states $|T\rangle^{\otimes t}$ as a resource state is now decomposed into a linear combination of stabilizer states as

$$|T\rangle\langle T|^{\otimes t} = \sum_i x_i \sigma_i, \tag{2.9}$$

   where $\sum_i x_i = 1$.

2. Sample a stabilizer state $\sigma_i$ with probability

$$p_i = \frac{|x_i|}{\sum_i |x_i|}.$$

3. Calculate $M_i = \mathrm{sign}(x_i) \sum_i |x_i| \langle A \rangle_{\sigma_i}$, where $\langle A \rangle_{\sigma_i}$ is defined as

$$\langle A \rangle_{\sigma_i} \coloneqq 2^t \,\mathrm{Tr}\left[\left(A \otimes |0\rangle\langle 0|^{\otimes t}\right) U_{\mathrm{cl}} \left(|0\rangle\langle 0|^{\otimes n} \otimes \sigma_i\right) U_{\mathrm{cl}}^{\dagger}\right], \tag{2.10}$$

   and can be calculated efficiently.

4. By repeating steps 2 and 3, the expectation value $\mathrm{Ex}(M_i)$ of $M_i$ is estimated.

From Eqs. (2.9) and (2.10), we have

$$\begin{aligned}
\langle A \rangle &= 2^t \sum_i x_i \,\mathrm{Tr}\left[\left(A \otimes |0\rangle\langle 0|^{\otimes t}\right) U_{\mathrm{cl}} \left(|0\rangle\langle 0|^{\otimes n} \sigma_i\right) U_{\mathrm{cl}}^{\dagger}\right] \\
&= \sum_i p_i \left(\sum_j |x_j|\right) \mathrm{sign}(x_i) \langle A \rangle_{\sigma_i} \\
&= \sum_i p_i M_i.
\end{aligned}$$

Therefore, $M_i$ is an unbiased estimator of $\langle A \rangle$. Since the sampling according to quasiprobability distribution is simulated by the postprocessing, we call it a "quasiprobability method."

By use of the Hoeffding inequality [43], the number of samples necessary to obtain the expectation value within an additive error $\delta$ with probability of at

least $1-\epsilon$ is given by

$$N_{\text{stabilizer}} = \left(\sum_i |x_i|\right)^2 \frac{2}{\delta^2} \ln\left(\frac{2}{\epsilon}\right).$$

The sampling cost is proportional to the square of $\sum_i |x_i|$.

Until now, we have considered that the resource state is in a pure state $|T\rangle\langle T|$. However, in general, the resource state can be in a mixed state possibly due to noise on the $T$ gate. In the following, we simply denote a resource state by $\rho$ in general. If $\rho$ is a probabilistic mixture of stabilizer states, for example, all the coefficients $x_i$ are positive by definition, and $\sum_i |x_i| = 1$. Hence, the sampling cost does not increase. Otherwise, some coefficients are inevitably negative, and the sampling cost $N_{\text{stabilizer}}$ increases according to the amount of $\sum_i |x_i|$. In this sense, $\sum_i |x_i|$ quantifies the simulation cost of the universal quantum computation.

With use of the minimization for all possible stabilizer decompositions, the Robustness of Magic (ROM) of a resource state $\rho$ is defined as follows

$$\mathcal{R}(\rho) = \min_{x_i} \left\{ \sum_i |x_i| ; \rho = \sum_i x_i \sigma_i \right\},$$

which determines the minimum cost to simulate a Clifford circuit with an input state $\rho$ by stabilizer-state sampling. However, calculation of the ROM is intractable if the number of qubits increases. Even in this case, we can calculate an upper bound of the ROM by using the submultiplicativity,

$$\mathcal{R}(\rho \otimes \rho') \leq \mathcal{R}(\rho)\mathcal{R}(\rho').$$

Specifically, for the resource state $|T\rangle\langle T|^{\otimes t}$, it has been estimated that

$$\mathcal{R}(|T\rangle\langle T|^{\otimes 5}) = 3.68705$$

and hence

$$\left\{\mathcal{R}\Big(|T\rangle\langle T|^{\otimes t}\Big)\right\}^2 < \left\{\mathcal{R}\Big(|T\rangle\langle T|^{\otimes 5}\Big)\right\}^{\frac{2t}{5}} \approx 2^{0.75298t}$$

as explained in Ref. [38]. On the other hand, the upper bound of the cost of the resource state $|T\rangle\langle T|^{\otimes t}$ is $2^t$ if we use $\mathcal{R}(|T\rangle\langle T|) = \sqrt{2}$. Consequently, optimizing the stabilizer decomposition over multiple copies of a resource state significantly reduces the simulation cost. In Ref. [39], it is shown that the channel robustness of $\mathcal{E}$ is equal or lower than the robustness of magic of the Choi state $|\Psi_{\mathcal{E}}\rangle\langle\Psi_{\mathcal{E}}|$:

$$R(\mathcal{E}) \geq \mathcal{R}(|\Psi_{\mathcal{E}}\rangle\langle\Psi_{\mathcal{E}}|).$$

This is because more stabilizer states are used to calculate RoM than channel robustness. Moreover, if the unitary operation $\mathcal{U}$ is in the third level of the Clifford hierarchy, then

$$R(\mathcal{U}) = \mathcal{R}(|\Psi_{\mathcal{U}}\rangle\langle\Psi_{\mathcal{U}}|).$$

### 2.7.2 Heisenberg propagation

Let us review Heisenberg propagation as proposed in Ref. [40]. In Heisenberg propagation, an observable to be measured evolves in the Heisenberg picture. In general, such a calculation requires exponential time. To handle this, we decompose the observable into a linear combination of Pauli operators. As described below, one Pauli operator is sampled at each step by using quasiprobability method as follows.

Consider an $n$-qubit quantum circuit consisting of $d$ quantum channels $\{\Lambda_i\}_{i=1}^{d}$. Each quantum channel acts on a constant number of qubits. We assume that both the initial state of the circuit $\rho$ and an observable $A$ are products of operators acting on a finite number of qubits. The expectation value of $A$ is written as

$$\begin{aligned}\langle A\rangle &= \mathrm{Tr}\left(A\Lambda_d\circ\cdots\circ\Lambda_2\circ\Lambda_1(\rho)\right)\\ &= \mathrm{Tr}\left(\rho\Lambda_1^\dagger\circ\cdots\circ\Lambda_{d-1}^\dagger\circ\Lambda_d^\dagger(A)\right),\end{aligned}$$

where $\Lambda^\dagger$ is the adjoint of $\Lambda$; that is,

$$\mathrm{Tr}\left[C\Lambda(B)\right] = \mathrm{Tr}\left[\Lambda^\dagger(C)B\right],$$

for any operators $B$ and $C$.

The Heisenberg propagation algorithm is as follows:

1. Decompose $A^{(i)}$ into Pauli operators $\sigma\in\mathcal{P}_n=\{I,X,Y,Z\}^{\otimes n}$:

$$A^{(i)} = \sum_{\sigma\in\mathcal{P}_n} c_\sigma\sigma,$$

   where $A^{(0)}=A$ and $A^{(i)}$ $(i=1,\ldots,d)$ is defined recursively below.

2. Sample a Pauli operator $\sigma^{(i)}$ with probability

$$p_\sigma = \frac{|c_\sigma|}{\sum_{\sigma\in\mathcal{P}_n}|c_\sigma|} = \frac{\left|\mathrm{Tr}\left(A^{(i)}\sigma\right)\right|}{2^n\mathcal{D}\left(A^{(i)}\right)},$$

   where $\mathcal{D}(A)\coloneqq 2^{-n}\sum_\sigma|\mathrm{Tr}(A\sigma)| = \sum_{\sigma\in\mathcal{P}_n}|c_\sigma|$, which is called the "stabilizer norm" in Ref. [45].

3. Define $A^{(i+1)}=\Lambda_{d-i}^\dagger\left(A^{(i)}\right)$.

4. Repeat steps 1-3 for $i=0,\ldots,d$ to obtain $A^{(d+1)}$, which is an operator still acting on a finite number of qubits. Then we calculate

$$M\left(\left\{\sigma^{(i)}\right\}\right)\coloneqq\mathrm{Tr}\left[A^{(d+1)}\rho\right]\prod_{i=0}^{d}\left[\mathrm{sign}(c_{\sigma^{(i)}})\mathcal{D}\left(A^{(i)}\right)\right].$$

5. Repeat step 4 to estimate the expectation value of $M(\{\sigma_i\})$.

The expectation value is given by

$$\sum_{\left\{\sigma^{(i)}\right\}}\left[\left(\prod_{i=0}^{d}p_{\sigma^{(i)}}\right)M\left(\left\{\sigma^{(i)}\right\}\right)\right]=\langle A\rangle\,,$$

where $\sum_{\left\{\sigma^{(i)}\right\}}$ indicates the summation taken over all possible trajectories. We used the fact that $\operatorname{sign}\left[\operatorname{Tr}\left(A^{(i)}\sigma^{(i)}\right)\right]\mathcal{D}\left(A^{(i)}\right)$ is an unbiased estimator for $A^{(i)}$ in step 3. The number of samples required for an additive error $\delta$ with probability of at least $1-\epsilon$ is bounded by the Hoeffding inequality [43]

$$N_{\text{Heisenberg}}=\left(\mathcal{D}(A)\prod_{i=1}^{d}\mathcal{D}\left(\Lambda_i^{\dagger}\right)\right)^2\frac{2}{\delta^2}\ln\left(\frac{2}{\epsilon}\right),\tag{2.11}$$

where the channel stabilizer norm for a channel $\Lambda$ is defined by

$$\mathcal{D}(\Lambda)\coloneqq\max_{\sigma\in\mathcal{P}_n}\mathcal{D}[\Lambda(\sigma)].\tag{2.12}$$

Since

$$\mathcal{D}(\Lambda\circ\Lambda')\leq\mathcal{D}(\Lambda)\mathcal{D}(\Lambda'),$$

we should choose the channel $\Lambda$ to be simulated appropriately so that the channel stabilizer norm is minimized while the dimension of $\Lambda$ is maintained tractable.

## 2.8 Summary and Discussion

In this chapter, we have reviewed the basics of quantum computation and then classically efficiently simulable quantum circuits, Clifford circuits and fermionic linear optics (FLO). Moreover, we review the quasiprobability-based sampling simulation algorithms, which sample a CSP channel, a stabilizer state, or a Pauli operator.

Through the stabilizer-state sampling simulation algorithm, the classical computation cost of a quantum circuit can be quantified as the sampling cost of the simulation. However, unlike the Heisenberg propagation, the existing stabilizer-state sampling has not been optimized to simulate noisy quantum circuits. In Chapter 3, we will extend the stabilizer-state sampling to the noisy case and compare the extended stabilizer-state sampling with the Heisenberg propagation in terms of the sampling cost. Furthermore, we will show that possible quantum advantages can be squeezed by estimating the sampling cost of the stabilizer-state sampling algorithm.

Clifford circuits are classically efficiently simulatable by the Gottesman-Knill theorem. One of the most important applications of Clifford circuits is quantum error correction (QEC). Whereas most of numerical calculations of QEC

assume that the noise is described by Pauli operators, quantum devices suffer from coherent noise, which cannot be represented by Pauli operators, such as an over-rotation noise. Based on the review of quasiprobability-based simulation algorithms, we expect that coherent noise can be simulated by decomposing the noise over CSP channels, thereby sampling one CSP channel. We will see the simulation method for QEC under the over-rotation noise using the quasiprobability-based simulation algorithm in Chapter 4.

Although we have reviewed the quasiprobability-based simulation algorithms based on Clifford circuits, the classically efficiently simulable quantum circuit should be chosen according to a quantum algorithm or a quantum circuit. The simulation of fermionic systems is one of the most promising candidates for demonstrating quantum advantages, and the Google Quantum AI group performed several quantum simulations of a fermionic system recently [46], which is composed of free fermions. To narrow down possible quantum advantages by the simulation of fermionic systems, a quasiprobability-based simulation algorithm based on FLO would be more useful. We will show the quasiprobability-based simulation algorithm based on FLO and estimate the sampling cost of a concrete quantum circuit in Chapter 5.

# Chapter 3

# Comparative Study of Sampling-Based Simulation Costs of Noisy Quantum Circuits

In this chapter, we extend the stabilizer-state sampling to the noisy case, and compare its simulation cost with that of Heisenberg propagation. Noise in quantum operations often negates the advantage of quantum computation. However, most classical simulations of quantum computers calculate the ideal probability amplitudes either storing full state vectors or using sophisticated tensor network contractions. Here, we investigate sampling-based classical simulation methods for noisy quantum circuits. Specifically, we characterize the simulation costs of two major schemes, stabilizer-state sampling of magic states and Heisenberg propagation, for quantum circuits being subject to stochastic Pauli noise, such as depolarizing and dephasing noise. To this end, we introduce several techniques for the stabilizer-state sampling to reduce the simulation costs under such noise. It revealed that in the low noise regime, stabilizer-state sampling results in a smaller sampling cost, while Heisenberg propagation is better in the high noise regime. Furthermore, for a high depolarizing noise rate $\sim 10\%$, these methods provide better scaling compared to that given by the low-rank stabilizer decomposition. We believe that these knowledge of classical simulation costs is useful to squeeze possible quantum advantage on near-term noisy quantum devices as well as efficient classical simulation methods. This chapter is based on [Hakkaku and Fujii, Phys. Rev. Applied **15**, 064027 (2021)] with slight modifications to fit in the context.

## 3.1 Introduction

Quantum computers are expected to provide an exponential speedup compared to classical computers for certain problems such as factoring problems and quantum simulations. Recently, extensive effort has been expended for the realization of quantum computers, and the number of qubits is now more than 50 [9, 46–49]. Unfortunately, such a number of qubits is still too small to run sophisticated quantum algorithms such as Shor's algorithm for factorization. Nevertheless, quantum devices that have already been realized or will be realized soon. are thought to achieve quantum computational supremacy, providing an output of a particular task much faster than the known best effort on a classical computer. Recently, Google demonstrated a sampling task on its quantum processor, Sycamore, consisting of 53 qubits with high-fidelity single-qubit and two-qubit gates [9]. While Sycamore takes about 200 s to conduct the task, a state-of-the-art supercomputer would take, according to Google's estimation, approximately 10,000 years. After this experiment, IBM and Alibaba rebutted the estimated time for a classical simulation [50, 51]. Specifically, Alibaba estimated that the simulation takes less than 20 days by use of a sophisticated designed tensor network-based classical simulation algorithm [51]. While noise on quantum operations deteriorates the quantumness, which would reduce the classical simulation cost, the effect of the noise is not fully used in the abovementioned classical simulations. To compare quantum and classical computers fairly, a more-refined classical approach should be used to simulate quantum computers.

There has been another classical simulation approach based on sampling. Instead of computing the full probability amplitudes, a class of classically simulatable quantum computations, which is called a Clifford circuit, is used to save memory during a classical simulation [38]. More precisely, a quantum circuit is decomposed into the Clifford circuits and the preparation of a resource state which is the so-called magic state [25]. Then, by decomposition of the resource state into a linear combination of stabilizer states with a quasiprobability distribution, the resource state is replaced by sampling a stabilizer state with an appropriate postprocessing, where the Gottesman-Knill theorem [30] can efficiently simulate each realization. We refer to this sampling algorithm as "stabilizer-state sampling." The sampling cost of this quantum computation is determined by a measure called the "robustness of magic (ROM)."

Another sampling-based classical simulation algorithm is based on evolving a measured observable in the Heisenberg picture [40]. The observable evolved by an adjoint quantum channel is decomposed over the Pauli operators, and one of them is sampled by the quasiprobability method similarly to stabilizer-state sampling. This sampling algorithm is called "Heisenberg propagation." The simulation costs are characterized by a measure called a "stabilizer norm." A study on the simulation cost of a depolarized rotation gate showed that the depolarizing noise decreases the simulation costs [40]. However, it remains unclear whether Heisenberg propagation can simulate noisy quantum circuits more efficiently than stabilizer-state sampling.

In this study, we investigate the simulation costs of noisy quantum circuits in further detail. Specifically, we consider two algorithms, stabilizer-state sampling and Heisenberg propagation, to quantify the sampling costs of quantum circuits subject to stochastic Pauli noise. Unfortunately, the existing stabilizer-state sampling has not been optimized to simulate noisy quantum circuits. Unlike Heisenberg propagation, stabilizer-state sampling is not directly applicable to quantum circuits where nondiagonal noise, such as Pauli $X$ and $Y$ errors, occurs. Moreover, noise on the Clifford gates has yet to be fully used to reduce simulation costs. To address the former problem, we use the gate-teleportation technique [24] to transform the nondiagonal part to a diagonal noise. For the latter issue, we propose a method to collect noise on Clifford gates into a resource state. These techniques reduce the simulation costs for stabilizer-state sampling and allows us to compare the two sampling-based simulation algorithms. In addition, we introduce a reduced stabilizer basis to calculate a reasonable upper bound of the ROM for multiple copies of a noisy magic state in a feasible way.

For these two major sampling-based classical simulation algorithms, we compare the costs to simulate noisy quantum circuits and identify the more-suitable approach in different situations. Specifically, we consider noisy quantum circuits where each gate is followed by dephasing or depolarizing noise. We quantitatively analyze how such noise decreases the simulation costs for the two sampling-based simulation algorithms. We find that there is a crossover in the performance: up to a particular error rate, stabilizer-state sampling has better performance; however, as the error rate becomes higher, Heisenberg propagation outperforms stabilizer-state sampling. This knowledge is useful to pursue a better approach to simulate a noisy quantum circuit. Furthermore, specified classically simulatable regions would be also helpful to design quantum circuits that potentially have a quantum advantage avoiding these sampling-based classical simulations.

The rest of this chapter is organized as follows. In Section 2.7, we review two existing classical simulation algorithms: stabilizer-state sampling and Heisenberg propagation. The analysis includes the simulation costs, ROM and stabilizer norm. Then, in Section 3.3, we explain how to calculate the ROM of noisy quantum circuits through some examples. Finally, in Section 3.4, we compare the two sampling-based algorithms via noisy random quantum circuits (RQCs). Section V is devoted to the conclusions and a discussion.

## 3.2 Qualitative comparison of the two algorithms

The staiblizer-state sampling and Heisenberg propagation discussed in Section 2.7 are similar in the sense that if a quantum circuit consists only of Clifford gates, then the overhead does not grow exponentially. Both algorithms require an optimization procedure to estimate the simulation costs. That is, the size of the resource state in stabilizer-state sampling or the size of the support of the channel must be small to feasibly calculate the ROM or a channel stabilizer norm , respectively. For stabilizer-state sampling, the computationally hard

part is imposed by the preparation of a resource state, which can reduce the simulation cost for an arbitrary quantum circuit by preparing multiple copies of the resource state and decomposing them over stabilizer states. This could be advantageous against Heisenberg propagation because its simulation cost explicitly depends on the quantum circuit to be simulated instead of a resource state.

On the other hand, it is easier for Heisenberg propagation to use the noise effect to reduce the simulation cost. For example, depolarizing noise, which appears after the Clifford gate, helps to reduce the overhead in a straightforward manner. However stabilizer-state sampling requires a special treatment, as developed in the next section. Because of these complicated factors, it remains unclear which algorithm is better suited for a given noisy quantum circuit. This is one of the main targets to be clarified in this chapter.

## 3.3 Stabilizer-state sampling for noisy quantum circuits

Heisenberg propagation can simulate noisy quantum circuits straightforwardly. However, it is not straightforward for stabilizer-state sampling to use the noise effect, especially on the Clifford gate, to reduce the simulation cost. Here we provide several techniques to extend stabilizer-state sampling to the noisy case.

Below, we first consider the simulation cost of a diagonal gate followed by diagonal noise, such as dephasing noise. Second, we calculate the simulation cost when stochastic Pauli noise occurs after a non-Clifford gate. Third, we explain noise fusion, where the noise occurring in different gates is merged so that the noise on the Clifford gates can reduce the simulation cost of a non-Clifford gate. Finally, we explain how to reduce the number of stabilizer states as a basis to calculate a reasonable upper bound of the ROM of the noisy resource states, since an exact calculation of the ROM is hard.

### 3.3.1 Noise teleportation

Consider a single-qubit rotation gate about the $z$ axis subject to the dephasing noise. The ideal rotation gate and the corresponding resource state are defined in Eqs. (2.7) and (2.8), respectively. The single-qubit dephasing noise is defined as

$$\mathcal{E}_{\text{dephasing}}(\rho) \coloneqq (1-p)\rho + pZ\rho Z. \tag{3.1}$$

The $Z$ error in Eq. (3.1) acts as the $Z$ operator on the resource state $|U(\theta)\rangle$, as shown in Fig. 3.1. Thus, the resource state of the noisy rotation gate is given by

$$\rho = (1-p)\,|U(\theta)\rangle\langle U(\theta)| + pZ\,|U(\theta)\rangle\langle U(\theta)|\,Z.$$

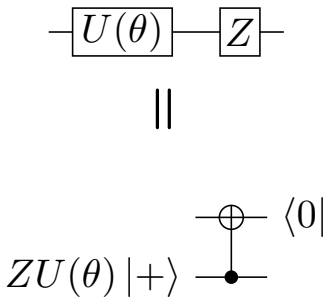


Figure 3.1: Top: Single-qubit rotation gate about the $z$ axis $U(\theta)$ followed by the $Z$ error. Bottom: Pushing the $Z$ error into the resource state.

Figure 3.2 shows the ROM of the resource state corresponding to the noisy rotation gate $\mathcal{R}(\rho)$, where we use a convex-optimization solver, CVXPY [52, 53], to calculate the ROM. As shown in Fig. 3.2, the ROM decreases as the error rate of the dephasing noise increases. Additionally, the smaller the rotation angle, the more easily the noise makes the ROM unity; that is, such a noisy resource state becomes a probabilistic mixture of stabilizer states. One implication of this is that we have to carefully design quantum circuits for noisy near-term quantum devices so that they cannot be simulated easily. For example, the variational quantum eigensolver (VQE) uses parameterized quantum circuits consisting of many rotation gates, whose angles are often small. A small amount of noise would be enough to make such circuits classically simulatable. It would be interesting to characterize applications of noisy near-term quantum devices in terms of the ROM if they satisfy the necessary condition for quantum advantage.

In the above case, the noise effect is considered straightforwardly by virtue of the dephasing noise. However, this argument is not directly applicable for an $X$ error or a $Y$ error because they are not diagonal with respect to the computational basis. To handle this, we propose a way to deal with nondiagonal errors through gate teleportation. Consider a diagonal non-Clifford single-qubit gate $U$ followed by the single-qubit depolarizing noise

$$\begin{aligned}\mathcal{E}_{\mathrm{depo1}}(\rho) &\coloneqq \left(1-\frac{3}{4}p\right)\rho + \frac{p}{4}\sum_{A\in\{X,Y,Z\}}[A]\rho \\ &= (1-p)\rho + p\frac{I}{2}\end{aligned}$$

where $[A]$ is a superoperator defined by $[A]\rho \coloneqq A\rho A^\dagger$. A $Z$ error is treated in the same way as mentioned before. Figure 3.3a corresponds to the gate teleportation of a diagonal gate $U$ followed by an $X$ error, where the $X$ error is rewritten as $HZH$. In Figure 3.3a the first $H$ gate is replaced by the gate teleportation of the $H$ gate (Fig. 3.3b). As a result, the $X$ error is taken as the $Z$ operator on the second ancilla qubit. Similarly, we treat the $Y$ error as the correlated $Z$ operator on the two ancilla qubits. In this way, the depolarizing

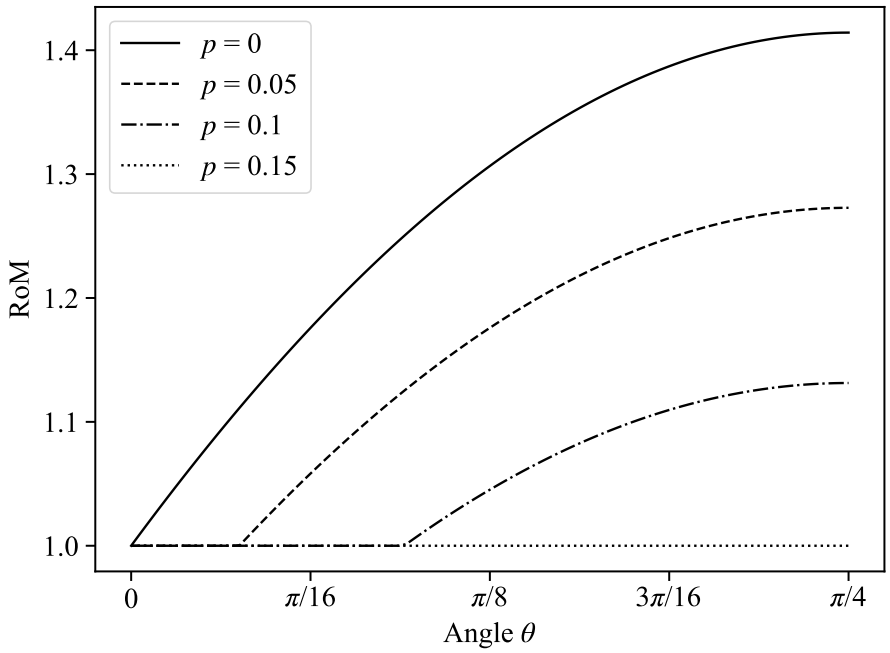


Figure 3.2: ROM of the resource state $\mathcal{E}_{\text{dephasing}}[|U(\theta)\rangle\langle U(\theta)|]$, which corresponds to the rotation gate about the $z$ axis followed by the dephasing noise with error rate $p$. The horizontal axis shows the angle $\theta$ of the rotation. The vertical axis shows the ROM, which quantifies the simulation cost of a Clifford circuit with a non-Clifford resource state for stabilizer-state sampling. The legend shows the error rates of the dephasing noise. The sampling cost increases as ROM becomes larger. When the ROM of a circuit is unity, the noisy resource state is a probabilistic mixture of stabilizer states.

noise is translated into correlated diagonal errors $\tilde{\mathcal{E}}_1$ on the ancilla qubits as follows:

$$\tilde{\mathcal{E}}_1 = \left(1 - \frac{3}{4}p\right)[I \otimes I] + \frac{p}{4}([Z_1] + [Z_2] + [Z_1 Z_2]).$$

This gives us the noisy resource state as

$$\tilde{\mathcal{E}}_1(\rho) = \left(1 - \frac{3}{4}p\right)\rho + \frac{p}{4}([Z_1] + [Z_2] + [Z_1 Z_2])\rho.$$

The noisy resource state obtained above is equivalent to the Choi state of the quantum channel $\mathcal{E}_{\text{depo1}} \circ \mathcal{U}$, where $\mathcal{U}(\rho) \coloneqq U\rho U^\dagger$ up to a local Clifford gate:

$$\tilde{\mathcal{E}}_1\left(\rho_{\text{CZ}|U\rangle|+\rangle}\right) = [I] \otimes \left([H] \circ \mathcal{E}_{\text{depo1}} \circ [U]\right)\left(\rho_{|\Psi^+\rangle}\right),$$

(a)

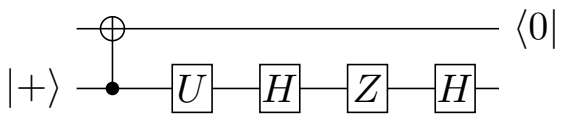


(b)

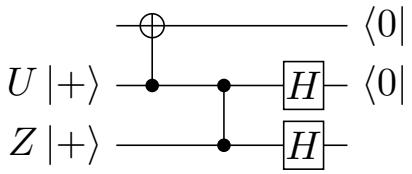


Figure 3.3: Noise teleportation of a diagonal gate $U$ followed by an $X$ error. (a) Gate teleportation of $U$ followed by an $HZH$ operator. (b) Gate teleportation of $U$ and an $X$ error by replacement of the first $H$ gate shown in (a) with the gate teleportation of the $H$ gate.

where

$$\rho_{(|\cdots\rangle)} = |\cdots\rangle\langle\cdots|\,,$$
$$|\Psi^+\rangle := \frac{|00\rangle + |11\rangle}{\sqrt{2}},$$

and CZ indicates the controlled-$Z$ gate. More generally, for a diagonal single-qubit gate $U$ and single-qubit stochastic Pauli noise $\mathcal{E}$, the classical simulation cost via the noise teleportation is quantified by a ROM of

$$[I] \otimes (\mathcal{E} \circ [U])\, \rho_{|\Psi^+\rangle}.$$

Recently, a similar measure for a quantum channel was developed in Ref. [39], which is called the "channel robustness." The channel robustness is also calculated from the ROM of the Choi state except the stabilizer states used to decompose the Choi state must satisfy the trace-preserving condition. Seddon and Campbell [39] show that for any $n$-qubit CPTP (completely positive trace-preserving) maps $\mathcal{E}$, ROM of the Choi state $\mathcal{R}(\rho_{\mathcal{E}})$, and channel robustness $\mathcal{R}_*(\mathcal{E})$, the following inequality holds:

$$\mathcal{R}(\rho_{\mathcal{E}}) \leq \mathcal{R}_*(\mathcal{E}),$$

where

$$\rho_{\mathcal{E}} := \left(\mathcal{E} \otimes I^{\otimes n}\right) |\Omega_n\rangle\langle\Omega_n|\,,$$
$$|\Omega_n\rangle := \frac{1}{\sqrt{2^n}} \sum_{j=0}^{2^n-1} |j\rangle\,|j\rangle\,.$$

(a)

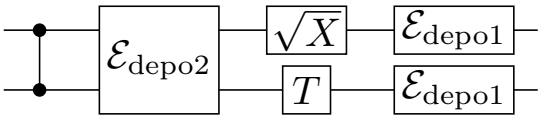


(b)

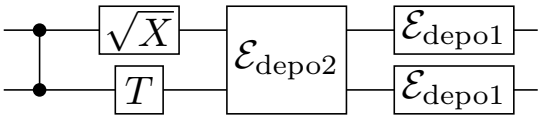


Figure 3.4: Noise fusion. (a) Depolarizing noise occurs at every gate. (b) Noise is collected around the $T$ gate to reduce the simulation cost of the $T$ gate.

We confirmed that the ROM of $\rho = \tilde{\mathcal{E}}_1(|T+\rangle\langle T+|)$, which is the resource state of the $T$ gate followed by the depolarizing noise, is equal to its channel robustness by numerical calculations. However, the ROM of the product state $\rho^{\otimes n}$ may be lower than the channel robustness of $\rho^{\otimes n}$. This is because the stabilizer states that do not result in trace-preserving operations are used in the stabilizer decomposition when a resource state is multiple copies of a state.

### 3.3.2 Noise fusion

In general, a quantum circuit consists of Clifford and non-Clifford gates. Both of these gates are subject to noise. Since Clifford gates can be simulated efficiently, noise on the Clifford gates should not directly reduce the classical simulation costs for stabilizer-state sampling. To reduce the ROM of a resource state, we construct a method to merge the noise on Clifford gates with the noise on a neighboring non-Clifford gate as follows.

Consider a quantum circuit consisting of arbitrary single-qubit and two-qubit gates, followed by single-qubit and two-qubit depolarizing noise, respectively. The single-qubit depolarizing noise and two-qubit depolarizing noise are given by

$$\mathcal{E}_{\text{depo1}} \coloneqq \left(1 - \frac{3}{4}p\right)[I] + \frac{p}{4} \sum_{A \in \{X,Y,Z\}} [A],$$
$$\mathcal{E}_{\text{depo2}} \coloneqq \left(1 - \frac{15}{16}p\right)[I^{\otimes 2}] + \frac{p}{16} \sum_{(A,B) \neq (I,I)} [A \otimes B].$$

Let $U_1$ and $U_2$ be arbitrary single-qubit and two-qubit gates, respectively. The unitary operator $U_1(U_2)$ commutes with the depolarizing channel $\mathcal{E}_{\text{depo1}}(\mathcal{E}_{\text{depo2}})$

(a)

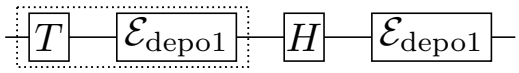


(b)

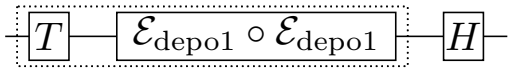


Figure 3.5: Circuits illustrating noise teleportation and noise fusion. (a) $T$ gate and $H$ gate followed by a single-qubit depolarizing channel. (b) Two single-qubit depolarizing channels are merged by the noise fusion.

as

$$\begin{aligned} \mathcal{E}_{\mathrm{depo1}} \circ [U_1] &= [U_1] \circ \mathcal{E}_{\mathrm{depo1}}, \\ \mathcal{E}_{\mathrm{depo2}} \circ [U_2] &= [U_2] \circ \mathcal{E}_{\mathrm{depo2}}. \end{aligned} \tag{3.2}$$

For example, consider the circuit shown in Fig. 3.4a. The two-qubit depolarizing noise forward is commuted with use of Eq. (3.2), which merges the single-qubit depolarizing noise and the two-qubit depolarizing noise [Fig. 3.4b]. In general, for a given noise channel

$$\mathcal{E} = \sum_i [E_i],$$

by replacing $\mathcal{E}$ with a unitary gate $U$, we have

$$\mathcal{E} \circ [U] = [U] \circ \mathcal{E}',$$

where

$$\mathcal{E}' \coloneqq \sum_i \left[U^\dagger E_i U\right].$$

If channel $\mathcal{E}$ is a stochastic Pauli channel and if $U$ is a gate in the third or lower level of the Clifford hierarchy, including the $T$ gate, then $\mathcal{E}'$ is a stochastic Clifford channel. In this case, the merging process reduces the ROM of the resource state. For clarity, we consider the simplest case, the depolarizing noise, below.

### 3.3.3 Illustrative example of noise teleportation and noise fusion

To confirm that noise teleportation and noise fusion can reduce the ROM, we calculate the ROM of the noisy circuit shown in Fig. 3.5a. We assume that single-qubit depolarizing noise always occurs after a single-qubit gate. The

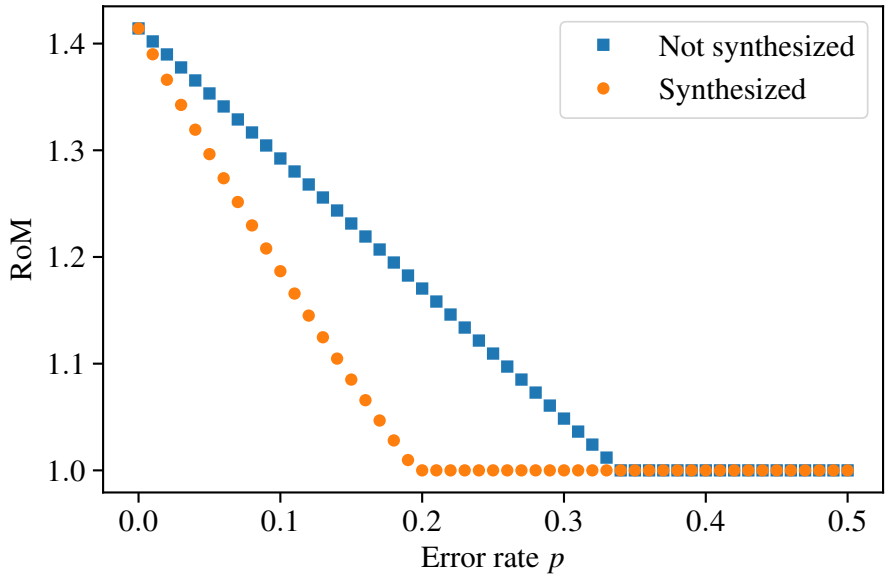


Figure 3.6: Comparison of the ROM with and without noise fusion. The horizontal axis shows the error rates of the single-qubit depolarizing noise. The vertical axis shows the ROM. The orange circles and blue squares correspond to the ROM defined in Eq. (3.3) with noise fusion and the ROM defined in Eq. (3.4) without noise fusion, respectively.

ROM of the resource state of the quantum channels surrounded by the dashed rectangle in Fig. 3.5a is given as

$$\mathcal{R}\Big(\tilde{\mathcal{E}}_1(|T+\rangle\langle T+|)\Big). \tag{3.3}$$

We replace the single-qubit depolarizing noise backward using the noise fusion as shown in Fig. 3.5b. The ROM of the resource state of the quantum channels surrounded by the dashed rectangle in Fig. 3.5b is given as

$$\mathcal{R}\Big(\tilde{\mathcal{E}}_1 \circ \tilde{\mathcal{E}}_1(|T+\rangle\langle T+|)\Big). \tag{3.4}$$

The ROM of the resource state is calculated in both cases with noise fusion and without noise fusion. The blue squares and orange circles in Fig. 3.6 correspond to the ROM defined in Eqs. (3.3) and (3.4), respectively. The ROM shown in Eq. (3.3) is unity when the error rate $p$ is equal to or greater than 0.34. On the other hand, the ROM shown in Eq. (3.4) is unity when the error rate $p$ is equal to or greater than 0.2. Hence, noise fusion successfully reduces the ROM.

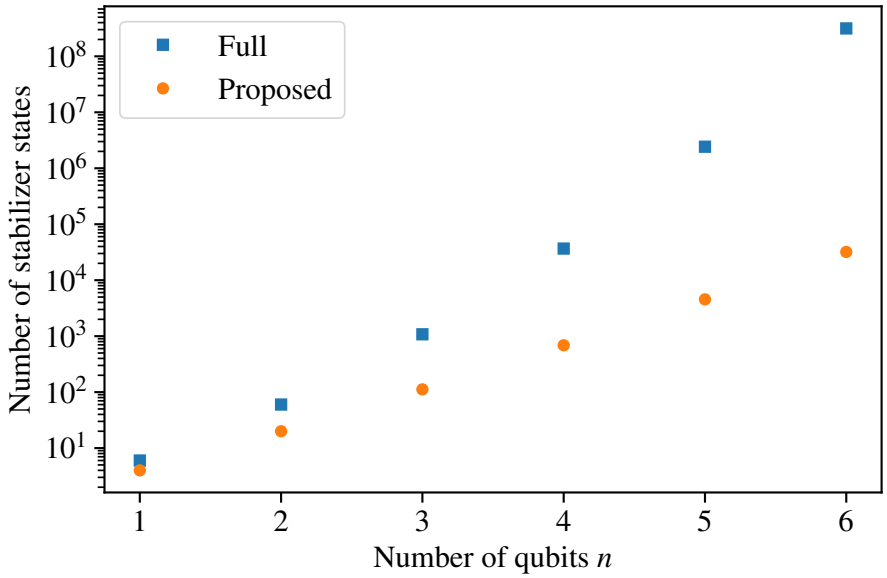


Figure 3.7: Comparison of the number of the stabilizer states used to calculate the exact ROM of $n$-fold copies of the magic state and the number of stabilizer states used to calculate its upper bound by our proposed method. The horizontal axis indicates the number of qubits. The vertical axis indicates the number of stabilizer states. Blue squares and orange circles correspond to the total number of stabilizer states and the number of stabilizer states needed to calculate the upper bound, respectively.

### 3.3.4 Reducing basis for stabilizer-state decomposition

Simulation costs can be reduced by decomposing $n$-fold copies of a resource state $\rho^{\otimes n}$ instead of decomposing $\rho$. Unfortunately, the number of stabilizer states used in the decomposition grows superexponentially as the number of qubits increases [30, 54]:

$$2^n \prod_{k=1}^{n} \left(2^k + 1\right). \tag{3.5}$$

Thus, it becomes intractable to calculate $\mathcal{R}\left(|T\rangle\langle T|^{\otimes n}\right)$ exactly as $n$ increases. However, not all stabilizer states contribute to the decomposition of the tensor product of the magic states. The decomposition of the magic state $|T\rangle\langle T|$ requires only $X$ and $Y$ components of stabilizer states. Hence, the stabilizer states whose stabilizer operators include $X$ and $Y$ operators are engaged in the decomposition.

Consider the upper bound of the ROM of two-copies of a magic state $|T\rangle\langle T|^{\otimes 2}$.

Table 3.1: Comparison of the exact ROM of $n$-fold copies of the magic state $|T\rangle$ and their upper bounds calculated by our proposed method.

| $n$ | Proposed method | Exact |
|---|---|---|
| 1 | 1.414214 | 1.414214 |
| 2 | 1.747547 | 1.747547 |
| 3 | 2.218951 | 2.218951 |
| 4 | 2.862742 | 2.862742 |
| 5 | 3.689298 | 3.687052 |

We use separable stabilizer states, all twofold tensor products of $\{|\pm\rangle, |\pm i\rangle\}$ and the entangled stabilizer states stabilized by

$$\begin{aligned} &\langle XX, YY\rangle, \quad \langle -XX, -YY\rangle, \\ &\langle XY, YX\rangle, \quad \langle -XY, -YX\rangle. \end{aligned} \tag{3.6}$$

Using these stabilizer states, we numerically find that the upper bound of the ROM of $|T\rangle\langle T|^{\otimes 2}$ is almost the same as the exact value. On the basis, we use the separable stabilizer states and bipartite entangled stabilizer states with respect to $X$ and $Y$ operators. To decompose $|T\rangle\langle T|^{\otimes n}$ over certain stabilizer states, we use the stabilizer states stabilized by one of the stabilizer groups shown in Eq. (3.6), for up to $\lfloor \frac{n}{2} \rfloor$ pairs. Thus, the number of basis elements to decompose $|T\rangle\langle T|^{\otimes n}$ from Eq. (3.5) is reduced to

$$4^n n! \sum_{k=0}^{\lfloor n/2 \rfloor} \left\{ 8^k k! (n-2k)! \right\}^{-1}.$$

Figure 3.7 compares the number of the stabilizer states used to calculate the ROM of $n$-fold copies of the magic state $\mathcal{R}\left(|T\rangle\langle T|^{\otimes n}\right)$ and its upper bound by our proposed method. The horizontal axis indicates the number of stabilizer states, while the vertical axis indicates the number of qubits. The blue squares and orange circles correspond to the total number of stabilizer states and the number of stabilizer states used by our proposed method, respectively. Our method uses fewer stabilizer states than the total number of stabilizer states. Table 3.1 compares the upper bounds of the ROM of $n$-fold copies of the magic state for our proposed method with the exact ROM calculated with all stabilizer states. The upper bound of the ROM is sufficiently close to the exact ROM up to four qubits. For $n = 5$, the upper bound of the ROM is slightly larger than the exact ROM. Therefore, our method provides a reasonable upper bound of the ROM.

This method is used in Sect. 3.4 in the caluclation of the ROM of twofold copies of the resource state of the depolarized $T$ gates. A more-efficient and more-precise method for calculating the upper bound of the ROM of $n$-fold copies of the magic state was proposed in Ref. [55], but the noisy case was not considered there.

(a)

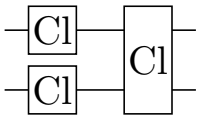


(b)

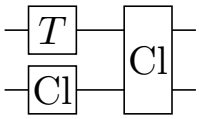


(c)

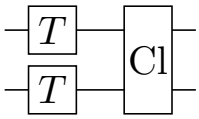


Figure 3.8: Three patterns of the unit cell constituting our RQCs: (a) unit cell 1, (b) unit cell 2, and (c) unit cell 3. Cl denotes a Clifford gate.

## 3.4 Comparison of sampling-based simulation algorithms

Here we compare the two sampling-based algorithms by calculating the simulation cost concretely for RQCs, which are similar to the circuits used in the quantum computational supremacy experiment [9], consisting of Clifford and $T$ gates followed by single-qubit or two-qubit depolarizing noise. We construct RQCs by alternately applying single-qubit gates chosen from $\left\{\sqrt{X}, \sqrt{Y}, T\right\}$ to each qubit, and then applying two-qubit Clifford gates to nonoverlapping nearest-neighbor pairs of two qubits. We call the sequential operations of applying single-qubit and two-qubit gates in turn a "cycle". After a certain number of cycles, all qubits are measured to obtain an expectation value of Pauli operator $P$.

The expectation value of $P$ with respect to an output state of a RQC becomes exponentially close to zero as the depth of a RQC increases. However, this is not the point in our comparison. The RQCs are just chosen as a representative of hardware-efficient quantum circuits that are expected to be used in near-term quantum devices. Regarding a single-qubit gate, the $T$ gate is the most adversarial in classical simulation, since the ROM of the associated resource state is the highest. We expect that the ROM of the hardware-efficient ansatz with the same arrangement of qubits will be much smaller. Therefore, our result will also give some insights into classical simulatability of such an ansatz.

The unit cell of these RQCs comprises two single-qubit gates followed by one two-qubit Clifford gate. We assume that single-qubit and two-qubit depolarizing noise occurs after each single-qubit gate and two-qubit gate, respectively.

Figure 3.8 shows the three patterns of the unit cell. Unit cell 1 consists of only Clifford gates. Unit cell 2 consists of one $T$ gate and two Clifford gates, while unit cell 3 consists of two $T$ gates and one Clifford gate. This structure can provide the upper bound for the simulation cost of a noisy RQC.

In the case of Heisenberg propagation, the upper bound of the simulation cost of n RQC can be estimated from the simulation costs of unit cells 1, 2, and 3 straightforwardly by Eq. (2.11). First we calculate the channel stabilizer norm using the Pauli transfer matrix (PTM) of a quantum channel [40]. For a quantum channel $\Lambda$ that takes $n$ qubits to $n$ qubits, the corresponding PTM is defined as

$$(R_\Lambda)_{ij} \coloneqq \frac{1}{2^n} \operatorname{Tr}\left[P_i \Lambda(P_j)\right].$$

Combining the definition of the PTM with that of the channel stabilizer norm [see Eq. (2.12)], we obtain

$$\mathcal{D}\big(\Lambda^\dagger\big) = \|R_\Lambda\|_\infty,$$

where $\|\cdot\|_\infty$ is the largest row's L1 norm of the matrix $R_\Lambda$. The PTMs of the $T$ gate, single-qubit depolarizing noise, and two-qubit depolarizing noise are given by

$$R_T = \begin{bmatrix} 1 & 0 & 0 & 0 \\ 0 & \frac{1}{\sqrt{2}} & -\frac{1}{\sqrt{2}} & 0 \\ 0 & \frac{1}{\sqrt{2}} & \frac{1}{\sqrt{2}} & 0 \\ 0 & 0 & 0 & 1 \end{bmatrix}, \tag{3.7}$$

$$R_{\text{depo1}} = \operatorname{diag}(1, 1-p_1, 1-p_1, 1-p_1), \tag{3.8}$$

$$R_{\text{depo2}} = \operatorname{diag}(1, 1-p_2, \ldots, 1-p_2), \tag{3.9}$$

respectively. The PTMs of Clifford gates do not need to be considered because they are signed permutation matrices and the depolarizing noise is symmetric. Because unit cell 1 includes only Clifford gates, its channel stabilizer norm is unity. By multiplying the PTMs in Eqs. (3.7) to (3.9), the PTMs of unit cells 2 and 3 are written, respectively, as

$$\begin{aligned} R_{\text{unit 2}} &= (R_T \otimes I_4)(R_{\text{depo1}} \otimes I_4)(I_4 \otimes R_{\text{depo1}})R_{\text{depo2}}, \\ R_{\text{unit 3}} &= (R_T \otimes I_4)(I_4 \otimes R_T) \\ &\qquad (R_{\text{depo1}} \otimes I_4)(I_4 \otimes R_{\text{depo1}})R_{\text{depo2}}. \end{aligned}$$

The channel stabilizer norms of unit cells 2 and 3 are given, respectively, by

$$\begin{aligned} \mathcal{D}_{\text{unit 2}} &= \max\Big(1, \sqrt{2}(p_1-1)(p_2-1)\Big), \\ \mathcal{D}_{\text{unit 3}} &= \max\Big(1, \sqrt{2}(p_1-1)(p_2-1), -2(p_1-1)^2(p_2-1)\Big). \end{aligned}$$

On the other hand, for stabilizer-state sampling, we calculate the ROM of unit cells 2 and 3 with the depolarizing noise. The error-free resource states of unit cells 2 and 3 are given by

$$\rho_{|T+++\rangle} = |T+++\rangle\langle T+++|\,,$$
$$\rho_{|T+T+\rangle} = |T+T+\rangle\langle T+T+|\,,$$

respectively. We add the correlated diagonal noise on them to consider the depolarizing noise, and calculate the ROM of depolarized unit cells 2 and 3. The noisy resource states of unit cells 2 and 3 are given, respectively, by

$$\rho_{\text{unit2}} = \tilde{\mathcal{E}}_2 \circ \left(\tilde{\mathcal{E}}_1 \otimes I\right) \circ \left(I \otimes \tilde{\mathcal{E}}_1\right)(\rho_{|T+++\rangle}),$$
$$\rho_{\text{unit3}} = \tilde{\mathcal{E}}_2 \circ \left(\tilde{\mathcal{E}}_1 \otimes I\right) \circ \left(I \otimes \tilde{\mathcal{E}}_1\right)(\rho_{|T+T+\rangle}),$$

where

$$\tilde{\mathcal{E}}_2 \coloneqq \left(1 - \frac{15}{16}p\right)\left[I^{\otimes 4}\right] + \frac{p}{16}\sum_{(A,B)\in S} A\otimes B,$$
$$S \coloneqq \left\{(A,B)|A,B \in \left\{I^{\otimes 2}, Z_1, Z_2, Z_1Z_2\right\}\right\} \setminus \left\{\left(I^{\otimes 2}, I^{\otimes 2}\right)\right\}$$

To reduce the simulation cost, we also calculate the upper bound for the ROM of twofold copies of $\rho_{\text{unit}i}$ $(i = 2, 3)$. We call stabilizer-state sampling with twofold copies of a resource state "optimized stabilizer-state sampling." In this case, the RoM per unit cell $i$ is given by $\left\{\mathcal{R}\left(\rho_{\text{unit}i}^{\otimes 2}\right)\right\}^{\frac{1}{2}}$. The corresponding simulation cost of unit $i$ is proportional to $\mathcal{R}\left(\rho_{\text{unit}i}^{\otimes 2}\right)$. Throughout the optimization, we use the basis reduction method as explained in Section 3.3.4 because the decomposition of an eight-qubit resource state is intractable for a current classical computer. To decompose the resource states of depolarized Clifford+$T$ circuits over certain stabilizer states, we use the stabilizer states stabilized by one of the stabilizer groups shown in Eq. (3.6) for the qubit pairs applied by the $T$ gate in the resource state. For the other qubits, which are not applied by the $T$ gate in the resource state, we use the stabilizer state $|+\rangle$ or $|-\rangle$.

The ratio of the simulation cost of a circuit for calculating the expectation value of $P$ via Heisenberg propagation to that via stabilizer-state sampling is given by

$$\frac{N_{\text{Heisenberg}}}{N_{\text{stabilizer}}} = \left(\frac{\prod_{i=1}^{d}\mathcal{D}\left(\Lambda_i^{\dagger}\right)}{\mathcal{R}(\rho)}\right)^2,$$

where we use $\mathcal{D}(P) = 1$. Therefore, we can compare the simulation costs for the two sampling-based classical simulation methods by calculating the ROM and the product of channel stabilizer norms.

Figure 3.9 (a) and (b) show the resultant simulation costs of unit cells 2 and 3, respectively. For simplicity, we assume that $p_1 = p_2 = p$. The blue squares,

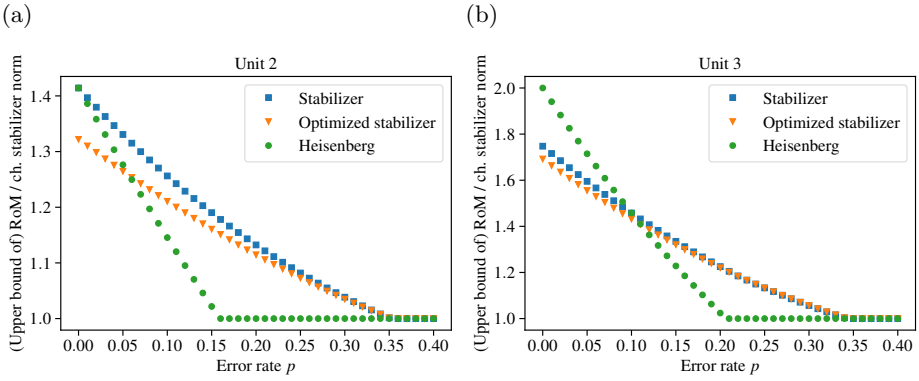


Figure 3.9: Comparison of the simulation costs of faulty unit cell 2 (a) and faulty unit cell 3 (b). The horizontal axis displays the error rates of the single-qubit and two-qubit depolarizing noise. The vertical axis displays the ROM, the upper bound of the ROM, or the channel (ch.) stabilizer norms, each of which quantifies the simulation cost of the corresponding method under consideration. The Blue squares, orange triangles, and green circles stand for simulation costs for stabilizer-state sampling $[\mathcal{R}(\rho_{\mathrm{unit}i})]$, optimized stabilizer-state sampling $\left(\left\{\mathcal{R}(\rho_{\mathrm{unit}i})^{\otimes 2}\right\}^{\frac{1}{2}}\right)$, and Heisenberg propagation $(\mathcal{D}_{\mathrm{unit}i})$, respectively, where $i = 2, 3$.

orange triangles, and green circles stand for simulation costs for stabilizer-state sampling $[\mathcal{R}(\rho_{\mathrm{unit}i})]$, optimized stabilizer-state sampling $\left(\left\{\mathcal{R}(\rho_{\mathrm{unit}i})^{\otimes 2}\right\}^{\frac{1}{2}}\right)$, and Heisenberg propagation $(\mathcal{D}_{\mathrm{unit}i})$, respectively, where $i = 2, 3$. In the low-noise region, the simulation costs for stabilizer-state sampling are much smaller than those of Heisenberg propagation. This is because the simulation costs are reduced by optimization of the stabilizer-state decomposition by use of multiple copies of a resource state. However, this is not the case for Heisenberg propagation. Suppose a channel stabilizer norm is calculated for a merged channel over several patterns of the unit cell. In this case, the simulation cost should be further reduced, whereas the dimensions of the PTM increase exponentially. However, we do not consider merging multiple patterns of the unit cell because the simulation cost of Heisenberg propagation depends explicitly on quantum channels. The dependence on quantum channels makes optimization of the channel stabilizer norm by merging the quantum channels problematic due to the enormous number of possible merging patterns.

In the high-noise region, Heisenberg propagation provides lower simulation costs. This is attributed to the difference in the effect of the depolarizing noise in both algorithms. To explain this in detail, we first consider the simulation cost of $\mathcal{E}_A \circ [T]$ for stabilizer-state sampling, where we set $\mathcal{E}_A$ $(A = X, Y, Z)$ a

single-qubit general dephasing noise:

$$\mathcal{E}_A \coloneqq (1-p)[I] + p[A].$$

We numerically calculate the ROM of the resource states of $\mathcal{E}_A \circ [T]$ for $A = X$, $Y$, and $Z$. The ROM of the resource state of $\mathcal{E}_Z \circ [T]$ is smallest for all $p$. As a result, for stabilizer-state sampling, the $Z$ error in the single-qubit depolarizing noise has a larger impact on the simulation costs of noisy quantum circuits compared with other Pauli errors: the $X$ and $Y$ errors. On the other hand, for Heisenberg propagation, the two Pauli errors in the depolarizing noise always help reduce the simulation costs. Let $\Lambda_{\rm Pauli}$ be the single-qubit stochastic Pauli noise defined as follows:

$$\Lambda_{\rm Pauli} \coloneqq \left(1 - \frac{p_X + p_Y + p_Z}{4}\right)[I] + \sum_{A=X,Y,Z} \frac{p_A}{4}[A].$$

The PTM of $\Lambda_{\rm Pauli} \circ [T]$ is given by

$$\begin{bmatrix} 1 & 0 & 0 & 0 \\ 0 & \frac{1}{\sqrt{2}}\left(1 - \frac{p_Y+p_Z}{2}\right) & \frac{1}{\sqrt{2}}\left(1 - \frac{p_Y+p_Z}{2}\right) & 0 \\ 0 & \frac{-1}{\sqrt{2}}\left(1 - \frac{p_X+p_Z}{2}\right) & \frac{1}{\sqrt{2}}\left(1 - \frac{p_X+p_Z}{2}\right) & 0 \\ 0 & 0 & 0 & 1 - \frac{p_X+p_Y}{2} \end{bmatrix},$$

so

$$\mathcal{D}(\Lambda_{\rm Pauli} \circ [T]) = \max\left\{1, \sqrt{2}\left(1 - \frac{p_X + p_Z}{2}\right), \sqrt{2}\left(1 - \frac{p_Y + p_Z}{2}\right)\right\}.$$

We see that the two Pauli errors, $\{X, Y\}$ or $\{Y, Z\}$, decrease the simulation cost of $\Lambda_{\rm Pauli} \circ [T]$ for Heisenberg propagation. This explains why the simulation costs for Heisenberg propagation decrease faster than for stabilizer-state sampling according to the error rate of the depolarizing noise.

In short, in Fig. 3.9, there is a crossover between which algorithm is better. In the low-noise region, stabilizer-state sampling outperforms Heisenberg propagation. However, the opposite is observed in the high-noise region. The crossover appears around $p \geq 0.05$ for unit cell 2 and $p \geq 0.11$ for unit cell 3.

Next we calculate the total amount of simulation costs of the noisy RQCs on a rectangular lattice consisting of $m \times n$ qubits and $d$ cycles. The total number of unit cells is roughly $D = mnd/2$. The numbers of unit cells 1, 2, and 3 are roughly $\frac{4}{9}D$, $\frac{4}{9}D$, and $\frac{1}{9}D$, respectively, since single-qubit gates are chosen randomly from $\left\{\sqrt{X}, \sqrt{Y}, T\right\}$. The simulation costs for Heisenberg propagation are proportional to

$$\left[\left\{\max\left(1, \sqrt{2}(p-1)^2\right)\right\}^{\frac{4D}{9}} \left\{\max\left(1, (p-1)^2, -2(p-1)^3\right)\right\}^{\frac{D}{9}}\right]^2.$$

On the other hand, the simulation costs for stabilizer-state sampling are proportional to

$$\left[\mathcal{R}(\rho_{\rm unit2})^{\frac{4D}{9}} \mathcal{R}(\rho_{\rm unit3})^{\frac{D}{9}}\right]^2.$$

Since the number of $T$ gates $t$ is relevant in the comparison of the simulation costs in both algorithms, we calculate the simulation costs as a function of $t$, which is related to $D$ by $\frac{3}{2}D$. Figure 3.10 shows the simulation costs of the two algorithms for $p = 0, 0.05, 0.1, 0.15, 0.2$. The blue, orange, and green lines correspond to the simulation costs as a function of $t$ for stabilizer-state sampling, optimized stabilizer-state sampling, and Heisenberg propagation, respectively. If the error rate $p$ is low, the optimized stabilizer-state sampling is the best choice [Figs. 3.10a and 3.10b], otherwise, Heisenberg propagation is superior to stabilizer-state sampling [Figs. 3.10c to 3.10e].

We also investigate the scaling factor $\alpha$ of the simulation costs $2^{\alpha t}$ with various error rates of the single-qubit and two-qubit depolarizing noise $p$ (Fig. 3.11). The blue, orange, and green lines correspond to the scaling for stabilizer-state sampling, optimized stabilizer-state sampling, and Heisenberg propagation, respectively. The sampling cost of error-free RQCs for the optimized stabilizer-state sampling is the lowest, while that for Heisenberg propagation is the highest. In this case, the scaling based on Heisenberg propagation is $2^t$, which is the same as the scaling based on stabilizer-state sampling when the resource state is decomposed over only separable stabilizer states. Furthermore, when the error rate is high, the simulation costs of noisy quantum circuits for stabilizer-state sampling and Heisenberg propagation are lower than the simulation costs for the stabilizer rank algorithm $2^{0.468t}$, [56, 57], which is a well-known sampling-based simulator for pure states. Specifically, scaling based on Heisenberg propagation and optimized stabilizer-state sampling is lower than scaling based on the stabilizer rank when $p \geq 0.1$ and $p \geq 0.13$, respectively. Additionally, Fig. 3.11 confirms that the threshold error rate of classical simulatability of Heisenberg propagation is lower than that of stabilizer-state sampling.

Finally, we consider the time required to calculate these noisy RQCs. We assume that we can estimate the expectation value within an additive error $\delta = 10^{-3}$, with a success probability of at least $1 - \epsilon = 1 - 10^{-2}$ and the error rate of the single-qubit and two-qubit depolarizing noise $p = 0.05$. For $p = 0.05$, $\alpha = 0.66$ and $\alpha = 0.73$ for optimized stabilizer-state sampling and Heisenberg propagation, respectively. Combining the above information, we find that the simulation of the noisy random circuits with $t = 40$ requires approximately $8.9 \times 10^{14}$ samples for the optimized stabilizer-state sampling and $6.2 \times 10^{15}$ samples for Heisenberg propagation. We also assume that we have a classical computer with $10^6$ CPU cores, and each CPU core takes 1 ms to calculate one sample, which is what a typical implementation of this algorithm takes. In this case, the computer needs about 10 s using optimized stabilizer-state sampling and 70 s using Heisenberg propagation.

## 3.5 Conclusions and discussion

We evaluate the simulation costs of noisy quantum circuits by two sampling-based classical algorithms: stabilizer-state sampling and Heisenberg propagation. We extend and improve the existing stabilizer-state sampling algorithm

for noisy quantum circuits. To compare the two sampling-based classical simulation algorithms, we also investigate the simulation costs of noisy RQCs. We find that for a low error rate, stabilizer-state sampling is the better algorithm, otherwise, Heisenberg propagation is the better. Scaling based on the simulation costs of noisy RQCs via Heisenberg propagation and optimized stabilizer-state sampling is lower than that by the stabilizer-rank simulator [56, 57] when $p \leq 0.1$ and $p \leq 0.13$, respectively.

Recently, Seddon *et al.* [41] presented classical sampling algorithms and their associated magic monotones, where a resource state is decomposed, instead of using density operators of stabilizer states, into a matrix spanned by pure stabilizer states, so-called stabilizer dyads. Since they showed that the dyadic frame simulator is faster than stabilizer-state sampling, it will be interesting to apply a dyadic frame simulator for noisy quantum circuits.

We believe that the knowledge obtained regarding the sampling-based classical simulation methods is useful not only for the classical simulation itself but also for designing applications of near-term quantum devices. Specifically, one of the most-promising applications of near-term quantum devices, VQE, uses parameterized quantum circuits, which consist of many rotation gates. In particular, the angles of the rotation gates of the unitary coupled-cluster ansatz with the Trotter decomposition are typically very small. As discussed in Section 3.3, a small-angle rotation gate can be easily simulated by stabilizer-state sampling. Even if a unitary coupled-cluster ansatz without Trotterization or a hardware-efficient ansatz is used, the angles would be small if a target molecule is a weakly correlated electron system, where the Hartree-Fock method gives a good approximation. This is because a Hartree-Fock state as the initial state of the VQE is a good approximation of the ground state. In Ref. [58], a perturbative approach is sufficient to describe the VQE with a hardware-efficient ansatz, implying the rotations are very small. Furthermore, for the unitary coupled-cluster ansatz, many two-qubit Clifford gates are used to construct the ansatz. Noise on two-qubit Clifford gates deteriorates the ROM of the rotation gates, which would make the parameterized circuit classically simulatable more easily. With these points in mind, we have to design the parameterized quantum circuits under noise carefully so that the VQE has a potential quantum advantage. It would be interesting to characterize the Hamiltonian and the ansatz of the VQE with respect to the ROM of the quantum circuit generating an optimal variational solution.

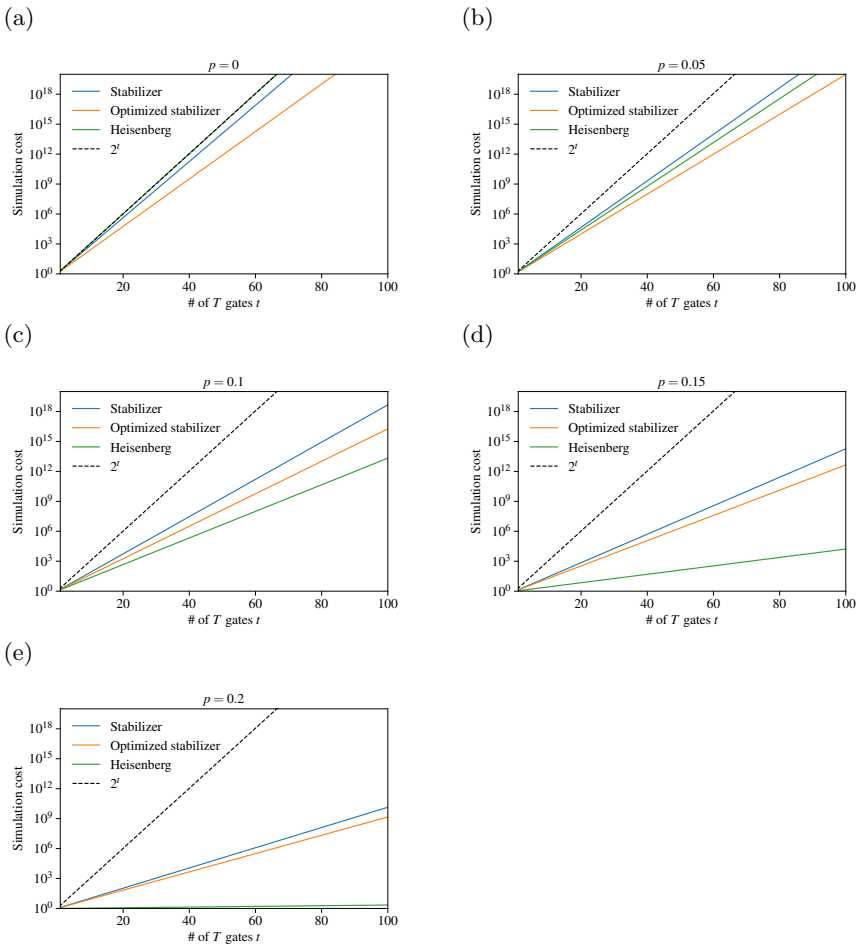


Figure 3.10: Comparison of the simulation costs of depolarized RQCs with various error rates of the single-qubit and two-qubit depolarizing noise $p$ through stabilizer-state sampling and Heisenberg propagation. The horizontal axis shows the number of $T$ gates $t$ in the circuits. The vertical axis shows the squared products of the upper bounds of the ROM or those of the channel stabilizer norms. Both are proportional to the simulation costs. Blue, orange, and green lines correspond to the simulation costs as a function of $t$ for stabilizer-state sampling, optimized stabilizer-state sampling, and Heisenberg propagation, respectively. The simulation costs with $p = 0, 0.05, 0.1, 0.15, 0.2$ are shown in from (a) to (e), respectively.

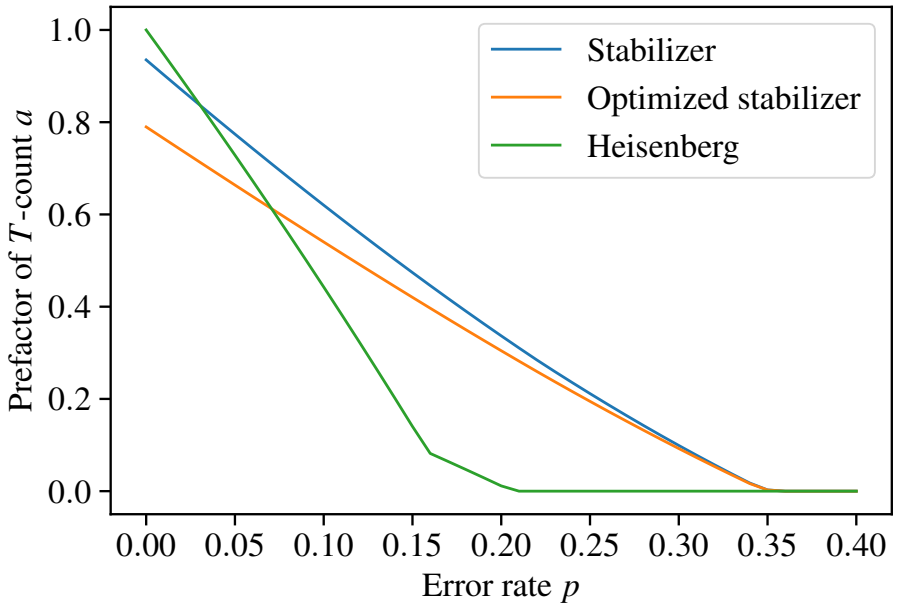


Figure 3.11: Scaling factors of the simulation costs as a function of the error rate $p$ of single-qubit and two-qubit depolarizing noise. The horizontal axis shows the error rates of the depolarizing noise $p$. The vertical axis shows the prefactor of the exponent $\alpha$ of the simulation costs $2^{\alpha t}$, where $t$ is the number of $T$ gates in a RQC. Blue, orange, and green lines correspond to the scaling using stabilizer-state sampling, optimized stabilizer-state sampling, and Heisenberg propagation, respectively.

# Chapter 4

# Sampling-Based Quasiprobability Simulation for Fault-Tolerant Quantum Error Correction on the Surface Codes under Coherent Noise

We propose a sampling-based simulation for fault-tolerant quantum error correction under coherent noise. A mixture of incoherent and coherent noise, possibly due to over-rotation, is decomposed into Clifford channels with a quasiprobability distribution. Then, an unbiased estimator of the logical error probability is constructed by sampling Clifford channels with an appropriate postprocessing. We characterize the sampling cost via the channel robustness and find that the proposed sampling-based method is feasible even for planar surface codes with relatively large code distances intractable for full state-vector simulations. As a demonstration, we simulate repetitive faulty syndrome measurements on the planar surface code of distance 5 with 81 qubits. We find that the coherent error increases the logical error rate. This is a practical application of the quasiprobability simulation for a meaningful task and would be useful to explore experimental quantum error correction on the near-term quantum devices. This chapter is based on [Hakkaku, Mitarai, and Fujii, Phys. Rev. Research, **3**, 043130 (2021)] with slight modifications to fit in the context.

## 4.1 Introduction

Quantum error correction (QEC) is an essential ingredient for developing scalable fault-tolerant quantum computers because quantum information is vulnerable to environmental noise [5, 6]. QEC counteracts noise by encoding quantum information into a subspace of multiple qubits, which assures computation with arbitrary precision in quantum computers. Massive experimental efforts have been devoted to demonstrating small-scale QEC circuits as testbeds toward large-scale QEC circuits in the future as well as numerical simulations [16–18]. It is thus important to investigate performances of QEC codes theoretically to establish a plausible goal for experiments.

Most numerical studies for QEC have been conducted by assuming stochastic Pauli noise to exploit the efficient simulatability of stabilizer states [29, 30]. Specifically, Ref. [14] numerically calculated the threshold error rate of the rotated surface code under single- and two-qubit depolarizing channels with circuit-level noise and observed a threshold error rate of 0.57%. This result suggests that the surface code can cope with the error rate that current state-of-the-art quantum computers are reaching [18, 49]. While the computational overhead increases when compared with the Pauli noise, we can also efficiently simulate the Clifford noise such as stochastic Clifford gates and Pauli projections.

In practice, however, quantum devices often suffer from noise that cannot be described by Clifford operations. A major type of such noise is coherent unitary noise which is caused by the miscalibration of quantum gates which leads to over- or under-rotations. Reference [19] has developed a method to detect over-rotation errors using randomized benchmarking and detected $\pi/128$ over- or under-rotation errors in their superconducting qubit. While the error has been calibrated subsequently in Ref. [19], one can expect that a small amount of such errors beyond the experimental sensitivity are still present.

Analysis of the performance of QEC in such realistic situations still remains a challenge. QEC circuits under non-Clifford noise have been investigated either by brute-force simulations [20, 22] or by exploiting exact solvability of free fermion dynamics [21, 23]. However, full state-vector simulations require exponential computational resources with respect to the code distance and are currently limited to distance-3 surface code which uses 25 qubits [20]. While the use of approximate simulation using a tensor network [22] has pushed the limit to 153 qubits with perfect syndrome measurements, it is still difficult to scale up the simulation. On the other hand, free fermion simulations can handle coherent errors in a scalable manner. However, their usage is limited to certain cases: one-dimensional repetition codes with faulty syndrome measurements [21] which can only correct $X$ errors and surface codes with perfect syndrome measurements [23].

In this chapter, we propose a sampling-based simulation method widely applicable for fault-tolerant QEC circuits under a mixture of coherent and incoherent noise with multiple rounds of faulty syndrome measurements. The central idea is to decompose (possibly non-Clifford) noise channels into the sum of com-

pletely stabilizer preserving (CSP) channels [39]. We simulate the circuits by sampling CSP channels according to quasiprobability distributions, which are obtained from the decompositions [39, 59]. Each realization is efficiently simulable since the simulation of CSP channels involves only stabilizer states. Note that Bennink *et al.* have conducted similar simulations for small systems such as Steane's seven-qubit code [59]. We significantly improve the computational cost required for the simulation by providing more efficient decomposition of noise channels than Ref. [59]. This reveals that we can perform an efficient simulation in the presence of coherent errors without any additional overhead for a wide range of practically interesting parameter regions. Furthermore, even outside this region, the proposed quasiprobability method enables us to simulate a surface code of distance 5 with 81 qubits on a single workstation within a reasonable computational time.

As demonstrations, we simulate the planar surface code under the code capacity coherent noise with distance up to $d = 7$ and under the phenomenological coherent noise with distance up to $d = 5$. The result shows that such non-Clifford noise deteriorates the logical error rate as expected. We also evaluated how many samples are required to simulate the logical error rate reliably as a function of the noise parameters and the code distance. This reveals that the proposed method allows us to simulate the planar surface code with relatively large code distances, which are intractable for full state-vector simulations, with a reasonable computational overhead. The proposed method provides a benchmark for building small-scale fault-tolerant quantum computers in the noisy intermediate-sclae quantum (NISQ) era.

## 4.2 Simulation of QEC circuits under coherent noise

In this section, we discuss how to calculate a logical error rate of a QEC code by simulating quantum circuits with a quasiprobability sampling of CSP channels. QEC requires two types of qubits: data qubits, which constitute logical qubits, and measurement qubits, which are used for detecting errors on data qubits. The measurements extract eigenvalues of code stabilizers by measuring the latter, and these eigenvalues are called error syndromes. For a distance $d$ code, we repeat such measurements for $d$ rounds. We use a (noisy) Clifford circuit $\mathcal{E}_{\rm synd}$ for the repetitive syndrome measurements. The measurement qubits of different rounds are to be treated as different qubits to simplify the notation. Let $b$ be the error syndrome in space and time. When data qubits are initialized to $|0_L\rangle$, the probability of obtaining a specific error syndrome $b$ is given by

$$p(b) = \langle b|\mathrm{Tr}_{\rm data}\left[\mathcal{E}_{\rm synd}(|\mathbf{0}\rangle\langle\mathbf{0}|)\right]|b\rangle\,.$$

where $|b\rangle$ and $|0^{|b|}\rangle$ are final and initial states of the measurement qubits, respectively, and $|\mathbf{0}\rangle \coloneqq |0_L\rangle \otimes \left|0^{|b|}\right\rangle$ After the extraction of the error syndrome, we feed $b$ to decoding algorithms such as a minimum-weight perfect-matching

algorithm to find a possible recovery operation $\mathcal{R}_b$ which corrects errors on data qubits. The error corrected state $\rho_{\text{corrected}}$ is given by

$$\rho_{\text{corrected}} = \sum_b \mathcal{R}_b \circ \mathcal{P}_b \circ \mathcal{E}_{\text{synd}}(|\mathbf{0}\rangle\langle\mathbf{0}|),$$

where $\mathcal{P}_b$ is the projection onto $|b\rangle\langle b|$. Since the data qubits of $\rho_{\text{corrected}}$ are in the code space, the logical fidelity can be expressed by $\langle 0_L|\text{Tr}_{\text{meas}}(\rho_{\text{corrected}})|0_L\rangle$. Therefore the logical error rate $p_L$ can be written as

$$\begin{aligned} p_L &= 1 - \langle 0_L|\text{Tr}_{\text{meas}}(\rho_{\text{corrected}})|0_L\rangle \\ &= 1 - \sum_b \langle 0_L|\text{Tr}_{\text{meas}}(\mathcal{R}_b \circ \mathcal{P}_b \circ \mathcal{E}_{\text{synd}}(|\mathbf{0}\rangle\langle\mathbf{0}|))|0_L\rangle\,. \end{aligned} \tag{4.1}$$

If the noise introduced in $\mathcal{E}_{\text{synd}}$ is a stochastic Pauli or Clifford error, one can simulate $\mathcal{E}_{\text{synd}}$ efficiently and can estimate the logical error rate $p_L$. However, efficient simulatability vanishes if noise involves non-Clifford channels.

We now describe an idea to deal with more general noise by a quasiprobability method [37–39, 41, 59–62]. $\mathcal{E}_{\text{synd}}$ can be decomposed into (noisy) elementary operations as $\mathcal{E}_{\text{synd}} = \mathcal{E}^{(L)} \circ \cdots \circ \mathcal{E}^{(1)}$. Here $L$ is the total number of quantum operations in $\mathcal{E}_{\text{synd}}$. $\mathcal{E}^{(i)}$ can be decomposed over CSP and completely positive trace-preserving (CPTP) channels $\mathcal{S}_k^{(i)}$ in terms of a quasiprobability distribution $c_k^{(i)}$ as

$$\mathcal{E}^{(i)} = \sum_k c_k^{(i)} \mathcal{S}_k^{(i)}.$$

This decomposition can alternatively be written as

$$\mathcal{E}^{(i)} = \sum_k p_k^{(i)} R_*\left(\mathcal{E}^{(i)}\right) \text{sgn}\left(c_k^{(i)}\right) \mathcal{S}_k^{(i)},$$

where

$$\begin{aligned} R_*(\mathcal{E}) &\coloneqq \min_{\{c_k\}} \left\{ \sum_k |c_k| ; \mathcal{E} = \sum_k c_k \mathcal{S}_k \right\}, \\ p_k^{(i)} &\coloneqq \frac{\left|c_k^{(i)}\right|}{R_*\left(\mathcal{E}^{(i)}\right)}. \end{aligned}$$

$R_*(\mathcal{E})$ is called channel robustness [39], the square of which characterizes the sampling cost, as will be seen later. Using this decomposition for each $\mathcal{E}^{(i)}$, $\mathcal{E}_{\text{synd}}$ becomes

$$\mathcal{E}_{\text{synd}} = \sum_{\vec{k}} p_{\vec{k}} R_{*\text{tot}} \lambda_{\vec{k}} \mathcal{S}_{\vec{k}}, \tag{4.2}$$

where the summation is taken over all possible $\vec{k} = \left(k^{(1)}, k^{(2)}, \ldots, k^{(L)}\right)$, and

$$\begin{aligned} p_{\vec{k}} &\coloneqq \prod_{i=1}^{L} p^{(i)}_{k^{(i)}}, \\ \lambda_{\vec{k}} &\coloneqq \prod_{i=1}^{L} \mathrm{sgn}\left(c^{(i)}_{k^{(i)}}\right), \\ \mathcal{S}_{\vec{k}} &\coloneqq \mathcal{S}^{(L)}_{k^{(L)}} \circ \cdots \circ \mathcal{S}^{(1)}_{k^{(1)}}, \\ R_{*\mathrm{tot}} &\coloneqq \prod_{i=1}^{L} R_*\left(\mathcal{E}^{(i)}\right). \end{aligned}$$

Finally, combining Eqs. (4.1) and (4.2), we conclude

$$p_L = 1 - \sum_{b,\vec{k}} p_{\vec{k}} R_{*\mathrm{tot}} \lambda_{\vec{k}} \langle 0_L | \mathrm{Tr}_{\mathrm{meas}} \left(\mathcal{R}_b \circ \mathcal{P}_b \circ \mathcal{S}_{\vec{k}}(|\mathbf{0}\rangle\langle\mathbf{0}|)\right) |0_L\rangle .$$

This implies that, when $\vec{k}$ is sampled from $p_{\vec{k}}$, $1 - R_{*\mathrm{tot}} \lambda_{\vec{k}} \langle 0_L | \mathrm{Tr}_{\mathrm{meas}} \left(\mathcal{R}_b \circ \mathcal{P}_b \circ \mathcal{S}_{\vec{k}}(|\mathbf{0}\rangle\langle\mathbf{0}|)\right) |0_L\rangle$ is an unbiased estimator for $p_L$. Since it is bounded in a range $[-R_{*\mathrm{tot}}, R_{*\mathrm{tot}}]$, from Hoeffding inequality [43], the number of samples $M$ needed to estimate $p_L$ within additive error $\epsilon$ with probability at least $1 - \delta$ is given by

$$M = \frac{2}{\epsilon^2} R^2_{*\mathrm{tot}} \ln\left(\frac{2}{\delta}\right). \tag{4.3}$$

Note that, when we only consider Clifford noise, $\frac{2}{\epsilon^2} \ln\left(\frac{2}{\delta}\right)$ samples suffice to achieve the same accuracy. Therefore $R^2_{*\mathrm{tot}}$ quantifies the additional overhead required for including the effect of non-Clifford channels.

## 4.3 Planar surface codes under coherent noise

To demonstrate the feasibility of the proposed method, we consider the planar surface code introduced in Ref. [13], which is thought to be one of the most promising candidates for an experimental realization of QEC, as they require only single- and nearest-neighbor two-qubit gates on two-dimensional arrays of qubits [14, 63]. The planar surface code with code distance $d$ has a $(2d-1) \times (2d-1)$ square grid of qubits of which $d^2 + (d-1)^2$ data qubits are used to encode the logical qubit and $2d(d-1)$ measurement qubits are used to extract the syndromes. In Fig. 4.1, we show the layout of $d = 3$ planar surface code as an example.

In numerical simulations, the ideal logical state $|0\rangle_L$ followed by single-qubit noise is prepared as the initial state. We assume two types of noise model: a code-capacity noise model, where the noise occurs in all data qubits with perfect syndrome measurements, and a phenomenological noise model, where the noise occurs in all data qubits and measurement qubits just before the

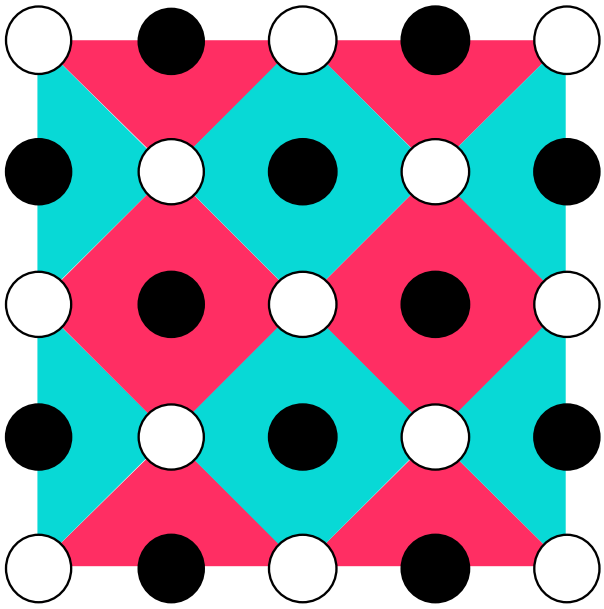

Figure 4.1: Layout of $d = 3$ planar surface code. The white and black circles represent data and measurement qubits, respectively. The light blue square and triangular patches show $X$ stabilizers. The red square and triangular patches show $Z$ stabilizers.

syndrome measurements. The number of rounds of the syndrome measurement in the latter case is $d$. We also assume that the syndrome measurements are performed perfectly at the final cycle. In both cases, $Z$-type and $X$-type errors are uncorrelated, and hence only $X$-type errors and syndrome measurements are simulated for simplicity. The specific noise channel $\mathcal{N}_{\rm coh}$ simulated in this chapter is a mixture of coherent and incoherent noise which is modeled by the over-rotation noise followed by the bit-flip $X$ error as

$$\begin{aligned} \mathcal{N}_{\rm coh} &\coloneqq \mathcal{N}_{\text{bit-flip}} \circ \mathcal{N}_{\text{over-rot}}, \\ \mathcal{N}_{\text{over-rot}} &\coloneqq \left[e^{ir\theta X}\right], \\ \mathcal{N}_{\text{bit-flip}} &\coloneqq (1-p)[I] + p[X], \end{aligned}$$

where $\theta$ is chosen such that $p = \sin^2\theta$. We vary the parameters $(r, p)$ and evaluate the performance of the code by using the method described in Sec. 4.2.

We first examine the sampling cost of our simulation which is characterized by the channel robustness $R_{*\rm coh}(r,p)$ of $\mathcal{N}_{\rm coh}$ [38, 39, 61]. The CSP channels employed to decompose $\mathcal{N}_{\rm coh}$ are $[I]$, $[X]$, $\left[e^{-i(\pi/4)X}\right]$, and $\left[Xe^{-i(\pi/4)X}\right]$. Figure 4.2 shows the values of $R_{*\rm coh}(r,p)$. From Fig. 4.2, we confirm that the channel robustness increases as the noise coherence becomes larger as expected. Importantly, for a small $r$ with a sufficiently large $p$, the channel robustness

decreases and hits unity, where an efficient simulation of coherent errors can be performed. This is because $r\theta$ is small in this region, resulting in the low channel robustness of $\mathcal{N}_{\text{over-rot}}$. Thus, the bit-flip noise with large $p$ can easily make the channel robustness unity. On the other hand, at $p = 0$, the channel robustness of $\mathcal{N}_{\text{over-rot}}$ is unity even if $r > 0$ since we set $p = \sin^2\theta$. Therefore a certain mixture of incoherent and coherent errors, for example, with $p = 1\%$ ($0.1\%$) and $r = 0.10$ ($r = 0.46$), can be efficiently simulated without any additional overhead, which is in an experimentally important parameter region. This greatly improves the simulation cost over Ref. [59] which is a result of decomposing $\mathcal{N}_{\text{coh}}$ as a whole rather than decomposing $\mathcal{N}_{\text{over-rot}}$ and $\mathcal{N}_{\text{bit-flip}}$ individually.

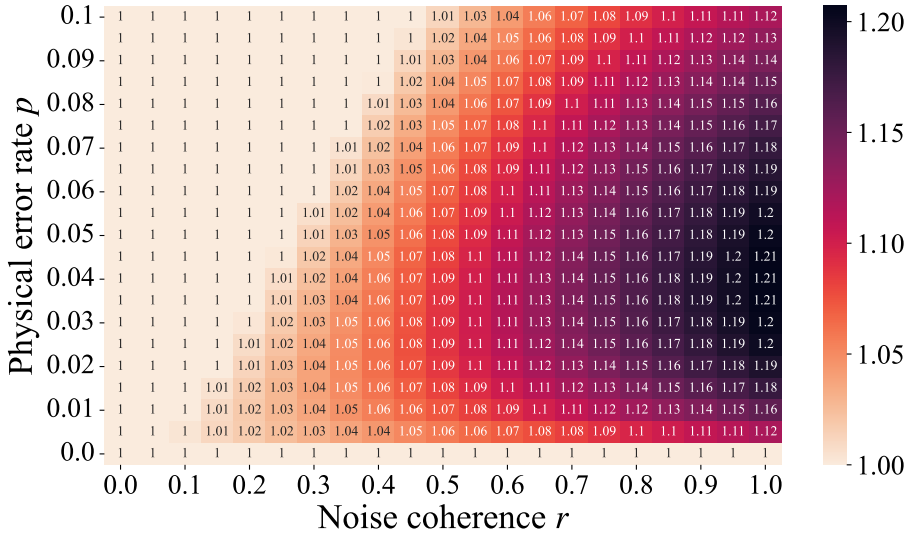


Figure 4.2: Channel robustness of the coherent noise $R_{*\text{coh}}(r, p)$. The horizontal and vertical axes display the noise coherence $r$ and physical error rate $p$, respectively. Numbers in each cell show the value of $R_{*\text{coh}}(r, p)$.

The number of samples needed for accurate results is determined by $R^2_{*\text{tot}}$ via Eq. (4.3). In the case of the code capacity noise, $\mathcal{N}_{\text{coh}}$ is applied $d^2 + (d-1)^2$ times, which corresponds to the number of data qubits. Therefore $R^2_{*\text{tot}} = (R_{*\text{coh}}(r, p))^{2\left(d^2+(d-1)^2\right)}$. In the case of the phenomenological noise, $\mathcal{N}_{\text{coh}}$ is applied to each of the $d^2+(d-1)^2$ data qubits $d$ times and to each of the $d(d-1)^2$ measurement qubits for $X$-type errors $d-1$ times since we assume perfect measurement in the final round. Overall, $\mathcal{N}_{\text{coh}}$ is applied $d\left(3d^2-4d+2\right)$ times, which means $R^2_{*\text{tot}} = (R_{*\text{coh}}(r, p))^{2d\left(3d^2-4d+2\right)}$ in this case. These formulas for $R^2_{*\text{tot}}$ provide us estimates of the simulation cost for a given $(p, r, d)$, based on which we choose the parameter range investigated below.

Figure 4.3 shows the logical error rate $p_L$ as a function of physical error

rate $p$ and noise coherence $r$, where the parameters are chosen such that our workstation with Intel Xeon CPU v4 CPU (E5-2687W), 24 cores, 3.00GHz, can calculate each point within a few days at most. We confirmed that the standard error of each data point is below $10^{-3}$. From Fig. 4.3, the logical error rate increases as the noise coherence grows, which implies that the impact of the coherent noise on the logical error probability is not negligible even for a relatively large code distance. Note that the $d = 5$ code, which requires 81 qubits, is well beyond the reach of naive full state-vector simulation. Furthermore, it is the first analysis of this region with faulty syndrome measurements to the best of our knowledge. Finally, let us discuss with which parameters and code distance the proposed method works. Figure 4.4 shows the dependence of $R^2_{*\mathrm{tot}}$ with respect to $d$ for the phenomenological noise model. Note that for the parameters where $R_{*\mathrm{coh}}(r, p) = 1$ in Fig. 4.2, we can simulate without any additional overhead as mentioned before. We will be able to simulate large code distances in that region. Outside of that, we expect that regions with $R_{*\mathrm{tot}} < 10^3$ are within reach if a high-performance parallel computer of $10^6$ CPU cores is available. For example, realistic parameters such as $(p, r, d) = (1.5\%, 0.15, 7)$ and $= (0.2\%, 0.05, 13)$ result in $R_{*\mathrm{tot}} < 10^3$. Full state-vector simulation would not work for these numbers of qubits; we need 169 qubits for $d = 7$ and 625 qubits for $d = 13$.

## 4.4 Conclusion

We have proposed a sampling-based method to estimate the logical error rate of QEC codes under coherent noise such as an over-rotation error. The simulation protocol is based on the quasiprobability decomposition of noise channels into Clifford operations. It is interesting to note that the QEC process is simulated as usual for sampled CSP channels, and hence the probability distribution for the syndrome measurements is far different from the true one $p(b)$. However, if we sample whether the decoding successds or fails with the quasiprobability method, we can estimate the logical error rate. By calculating the channel robustness for the mixture of coherent and incoherent errors, we reduce the simulation costs substantially, which allows us to simulate a practically important parameter region with a relatively large code distance without any additional overhead or with a reasonable additional overhead. While we have only considered the phenomenological noise model, it is straightforward to extend our method to the circuit-level noise model, where each elementary gate is followed by noise. We leave these problems for future works. We believe that this chapter helps to analyze the performance of the near-term small-scale QEC in realistic situations.

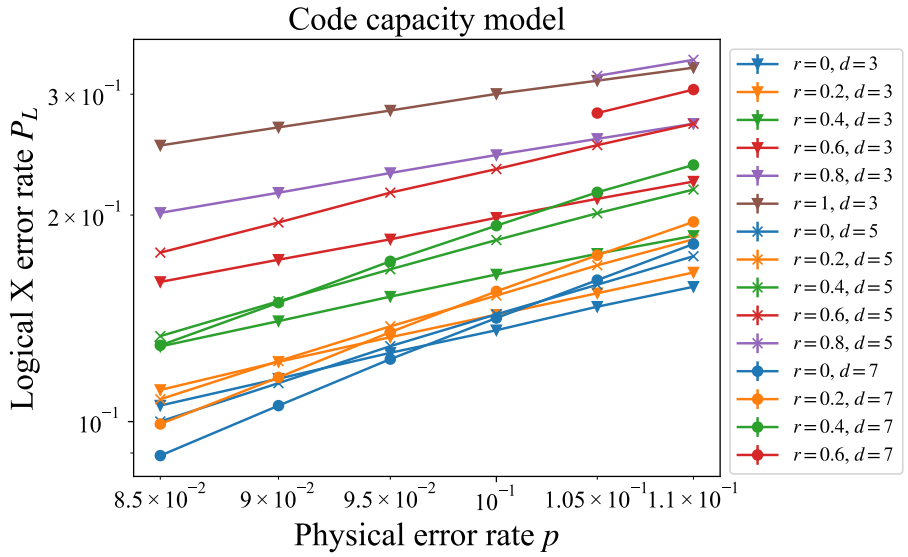


(a)

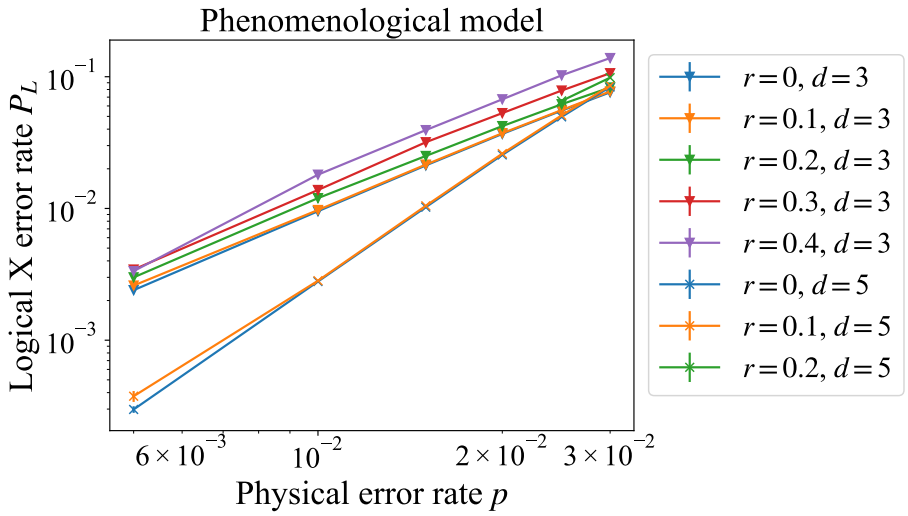


(b)

Figure 4.3: Logical $X$ error rate of the planar surface code under the coherent noise as a function of the physical error rate $p$ and noise coherence $r$ in the case of code capacity (a) and phenomenological (b) noise. The horizontal axis shows the physical error rate $p$, and the vertical axis shows the logical $X$ error rate $p_L$. The triangles, crosses, and circles stand for $d = 3, 5, 7$, respectively. The color shows the noise coherence.

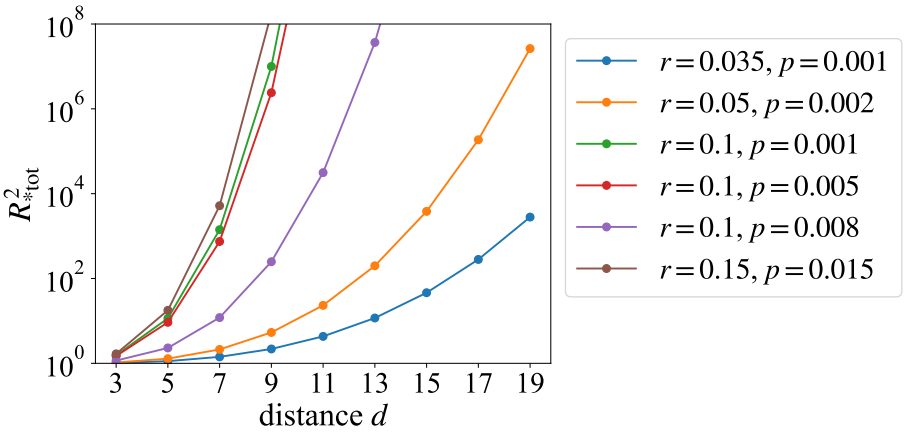


Figure 4.4: Scaling of the overhead caused by the quasiprobability sampling, $R^2_{*\mathrm{tot}}$, as a function of the code distance $d$.

# Chapter 5

# Quantifying Fermionic Nonlinearity of Fermionic Quantum Circuits

In this chapter, we propose another quasiprobability-based simulation method using fermionic linear optics. Variational quantum algorithms (VQAs) have been proposed as one of the most promising approaches to demonstrate quantum advantage on noisy intermediate-scale quantum (NISQ) devices. However, it has been unclear whether VQA can maintain quantum advantage under the intrinsic noise of the NISQ devices, which deteriorates the quantumness. Here we propose a measure, called *fermionic nonlinearity*, to quantify the classical simulatability of quantum circuits designed for simulating fermionic Hamiltonians. Specifically, we construct a Monte-Carlo type classical algorithm based on the classical simulatability of fermionic linear optics, whose sampling overhead is characterized by the fermionic nonlinearity. As a demonstration of these techniques, we calculate the upper bound of the fermionic nonlinearity of a rotation gate generated by four-body fermionic interaction under the dephasing noise. Moreover, we estimate the sampling costs of the unitary coupled cluster singles and doubles (UCCSD) quantum circuits for hydrogen chains subject to the dephasing noise. We find that, depending on the error probability and atomic spacing, there are regions where the fermionic nonlinearity becomes very small or unity, and hence the circuits are classically simulatable. We believe that our method and results help to design quantum circuits for fermionic systems with potential quantum advantages. This chapter is based on [Hakkaku, Tashima, Mitarai, Mizukami, and Fujii, arXiv:2111.14599].

## 5.1 Introduction

Quantum computers have attracted much attention because of their capability to solve classically intractable problems. Among them, the first industrial application is expected to be a quantum chemistry calculation, which uses quantum computers for simulating fermionic many-body systems. It has been predicted that a fault-tolerant quantum computer with about a million physical qubits can simulate both Fermi-Hubbard and molecular electronic structure Hamiltonians beyond classical approaches [64]. The application has also been anticipated for NISQ devices through the variational quantum eigensolver (VQE) [11, 65–71].

It is essential to predict at what scale quantum computers can have advantages over classical ones for those applications. One way is to estimate the computational cost required for fault-tolerant quantum computers to simulate fermionic systems that are well beyond the reach of classical supercomputers [64, 72, 73]. However, this approach highly depends both on the objective system and algorithms employed in classical or quantum computers. As another approach, we can ask a question the other way around; given a quantum circuit that simulates a fermionic system, what is the cost of classical computation to simulate that circuit? If there exists a quantum advantage, at least such a quantum circuit has to be hard for a classical computer to be simulated.

One way to evaluate the classical simulatability of quantum circuits is to quantify the simulation cost of a specific quasiprobability-based simulator [37–41, 61]. The central idea of quasiprobability simulators is to decompose a complex operator (operation) $A$ over a discrete set of classically tractable operators (operations) $\{B_i\}$, i.e., $A = \sum_i q_i B_i$. The examples of the classically tractable operators $\{B_i\}$ are pure stabilizer states [38, 61] and Pauli operators [40]. The coefficients of the decomposition $\{q_i\}$ are called "quasiprobability distribution", and the L1 norm of the quasiprobability distribution $\sum_i |q_i|$ determines a sampling cost. Any set of operations that can be efficiently simulated by classical computers can be used as operators $\{B_i\}$ in a quasiprobability-based simulator. Over the past years, Clifford circuits have become a popular class of such channels. [38, 39, 41, 61].

Here, we consider another popular class of classically simulatable circuits: fermionic linear optics (FLO) and matchgates [34, 74–76]. These classes represent the dynamics of free fermions, generated by quadratic fermionic Hamiltonians. It represents a restricted class of quantum circuits in the sense that, in general, natural fermionic interactions are described by not only two-body but also four-body fermion operators. For example, the four-body interactions appear in quantum circuits tailored to simulate fermionic systems, such as unitary coupled cluster (UCC) [11, 77] and Hamiltonian variational ansatze [67, 78]. Such four-body interactions make the quantum dynamics or variational circuit ansatze hard to be simulated on classical computers, which provides a potential advantage of using quantum computers. However, the required amount of the four-body interactions is limited in a certain (but common) situation where the Hartree-Fock calculation provides a good approximation. Hence, one may be able to classically simulate quantum circuits for such systems.

This paper presents a quasiprobability-based simulator exploiting FLO and the corresponding measure that quantifies the sampling cost. This simulator decomposes a fermionic non-Gaussian operation, such as a four-body fermionic interaction, over all possible free operations of FLO. The simulation cost is characterized by "fermionic nonlinearity," defined as the minimum of the L1 norm of the quasiprobability distribution. We calculate the upper bound of fermionic nonlinearity of a four-body fermionic interaction under stochastic Pauli noise as an example, thereby estimating the sampling cost to simulate famous VQE ansatzes for fermionic Hamiltonian. More specifically, we estimate the sampling cost of the noisy UCCSD quantum circuits for the hydrogen chain up to $H_8$ with several spacings using the optimized variational parameters obtained by full-vector simulations. A rough extrapolation from the results shows us that the noisy UCCSD quantum circuits for the hydrogen chain with the spacing of 0.8 Å at the error rate of the two-qubit dephasing noise $p = 0.02$ can be simulated up to $H_{22}$ within a reasonable sampling cost. Furthermore, if $p = 0.03$, the noisy UCCSD quantum circuit for the arbitrary-length hydrogen chain can be simulated because of vanishing fermionic nonlinearity. We believe that our method and results are helpful to design quantum circuits that simulate fermionic systems for potential quantum supremacy or quantum advantages.

## 5.2 Fermionic Nonlinearity of Quantum Circuits

### 5.2.1 Definition of fermionic nonlinearity

We describe a quasiprobability-based simulation method of general fermionic interactions via FLO. Given a non-FGO $\mathcal{E}$ and a set of all possible trace-preserving FGOs $\{\mathcal{S}_k\}$, we seek to express $\mathcal{E}$ as,

$$\begin{aligned}\mathcal{E} &= \sum_i q_i \mathcal{S}_i \\ &= \sum_i p_i \|q\|_1 \mathrm{sign}(q_i) \mathcal{S}_i, \end{aligned} \tag{5.1}$$

where

$$\begin{aligned}\|q\|_1 &= \sum_i |q_i|, \\ p_i &:= \frac{|q_i|}{\|q\|_1}. \end{aligned}$$

$p_i$ is a probability distribution because $p_i$ is non-negative and sum to unity. If this decomposition can be made, we can simulate the non-FGO by sampling a trace-preserving FGO with probability $p_i$ and multiplying the coefficient $\|q\|_1 \mathrm{sign}(q_i)$ to the results afterwards. The square of the L1 norm $\|q\|_1$ quantifies the classical simulation cost of this Monte-Carlo type simulation.

To be more concrete, let us consider the expectation value of a two-body fermionic interaction $\hat{c}_\mu \hat{c}_\nu$ with respect to $\mathcal{E}(\rho)$ for an FGS state $\rho$ and a non-FGO channel $\mathcal{E}$. The desired quantity can be written as,

$$\begin{aligned} \langle \hat{c}_\mu \hat{c}_\nu \rangle &= \mathrm{Tr}(\mathcal{E}(\rho)\hat{c}_\mu \hat{c}_\nu) \\ &= \sum_i p_i \|q\|_1 \mathrm{sign}(q_i) \langle \hat{c}_\mu \hat{c}_\nu \rangle_{\mathcal{S}_i} \end{aligned} \tag{5.2}$$

where

$$\langle \hat{c}_\mu \hat{c}_\nu \rangle_{\mathcal{S}_i} \coloneqq \mathrm{Tr}(\mathcal{S}_i(\rho)\hat{c}_\mu \hat{c}_\nu).$$

From Eq. (5.2), we can calculate the desired quantity $\langle \hat{c}_\mu \hat{c}_\nu \rangle$ by sampling an index $i$ with probability $p_i$ and calculating $\|q\|_1 \mathrm{sign}(q_i) \langle \hat{c}_\mu \hat{c}_\nu \rangle_{\mathcal{S}_i}$ efficiently, since $\langle \hat{c}_\mu \hat{c}_\nu \rangle_{\mathcal{S}_i}$ only involves an FGS and an FGO. Let $N$ be the number of samples. Then, $\|q\|_1 \mathrm{sign}(q_i) \langle \hat{c}_\mu \hat{c}_\nu \rangle_{\mathcal{S}_i}$ is an unbiased estimator of the desired quantity $\langle \hat{c}_\mu \hat{c}_\nu \rangle$. $\|q\|_1 \mathrm{sign}(q_i) \langle \hat{c}_\mu \hat{c}_\nu \rangle_{\mathcal{S}_i}$ is bounded in the interval $[-\|q\|_1, \|q\|_1]$, and thus the Hoeffding inequality shows that to estimate $\langle \hat{c}_\mu \hat{c}_\nu \rangle$ within additive error at most $\epsilon$ with probability at least $1-\delta$, we must set the number of samples such that

$$N \geq 2\|q\|_1^2 \frac{1}{\epsilon^2} \ln \frac{2}{\delta}.$$

Note that the expectation value of higher-order correlation function can be estimated in a similar way exploiting Wick's theorem.

Having seen that $\|q\|_1$ determines the sampling cost for simulations, we define the fermionic nonlinearity of a quantum channel $\mathcal{E}$ as follows:

$$W(\mathcal{E}) \coloneqq \min_{\{q_i\}} \left\{ \|q\|_1 | \mathcal{E} = \sum_i q_i \mathcal{S}_i \right\}. \tag{5.3}$$

$W(\mathcal{E})$ quantifies the minimum number of samples to execute the Monte-Carlo type simulation of a quantum circuit with FLO. Moreover, fermionic nonlinearity is submultiplicative under composition, i.e., $W(\mathcal{E}_2 \circ \mathcal{E}_1) \leq W(\mathcal{E}_2)W(\mathcal{E}_1)$ (See Ref. [79]). This property helps to estimate the upper bound of the sampling cost of an $n$-mode fermionic quantum channel when $n$ is too large to calculate the fermionic nonlinearity directly.

### 5.2.2 Concrete decomposition for four-body interactions

So far, we have assumed that there exists a decomposition of non-FGO in the form of Eq. (5.1). Here we consider how to explicitly calculate the decomposition and the fermionic nonlinearity of four-body fermionic interactions in the form of $\exp(i\theta \hat{c}_i \hat{c}_j \hat{c}_k \hat{c}_l)$. This type of operations appears in the simulation of interacting fermions and in VQE ansatze such as the UCC ansatz [11], and its variant, Jastrow-type ansatz [66, 80], or Hamiltonian variational ansatz (HVA)

[67, 78]. Without loss of generality, we consider the decomposition of the following operator,

$$\mathcal{E}_{\rm rot} = [\exp(-i\theta \hat{c}_1\hat{c}_2\hat{c}_3\hat{c}_4)],$$

where $[A]\rho \coloneqq A\rho A^\dagger$. This is because we can always perform transformation $\hat{c}_i \to \hat{c}_1$, $\hat{c}_j \to \hat{c}_2$, $\hat{c}_k \to \hat{c}_3$, and $\hat{c}_l \to \hat{c}_4$ by FGOs for mutually distinct indices $i$, $j$, $k$, and $l$. The four-body fermionic interaction operator $\hat{c}_1\hat{c}_2\hat{c}_3\hat{c}_4$ can be mapped to a Pauli operator by the Jordan-Wigner transformation. It maps $\hat{c}_k$ as follows.

$$\hat{c}_{2k-1} = X_k \prod_{j<k} Z_j,$$
$$\hat{c}_{2k} = Y_k \prod_{j<k} Z_j.$$

Hence, the fermionic interaction $\mathcal{E}_{\rm rot}$ can be rewritten as

$$\mathcal{E}_{\rm rot} = [\exp(i\theta Z \otimes Z)].$$

Theoretically, the fermionic nonlinearity should be calculated using all possible FGOs. However, in practice, it is difficult to calculate the fermionic nonlinearity using all possible FGOs because the number of all possible FGOs is infinite. Therefore, here we calculate the upper bound of the fermionic nonlinearity using a discrete set of the FGOs. Below, we will omit the term "upper bound" if there is no risk of confusion.

We adopt the following trace-preserving fermionic Gaussian channels as the basis channels to decompose $\mathcal{E}_{\rm rot}$:

$$\begin{aligned}&\left\{\left[e^{\pm i\frac{\pi}{4}Z}\right], [I], [Z]\right\}^{\otimes 2} \cup \{\mathcal{K}_{1,\alpha}, \mathcal{K}_{2,\alpha} | \alpha = \pm 1\} \\ \cup &\left\{\left[e^{\pm i\frac{\pi}{4}G}\right] | G \in \{XX, YY, XY, YX\}\right\},\end{aligned} \tag{5.4}$$

where

$$\mathcal{K}_{1,\alpha} \coloneqq \left[\frac{I+Z}{2} \otimes e^{i\alpha\frac{\pi}{4}Z}\right] + \left[\frac{I-Z}{2} \otimes e^{-i\alpha\frac{\pi}{4}Z}\right],$$
$$\mathcal{K}_{2,\alpha} \coloneqq \left[e^{i\alpha\frac{\pi}{4}Z} \otimes \frac{I+Z}{2}\right] + \left[e^{-i\alpha\frac{\pi}{4}Z} \otimes \frac{I-Z}{2}\right].$$

The sets of the channels in Eq. (5.4), $\left\{\left[e^{\pm i\frac{\pi}{4}Z}\right], [I], [Z]\right\}^{\otimes 2}$ and $\{\mathcal{K}_{1,\alpha}, \mathcal{K}_{2,\alpha}\}$, are adopted from Ref. [81], where the authors provided the way to simulate a two-qubit gate, such as $\mathcal{E}_{\rm rot}$, by sampling a single-qubit operation. Besides them, we add $\exp(\pm i\pi/4G)$ because they are the generators of FGOs and may be used for the decomposition. All of the elements in Eq. (5.4) are FGOs. Indeed, $IZ$, $XX$, $XY$, $YX$, $YY$, $ZI$ can be rewritten as

$$I_kZ_{k+1} = -i\hat{c}_{2k+1}\hat{c}_{2k+2}, \quad X_kX_{k+1} = -i\hat{c}_{2k}\hat{c}_{2k+1},$$
$$X_kY_{k+1} = -i\hat{c}_{2k}\hat{c}_{2k+2}, \quad Y_kX_{k+1} = i\hat{c}_{2k-1}\hat{c}_{2k+1},$$
$$Y_kY_{k+1} = i\hat{c}_{2k-1}\hat{c}_{2k+2}, \quad Z_kI_{k+1} = -i\hat{c}_{2k-1}\hat{c}_{2k}.$$

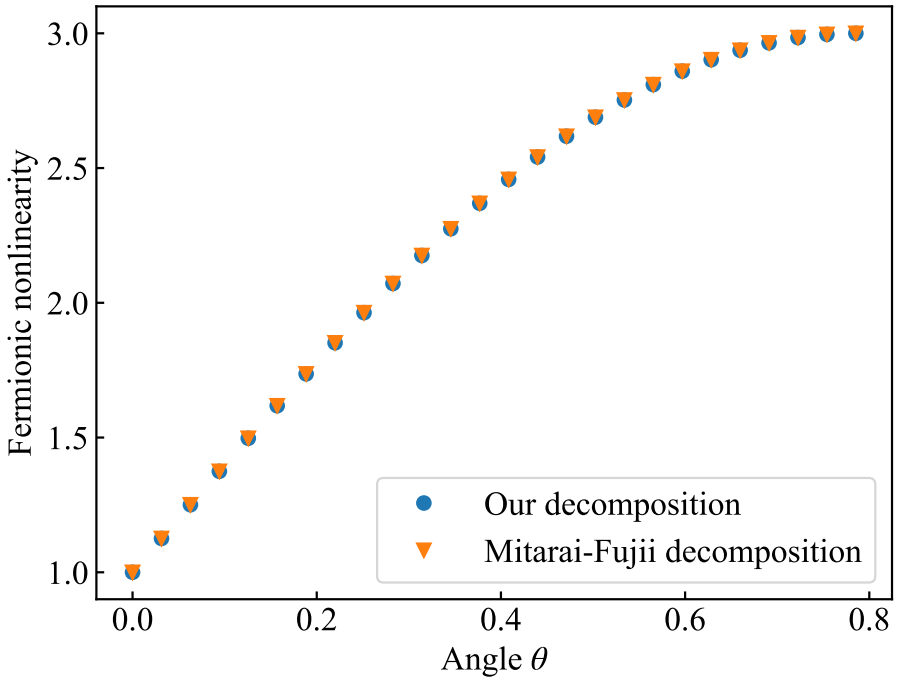


Figure 5.1: Fermionic nonlinearity of $\mathcal{E}_{\mathrm{rot}} = \left[e^{i\theta \hat{c}_1 \hat{c}_2 \hat{c}_3 \hat{c}_4}\right]$ as a function of the angle $\theta$. The horizontal axis shows the angle $\theta$. The vertical axis shows the fermionic nonlinearity. The blue circle illustrates the fermionic nonlinearity obtained by the basis channels in Eq. (5.4). The orange triangle shows the fermionic nonlinearity obtained by the decomposition in Ref. [81].

Thus the exponentials of these operators in Eq. (5.4) are FGOs. Moreover, the projective measurements in $\mathcal{K}_{i,\alpha}$ $(i = 1, 2)$ are FGOs [34].

We calculate the fermionic nonlinearity of $\mathcal{E}_{\mathrm{rot}}$ by solving the minimization problem in Eq. (5.3) using the basis channels in Eq. (5.4). To calculate fermionic nonlinearity, we use a convex-optimization solver CVXPY [52, 53]. The results are shown in Fig. 5.1. Also the fermionic nonlinearity using the decomposition in Ref. [81] is shown in Fig. 5.1 to compare with our results. According to Fig. 5.1, the fermionic nonlinearity is the same as when one uses the decomposition in Ref. [81]. Also, we have confirmed that the generators $\exp(\pm i\pi/4G)$ for $G \in \{XX, XY, YX, YY\}$ do not contribute to the decomposition by examining the coefficients of the decomposition. Moreover, we have numerically checked that the fermionic nonlinearity does not decrease even if we add the basis channels whose rotation angles are changed from $\pi/4$ to $\pi/8$, or $\pi/16$ in Eq. (5.4). Therefore, a measurement of a qubit in $Z$ basis, $\pm\pi/2$ rotations around the $Z$ axis, and Pauli $Z$ contribute significantly to the fermionic nonlinearity.

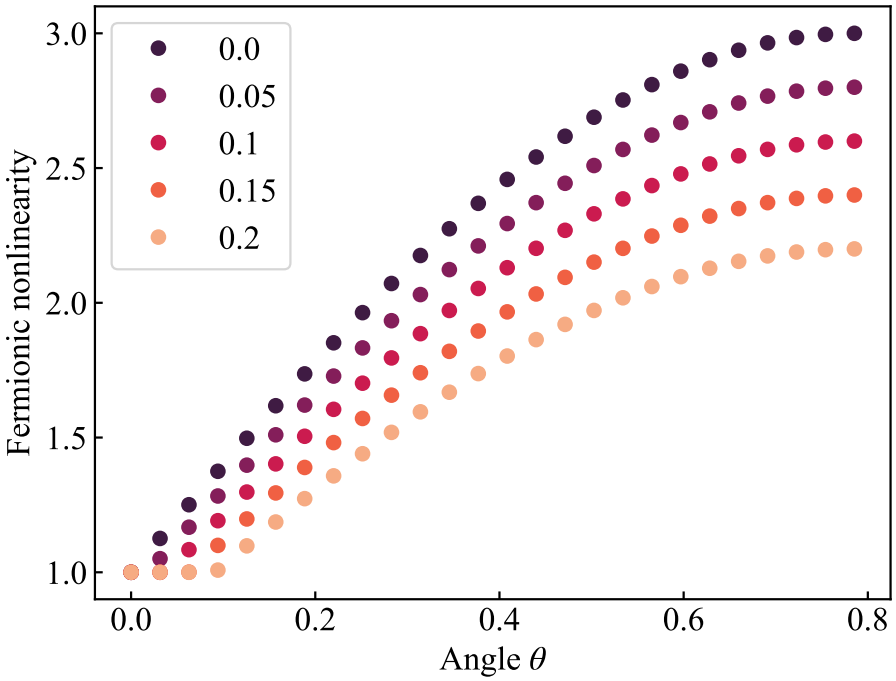


Figure 5.2: Fermionic nonlinearity of $\mathcal{E}_{\text{noisy rot}} \coloneqq \mathcal{N}_{\text{dep}} \circ \mathcal{E}_{\text{rot}}$ as a function of the angle $\theta$ of $\mathcal{E}_{\text{rot}}$ and the error rate $p$ of the two-qubit dephasing noise $\mathcal{N}_{\text{dep}}$. The horizontal axis shows the angle $\theta$ of $\mathcal{E}_{\text{rot}}$. The vertical axis shows the fermionic nonlinearity. The basis channels decomposing $\mathcal{E}_{\text{noisy rot}}$ are shown in Eq. (5.4). The legend shows the error rate $p$ of $\mathcal{N}_{\text{dep}}$.

### 5.2.3 Fermionic nonlinearity of noisy channels and application to the VQE simulation

Next, we consider the fermionic nonlinearity of $\mathcal{E}_{\text{rot}}$ being subject to noise:

$$\mathcal{E}_{\text{noisy rot}} \coloneqq \mathcal{N}_{\text{dep}} \circ \mathcal{E}_{\text{rot}},$$

where $\mathcal{N}_{\text{dep}}$ is the two-qubit dephasing noise

$$\mathcal{N}_{\text{dep}} \coloneqq (1-p)\left[I^{\otimes 2}\right] + \frac{p}{3}([IZ] + [ZI] + [ZZ])$$

$p$ is the error rate of the dephasing noise. Figure 5.2 shows the fermionic nonlinearity of $\mathcal{E}_{\text{noisy rot}}$ as a function of the angle of $\mathcal{E}_{\text{rot}}$ and the error rate of $\mathcal{N}_{\text{dep}}$. We see that the fermionic nonlinearity decreases as the error rate of $\mathcal{N}_{\text{dep}}$ increases. In addition, the smaller the rotation angle, the more easily the noise makes the fermionic nonlinearity unity, that is, such a noisy fermionic interaction becomes a probabilistic mixture of FGOs. One implication of these results

is as follows. For VQEs of fermionic problems, if the Hartree-Fock approach is a good first-order approximation and hence fermionic nonlinearity of the ansatz stays small even after the optimization, such a quantum circuit is fragile against noise in the sense that it readily becomes simulatable by the proposed sampling method.

To analyze more practical cases, we estimate the sampling cost of VQE that aims to obtain the ground state of the electronic Hamiltonian of the hydrogen chain $H_m$. Such a Hamiltonian is often used to benchmark the performance of classical quantum chemistry simulations [82–90] and VQE [58] numerically. This is because it exhibits rich phenomena, including metal-insulator transitions, and one can benchmark methods in both strong and weak correlation regimes. In particular, the Hamiltonian of the hydrogen chain with the use of the STO-3G basis set has a connection with the Hubbard model; the large spacing of the hydrogen chain corresponds to the Hubbard model in the large coupling limit, and vice versa. As for VQE, the authors of Ref. [46] have demonstrated that their quantum computer can prepare the Hartree-Fock state of $H_{12}$ using VQE, although their variational ansatz circuit is classically efficiently simulatable by FLO because the quantum circuit consists of two-body fermionic interactions. In the following numerical simulation, the Hamiltonians are generated by OpenFermion [91] and PySCF [92, 93] with the use of the STO-3G basis set, and then the Jordan-Wigner transformation maps them to qubit Hamiltonians, resulting in $2m$-qubit Hamiltonian for an $m$-hydrogen chain $H_m$. We take the Hartree-Fock (HF) state $|\mathrm{HF}\rangle$ as the reference state for the VQE.

We consider the UCC ansatz [94–99], which is a chemically inspired ansatz and often used in VQEs [11, 77]. In particular, we consider the UCCSD ansatz that only includes single and double excitations. The UCCSD ansatz is defined as

$$\begin{aligned} U &= e^{(T_1 - T_1^\dagger) + (T_2 - T_2^\dagger)}, \\ T_1 &\coloneqq \sum_{a \in \mathrm{virt}, i \in \mathrm{occ}} t_{ai} \hat{a}_a^\dagger \hat{a}_i, \\ T_2 &\coloneqq \sum_{a,b \in \mathrm{virt}, i,j \in \mathrm{occ}} t_{abij} \hat{a}_a^\dagger \hat{a}_b^\dagger \hat{a}_i \hat{a}_j, \end{aligned}$$

where occ and virt represent the sets of occupied and virtual orbitals, respectively, and $t_{ai}$ and $t_{abij}$ are variational parameters. Usually, the UCCSD is implemented as a quantum circuit by Trotter expansion of $U$:

$$\tilde{U} = \left[ \prod_{a \in \mathrm{virt}, i \in \mathrm{occ}} \exp\left( \frac{t_{ai}}{N_{\mathrm{trot}}} (\hat{a}_a^\dagger \hat{a}_i - \hat{a}_i^\dagger \hat{a}_a) \right) \right. \\ \left. \prod_{a,b \in \mathrm{virt}, i,j \in \mathrm{occ}} \exp\left( \frac{t_{abij}}{N_{\mathrm{trot}}} (\hat{a}_a^\dagger \hat{a}_b^\dagger \hat{a}_i \hat{a}_j - \hat{a}_j^\dagger \hat{a}_i^\dagger \hat{a}_b \hat{a}_a) \right) \right]^{N_{\mathrm{trot}}}$$

In the following, we consider the UCCSD ansatz with $N_{\mathrm{trot}} = 1$. Note that the fermion operator $\hat{a}_i$ is associated with the Majorana fermion operators $\hat{c}_{2i-1}, \hat{c}_{2i}$

as follows:

$$\hat{c}_{2i-1} = \hat{a}_i + \hat{a}_i^\dagger,$$
$$\hat{c}_{2i} = -i\Big(\hat{a}_i - \hat{a}_i^\dagger\Big).$$

Using this relation, a four-body interaction constituting $\tilde{U}$ can be rewritten by the Majorana fermion operators as follows:

$$\begin{aligned}
&e^{t_{abij}\left(\hat{a}_a^\dagger \hat{a}_b^\dagger \hat{a}_i \hat{a}_j - \hat{a}_j^\dagger \hat{a}_i^\dagger \hat{a}_b \hat{a}_a\right)} \\
=&e^{-i\frac{t_{abij}}{8}\hat{c}_{2a-1}\hat{c}_{2b-1}\hat{c}_{2i-1}\hat{c}_{2j}} e^{-i\frac{t_{abij}}{8}\hat{c}_{2a-1}\hat{c}_{2b-1}\hat{c}_{2i}\hat{c}_{2j-1}} \\
&e^{-i\frac{t_{abij}}{8}\hat{c}_{2a-1}\hat{c}_{2b}\hat{c}_{2i-1}\hat{c}_{2j-1}} e^{i\frac{t_{abij}}{8}\hat{c}_{2a-1}\hat{c}_{2b}\hat{c}_{2i}\hat{c}_{2j}} \\
&e^{-i\frac{t_{abij}}{8}\hat{c}_{2a}\hat{c}_{2b-1}\hat{c}_{2i-1}\hat{c}_{2j-1}} e^{i\frac{t_{abij}}{8}\hat{c}_{2a}\hat{c}_{2b-1}\hat{c}_{2i}\hat{c}_{2j}} \\
&e^{i\frac{t_{abij}}{8}\hat{c}_{2a}\hat{c}_{2b}\hat{c}_{2i-1}\hat{c}_{2j}} e^{i\frac{t_{abij}}{8}\hat{c}_{2a}\hat{c}_{2b}\hat{c}_{2i}\hat{c}_{2j-1}}.
\end{aligned} \tag{5.5}$$

We consider the sampling cost for simulating UCCSD circuits when each of the Majorana rotation gates in Eq. (5.5) are subjected to dephasing noise.

The sampling cost of a UCCSD quantum circuit can be given by the upper bound of the fermionic nonlinearity, which can be calculated by the product of the fermionic nonlinearity of the four-body fermionic interactions. Note that, as mentioned before, the HF states used as the reference states are FGSs; therefore, there are no sampling costs due to the input states. We use the optimized variational parameters of error-free UCCSD quantum circuits, calculated by the full-vector simulations performed with Qulacs [100].

Figure 5.3 shows the upper bound of fermionic nonlinearity of the UCCSD quantum circuit as a function of the length $m$ of the hydrogen chains $\mathrm{H}_m$ and the error rate of the dephasing noise at different spacings of the hydrogen atoms. In the case of 0.5 Å and 0.8 Å, the Hamiltonian for the hydrogen chain embodies a weakly correlated electronic system. In contrast, the Hamiltonian in the case of 1.5 Å provides a strongly correlated electronic system. From Fig. 5.3, we find that the fermionic nonlinearity is smaller when the spacing of the hydrogen chain is smaller. This reflects that an HF state is a good approximation of the ground state when the spacing is small.

Finally, we discuss the size of the hydrogen chain that can be simulated within one day using $10^6$ CPU cores. Suppose that we want to estimate the expectation value of the Hamiltonian $H$ for the hydrogen chain within an additive error $\epsilon = \|H\|_{\mathrm{op}} 10^{-3}$, with a success probability of at least $1 - \delta = 1 - 10^{-2}$, where $\|A\|_{\mathrm{op}}$ is the operator norm of $A$. Assuming that each core takes at most 1 ms to calculate one sample of a quasiprobability distribution, a UCCSD quantum circuit whose fermionic nonlinearity is upper-bounded by $3 \times 10^3$ could be simulated within one day. We estimate the fermionic nonlinearity for $m > 8$ using the geometrical mean of fermionic nonlinearity of $\mathcal{E}_{\text{noisy rot}}$ in the noisy UCCSD quantum circuit at $m = 8$, $\overline{W(\mathcal{E}_{\text{noisy rot}})}_{m=8}$. Let $N_4$ be the number of four-body Majorana operators in $\hat{T}_2 - \hat{T}_2^\dagger$. We estimate the upper bound of

fermionic nonlinearity of $H_m$ ($m > 8$) by

$$\left[\overline{W(\mathcal{E}_{\text{noisy rot}})}_{m=8}\right]^{N_4}.$$

At $p = 0.02$ and the spacing of 0.8 Å, $\overline{W(\mathcal{E}_{\text{noisy rot}})}_{m=8}$ is 1.00012. Therefore, we estimate the UCCSD circuits for hydrogen chains under such conditions can be simulated up to $m = 22$ if this mean stays at the same level at larger $m$. Furthermore, we find $\overline{W(\mathcal{E}_{\text{noisy rot}})}_{m=8} = 1$ if $p \geq 0.03$ and the spacing is less than 0.8 Å, or if $p \geq 0.07$ and the spacing is 1.5 Å. We hence expect that the UCCSD circuits under such conditions can be simulated for arbitrary $m$.

Note that the energy expectation value obtained from simulations of noisy UCCSD circuits is slightly biased from the true value $\langle \text{HF}|U^\dagger H U|\text{HF}\rangle$. If we allow such a bias, we can take an alternative approach; we can utilize the classical coupled cluster (CC) theory to simulate UCC circuits. It is known that the CC theory can simulate up to large UCC systems with a small perturbative error when $t_{abij}$ (and $t_{ai}$) are small (i.e., small rotation angles $\theta$). The conventional CC can be solved in polynomial time using a non-variational projection method, assuming the Hartree-Fock state to be a good reference wave function. If this assumption holds, the accuracy of the non-variational CC is almost as good as that of variational UCC [101, 102]. An established way to diagnose the correctness of the premise is by examining the magnitude of the parameters of the CC wave function [103–108]. According to the rule of thumb in the classical CC, the maximum $t_{abij}$ is about 0.1 or less in the region where non-variational CC works well [108]. Besides, in systems where classical CC fails, the maximum $t_{abij}$ tends to be larger than 0.15 [108]. Our UCC calculations show that for $m = 8$, the maximum $t_{abij}$ is about 0.08 when the distance between the hydrogens is 0.8 Å and about 0.18 when the distance is 1.5 Å. Therefore, our results are in line with the empirical trend in classical computing.

Our results indicate that, to demonstrate the quantum supremacy or quantum advantages with the UCCSD ansatz, one has to choose target Hamiltonians that exhibit strong electronic correlations and execute the quantum circuits with sufficiently low error rates. Note that even if the gate error of a device is 1%, the effective physical error rate of the two-qubit dephasing noise in $\mathcal{E}_{\text{noisy rot}}$ would be much higher because, in general, the noise on the entangling gates to simulate non-local fermionic two-body or four-body rotations by physically allowed operations accumulates.

We note that we have discussed the classical simulatability of noisy UCCSD ansatz using the optimized variational parameters obtained by the error-free simulations and found that, under certain circumstances, they become classically simulatable. In such cases, even if sophisticated error mitigation and optimization strategies allowed us to perform the VQE successfully, we cannot achieve a quantum advantage because the resulting circuit can be simulated classically.

## 5.3 Conclusion

In this chapter, we propose a quasiprobability-based simulation algorithm using FLO and quantify its simulation cost by establishing the corresponding measure, fermionic nonlinearity $W(\mathcal{E})$. The sampling cost of the quasiprobability-based simulator is proportional to $W(\mathcal{E})^2$. As an example, we calculate the upper bound of fermionic nonlinearity of the noisy rotation gate generated by a four-body Majorana fermionic operator, which often appears in the parametrized quantum circuits in VQE. We find that the fermionic nonlinearity increases as the rotation angle becomes larger and decreases as the error rate of the dephasing noise increases. Based on the above observation, we discuss the simulatability of the quantum circuits for quantum chemistry with our proposed method. We estimate the sampling costs of the noisy UCCSD quantum circuits for the hydrogen chain, and discuss whether they can be simulated within one day when $10^6$ CPU cores are available. We find that the UCCSD circuits with the dephasing error rate $p = 0.02$ for hydrogen chains with the spacing of 0.8 Å can be simulated up to $H_{22}$. Furthermore, if $p \geq 0.03$, the noisy UCCSD circuits for hydrogen chain of arbitrary length with the same spacing can be simulated. Although this numerical result is pessimistic, it stimulates to investigate or design another VQE ansatz that retains quantumness against noise with the use of our results and method.

Our work leaves several open questions. Although we use the basis channels based on Ref. [81] to decompose the four-body Majorana fermionic interaction, there may exist more optimal basis channels. It is an interesting and nontrivial problem to choose the optimal discrete set of FGOs to decompose a given non-FGO. We formulate the classical simulatability of a quantum circuit for fermionic Hamiltonians in the channel picture, but it is also of great interest to establish such a formulation in the state picture, which should be compatible with the results shown in Ref. [109].

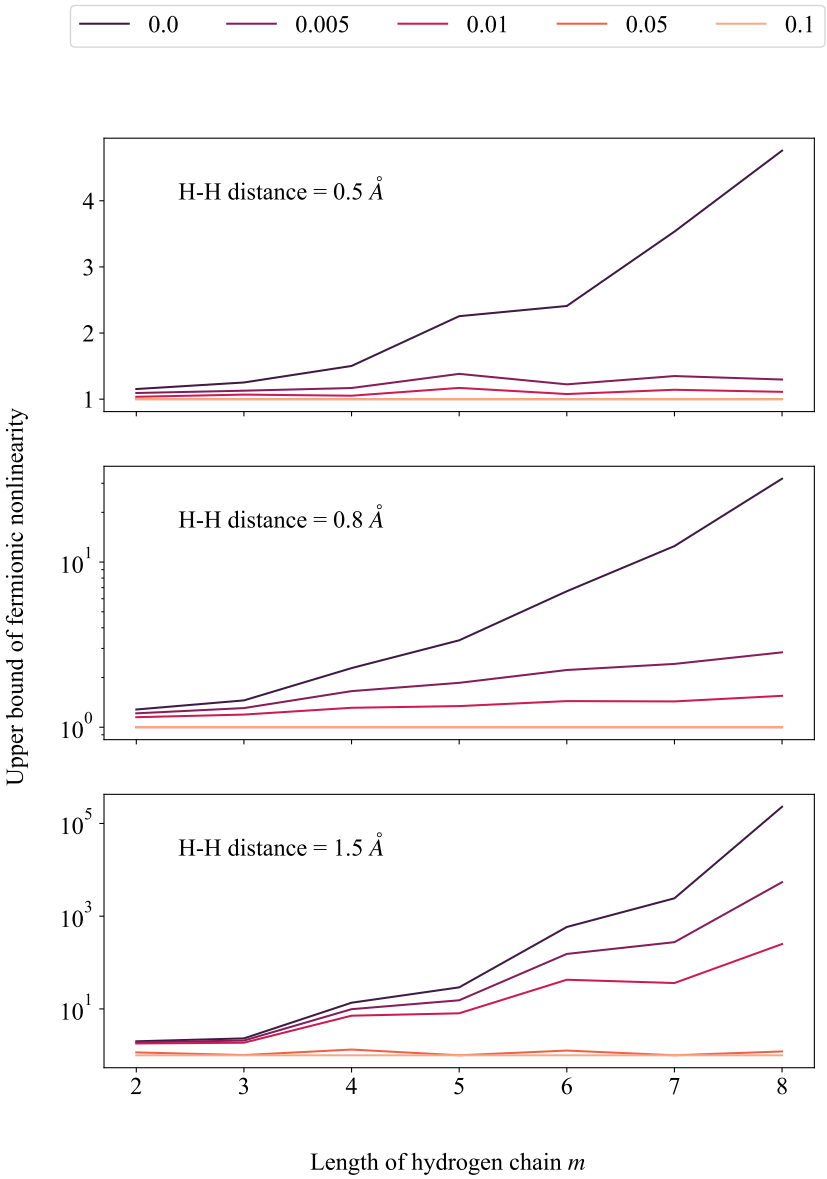


Figure 5.3: Upper bound of the fermionic nonlinearity of the UCCSD quantum circuit for the hydrogen chain up to $H_8$ at different spacings, 0.5 Å, 0.8 Å, and 1.5 Å. The horizontal axis shows the length of the hydrogen chain. The vertical axis shows the upper bound of the fermionic nonlinearity. The legend shows the error rate $p$ of the dephasing noise $\mathcal{N}_{\text{dep}}$.

# Chapter 6

# Conclusion

In this thesis, we have benchmarked noisy quantum computers through quasiprobability-based simulation algorithms. The reason for using the quasiprobability distribution is that it is possible to quantify the simulation cost of an arbitrary quantum computation based on a given class of classically simulatable quantum circuits. Moreover, the notion of a quasiprobability simulation algorithm allows us to systematically propose a better classical simulation algorithm by using a more suitable classically simulatable quantum circuit for each situation. Furthermore, quasiprobability simulation algorithms naturally incorporate the fact that noise reduces a quantumness of a quantum circuit and make the quantum circuit to be simulated more easily. Thus, through the quasiprobability-based simulation methods, we investigated whether quantum algorithms under noise have quantum advantages or not, and we also proposed a large-scale classical simulation method for noisy quantum computers. The details are as follows:

In Chap. 3, we extended the stabilizer-state sampling algorithm to the noisy case and compared the sampling cost with that of Heisenberg propagation. Many NISQ-oriented algorithms have recently been proposed to demonstrate a quantum advantage. However, researchers do not fully understand what kind of quantum circuits under how low error rates are sufficient. We improved the stabilizer-state sampling to simulate noisy quantum circuits more efficiently. Our improved algorithm surpasses Heisenberg propagation when the error rate of a stochastic Pauli noise is low by the numerical calculation. We also showed that quantum circuits that have many small-angle rotation gates can be classically efficiently simulated with a small amount of stochastic Pauli noise. It means that such quantum circuits are not suitable for demonstrating quantum advantage. We believe our proposed methods and results will help to design quantum circuits with the potential to demonstrate a quantum advantage.

In Chap. 4, we used the extended algorithm proposed in Chap. 3 to simulate a planar surface code under coherent noise. QEC is essential for building fault-tolerant quantum computers, and many analytical and numerical studies have been shown. Almost all of these studies used stochastic Pauli noise, although

quantum devices suffer from more general noise, such as over-rotation noise. We showed that our extended algorithm enables us to investigate a QEC code under the mixture of over-rotation noise and Pauli noise. We simulated repetitive faulty syndrome measurements on the planar surface code of distance 5 with 81 qubits. We have confirmed that the logical error rate increases as the strength of coherent noise grows. Moreover, we estimated that our method would simulate the planar surface code with $\mathcal{O}(1000)$ qubits using $10^6$ CPU cores. Although we have simulated the planar surface code, the rotated surface code is more suitable to simulate a larger code distance because the number of qubits of the rotated surface code is less than that of the planar surface code, which can be investigated by applying our method directly. Moreover, it is straightforward to extend our method to the more realistic noise allocation, i.e., circuit-level noise model, where each elementary gate is followed by noise. We believe that our simulation method sheds light on implementing and benchmarking a small-scale QEC code under realistic noise in the NISQ era.

In Chap. 5, we proposed a quasiprobability algorithm using free fermions and estimated the simulation cost of a quantum circuit for a fermionic Hamiltonian. Researchers anticipate an application to simulate fermionic many-body systems with a NISQ device. Thus, it is important to investigate how likely such a quantum circuit can demonstrate a quantum advantage. We presented the quasiprobability simulation algorithm using free fermions. This algorithm is better suitable to simulate a quantum circuit for a fermionic Hamiltonian than the existing quasiprobability algorithms. We investigated the simulation cost of UCCSD ansatz for the hydrogen chain quantitatively and discussed whether they can be simulated within one day if $10^6$ CPU cores are available. We found that one needs more sampling costs to simulate the UCCSD ansatz for the hydrogen chain with larger spacing. Combining these observations with the fact that the hydrogen chain with a large spacing corresponds to the strongly correlated material [90], we suggested that one should choose Hamiltonians of strongly correlated materials to demonstrate quantum advantage. Moreover, we found that, if the error rate of the two-qubit dephasing noise $p \geq 0.03$, the noisy UCCSD circuits for hydrogen chain of arbitrary length with the 0.8 can be simulated. Note that even if the gate error rate of a device is 1%, the effective noise in the two-qubit dephasing noise much higher because the noise on entangling gates to simulate non-local fermionic two-body or four-body rotations accumulates. Thus, we have to execute UCCSD ansatz with sufficiently low error rates. Whereas we have investigated the sampling cost of the UCCSD ansatz, it should be interesting to estimate the sampling cost of a quantum circuit to simulate the dynamics of a fermionic system. We believe that our algorithm and results are naturally helpful to demonstrate quantum advantage with the simulation of a fermionic Hamiltonian. Moreover, our proposed method is also interesting in the context of quantum resource theory. It is another interesting direction to establish a quasiprobability-based simulation algorithm that decomposes non-FGS over FGSs. With the quasiprobability simulation algorithm, one would estimate the "fermionic RoM" of molecular ground states and find the appropriate molecules to demonstrate a quantum advantage.

Quantum technology has progressed enough to execute the quantum supremacy experiment. It leads us to expect that NISQ devices will demonstrate a quantum advantage in a few decades. If such a quantum algorithm is developed, many practical quantum algorithms will be proposed and have an impact on other fields. To accelerate the movement, researchers should pursue the classical benchmarking methods to clarify and extend the classical simulatable regime and narrow down the candidates for quantum advantages. While researchers pursue the demonstration of quantum advantages, low-distance QEC codes are being implemented. Such low-distance QEC codes not only provide important insights for building large-scale fault-tolerant quantum computers but also may be used for practical application. To unlock the power of such a quantum computer, many error mitigation methods have been proposed. The probabilistic error cancellation is the error mitigation method using quasiprobability method [110]. In Ref. [111], it is shown that the probabilistic error cancellation can increase the code distance of a QEC code effectively. In Ref. [112], another application using the quasiprobability-based method to a quantum device has been proposed. The authors have proposed the quantum-assisted robustness of magic, which quantifies the overhead of simulating ideal resource states with noisy resource ones via quasiprobability-based simulation algorithms. Therefore, although we have seen the quasiprobability-based simulation algorithms are beneficial to benchmark quantum computers through their classical simulation, novel and useful applications have been emerging by combining quasiprobability-based simulation algorithms with quantum devices. We anticipate that our proposed quasiprobability simulation methods, when combined with quantum devices, could also be useful and interpolate between early fault-tolerant quantum computers and long-term fault-tolerant quantum computers.

# List of activities

## Publications

1. S. Hakkaku and K. Fujii, “Comparative Study of Sampling-Based Simulation Costs of Noisy Quantum Circuits”, Phys. Rev. Applied **15**, 064027 (2021).

2. S. Hakkaku, K. Mitarai, and K. Fujii, “Sampling-based quasiprobability simulation for fault-tolerant quantum error correction on the surface codes under coherent noise”, Phys. Rev. Research **3**, 043130 (2021).

3. S. Hakkaku, Y. Tashima, K. Mitarai, W. Mizukami and K. Fujii, “Quantifying Fermionic Nonlinearity of Quantum Circuits”, submitted, arXiv:2111.14599.

## International Conferences

### Poster presentations

1. S. Hakkaku and K. Fujii, “Comparative study for sampling-based simulation costs of noisy quantum circuits”, 24th Annual Conference on Quantum Information Processing, Online, (February, 2021).

2. S. Hakkaku and K. Fujii, “Comparative study for sampling-based simulation costs of noisy quantum circuits”, AQIS 2020 : 20th Asian Quantum Information Science (virtual) Conference, Online, (December, 2020).

## Domestic Conferences

### Oral presentations

1. 八角繁男, 御手洗光祐, 藤井啓祐, 「コヒーレントノイズ下の表面符号におけるフォールトトレラント量子誤り訂正のサンプリングに基づいたシミュレーション」, 第4回量子ソフトウェア研究会, (2021年10月)

2. 八角繁男, 藤井啓祐, 「ノイズのある量子回路のサンプリングシミュレーションコスト比較」, 第43回量子情報技術研究会, (2020年12月)

3. 八角繁男, 藤井啓祐, 「ノイズのあるトロッター展開型量子回路の古典シミュレーション可能性」, 日本物理学会第74回年次大会, (2019年3月)

4. 八角繁男, 藤井啓祐, 「ノイズのある量子回路の古典サンプリングコストの評価」, 日本物理学会秋季大会, (2018年9月)

### Poster presentations

1. 八角繁男, 藤井啓祐, 「コヒーレントノイズ下の表面符号におけるフォールトトレラント量子誤り訂正のサンプリングに基づいたシミュレーション」, 第4回量子ソフトウェア研究会, (2021年10月)

2. 八角繁男, 藤井啓祐, "Evaluation of the classical sampling cost for noisy quantum circuits", 物性研短期研究会量子情報・物性の新潮流, (2018年8月)

## Awards

1. 第4回量子ソフトウェア研究会学生奨励賞, (2022年3月)

2. 第39回量子情報技術研究会学生発表賞, (2019年5月)

3. 日本物理学会学生優秀発表賞, (2018年10月)

# Acknowledgments

Firstly, I would like to greatly thank my advisor, Prof. Keisuke Fujii, for his indispensable support throughout my graduate school program. I could not even imagine how much effort he devoted to giving other students and me the perfect environment for our research works. Despite his busy schedule, he patiently discussed my research with me and gave me critical comments on my manuscripts of our papers. Without his continuous support, I would not have completed my Ph.D. study this year.

Secondly, I would like to sincerely thank Prof. Kosuke Mitarai for many fruitful discussions and his insightful comments. He helped me not only with my research but also with a variety of matters. Thanks to his support, I have been able to finish my Ph.D. study this year.

Prof. Wataru Mizukami has provided me with much help in the field of quantum chemistry. I would like to thank him for educating me and also for publishing a joint work.

I appreciate the fruitful comments on this thesis from Prof. Masahiro Kitagawa, Prof. Takashi Yamamoto, and Prof. Wataru Mizukami, who are examiners of my dissertation.

I would like to thank all of my labmates for supporting me through this Ph.D. study. Thanks to them, I enjoyed my research life in my Ph.D. study.

I also thank the community of Kansai Student Chapter and all of the people who devoted their effort to the community.

Finally, I thank my beloved and dearest family.

# Bibliography


[1]P. W. Shor, "Algorithms for quantum computation: discrete logarithms and factoring", in Proceedings 35th Annual Symposium on Foundations of Computer Science (Nov. 1994), pp. 124–134.

[2]P. Shor, "Polynomial-Time Algorithms for Prime Factorization and Discrete Logarithms on a Quantum Computer", SIAM J. Comput. **26**, 1484–1509 (1997).

[3]A. W. Harrow, A. Hassidim, and S. Lloyd, "Quantum Algorithm for Linear Systems of Equations", Phys. Rev. Lett. **103**, 150502 (2009).

[4]S. Lloyd, "Universal Quantum Simulators", Science **273**, 1073–1078 (1996).

[5]P. W. Shor, "Scheme for reducing decoherence in quantum computer memory", Phys. Rev. A **52**, R2493–R2496 (1995).

[6]A. Steane, "Multiple-particle interference and quantum error correction", Proc. R. Soc. A **452**, 19960136 (1996).

[7]C. Gidney and M. Ekerå, "How to factor 2048 bit RSA integers in 8 hours using 20 million noisy qubits", Quantum **5**, 433 (2021).

[8]J. Preskill, "Quantum Computing in the NISQ era and beyond", Quantum **2**, 79 (2018).

[9]F. Arute, K. Arya, R. Babbush, D. Bacon, J. C. Bardin, R. Barends, R. Biswas, S. Boixo, F. G. S. L. Brandao, D. A. Buell, B. Burkett, Y. Chen, Z. Chen, B. Chiaro, R. Collins, W. Courtney, A. Dunsworth, E. Farhi, B. Foxen, A. Fowler, C. Gidney, M. Giustina, R. Graff, K. Guerin, S. Habegger, M. P. Harrigan, M. J. Hartmann, A. Ho, M. Hoffmann, T. Huang, T. S. Humble, S. V. Isakov, E. Jeffrey, Z. Jiang, D. Kafri, K. Kechedzhi, J. Kelly, P. V. Klimov, S. Knysh, A. Korotkov, F. Kostritsa, D. Landhuis, M. Lindmark, E. Lucero, D. Lyakh, S. Mandrà, J. R. McClean, M. McEwen, A. Megrant, X. Mi, K. Michielsen, M. Mohseni, J. Mutus, O. Naaman, M. Neeley, C. Neill, M. Y. Niu, E. Ostby, A. Petukhov, J. C. Platt, C. Quintana, E. G. Rieffel, P. Roushan, N. C. Rubin, D. Sank, K. J. Satzinger, V. Smelyanskiy, K. J. Sung, M. D. Trevithick, A. Vainsencher, B. Villalonga, T. White, Z. J. Yao, P. Yeh, A. Zalcman, H. Neven, and J. M. Martinis, "Quantum supremacy using a programmable superconducting processor", Nature **574**, 505–510 (2019).

[10]Y. ( Liu, X. ( Liu, F. ( Li, H. Fu, Y. Yang, J. Song, P. Zhao, Z. Wang, D. Peng, H. Chen, C. Guo, H. Huang, W. Wu, and D. Chen, "Closing the "quantum supremacy" gap: achieving real-time simulation of a random quantum circuit using a new Sunway supercomputer", in Proceedings of the International Conference for High Performance Computing, Networking, Storage and Analysis, SC '21 (Nov. 14, 2021), pp. 1–12.

[11]A. Peruzzo, J. McClean, P. Shadbolt, M.-H. Yung, X.-Q. Zhou, P. J. Love, A. Aspuru-Guzik, and J. L. O'Brien, "A variational eigenvalue solver on a photonic quantum processor", Nat. Commun. **5**, 4213 (2014).

[12]K. Mitarai, M. Negoro, M. Kitagawa, and K. Fujii, "Quantum circuit learning", Phys. Rev. A **98**, 032309 (2018).

[13]E. Dennis, A. Kitaev, A. Landahl, and J. Preskill, "Topological quantum memory", J. Math. Phys. **43**, 4452–4505 (2002).

[14]A. G. Fowler, A. C. Whiteside, and L. C. L. Hollenberg, "Towards Practical Classical Processing for the Surface Code", Phys. Rev. Lett. **108**, 180501 (2012).

[15]A. G. Fowler, M. Mariantoni, J. M. Martinis, and A. N. Cleland, "Surface codes: Towards practical large-scale quantum computation", Phys. Rev. A **86**, 032324 (2012).

[16]J. Kelly, R. Barends, A. G. Fowler, A. Megrant, E. Jeffrey, T. C. White, D. Sank, J. Y. Mutus, B. Campbell, Y. Chen, Z. Chen, B. Chiaro, A. Dunsworth, I.-C. Hoi, C. Neill, P. J. J. O'Malley, C. Quintana, P. Roushan, A. Vainsencher, J. Wenner, A. N. Cleland, and J. M. Martinis, "State preservation by repetitive error detection in a superconducting quantum circuit", Nature **519**, 66–69 (2015).

[17]L. Egan, D. M. Debroy, C. Noel, A. Risinger, D. Zhu, D. Biswas, M. Newman, M. Li, K. R. Brown, M. Cetina, and C. Monroe, "Fault-tolerant control of an error-corrected qubit", Nature **598**, 281–286 (2021).

[18]Z. Chen, K. J. Satzinger, J. Atalaya, A. N. Korotkov, A. Dunsworth, D. Sank, C. Quintana, M. McEwen, R. Barends, P. V. Klimov, S. Hong, C. Jones, A. Petukhov, D. Kafri, S. Demura, B. Burkett, C. Gidney, A. G. Fowler, A. Paler, H. Putterman, I. Aleiner, F. Arute, K. Arya, R. Babbush, J. C. Bardin, A. Bengtsson, A. Bourassa, M. Broughton, B. B. Buckley, D. A. Buell, N. Bushnell, B. Chiaro, R. Collins, W. Courtney, A. R. Derk, D. Eppens, C. Erickson, E. Farhi, B. Foxen, M. Giustina, A. Greene, J. A. Gross, M. P. Harrigan, S. D. Harrington, J. Hilton, A. Ho, T. Huang, W. J. Huggins, L. B. Ioffe, S. V. Isakov, E. Jeffrey, Z. Jiang, K. Kechedzhi, S. Kim, A. Kitaev, F. Kostritsa, D. Landhuis, P. Laptev, E. Lucero, O. Martin, J. R. McClean, T. McCourt, X. Mi, K. C. Miao, M. Mohseni, S. Montazeri, W. Mruczkiewicz, J. Mutus, O. Naaman, M. Neeley, C. Neill, M. Newman, M. Y. Niu, T. E. O'Brien, A. Opremcak, E. Ostby, B. Pató, N. Redd, P. Roushan, N. C. Rubin, V. Shvarts, D. Strain, M. Szalay, M. D. Trevithick, B. Villalonga, T. White, Z. J. Yao, P. Yeh, J. Yoo, A. Zalcman, H. Neven, S. Boixo, V. Smelyanskiy, Y. Chen,

A. Megrant, J. Kelly, and Google Quantum AI, "Exponential suppression of bit or phase errors with cyclic error correction", Nature **595**, 383–387 (2021).

[19]S. Sheldon, L. S. Bishop, E. Magesan, S. Filipp, J. M. Chow, and J. M. Gambetta, "Characterizing errors on qubit operations via iterative randomized benchmarking", Phys. Rev. A **93**, 012301 (2016).

[20]Y. Tomita and K. M. Svore, "Low-distance surface codes under realistic quantum noise", Phys. Rev. A **90**, 062320 (2014).

[21]Y. Suzuki, K. Fujii, and M. Koashi, "Efficient Simulation of Quantum Error Correction Under Coherent Error Based on the Nonunitary Free-Fermionic Formalism", Phys. Rev. Lett. **119**, 190503 (2017).

[22]A. S. Darmawan and D. Poulin, "Tensor-Network Simulations of the Surface Code under Realistic Noise", Phys. Rev. Lett. **119**, 040502 (2017).

[23]S. Bravyi, M. Englbrecht, R. König, and N. Peard, "Correcting coherent errors with surface codes", npj Quantum Inf. **4**, 55 (2018).

[24]X. Zhou, D. W. Leung, and I. L. Chuang, "Methodology for quantum logic gate construction", Phys. Rev. A **62**, 052316 (2000).

[25]S. Bravyi and A. Kitaev, "Universal quantum computation with ideal Clifford gates and noisy ancillas", Phys. Rev. A **71**, 022316 (2005).

[26]Michael A. Nielsen and Issac L. Chuang, *Quantum Computation and Quantum Information-10th Anniversary Edition*, 10th Anniversary Edition (Cambridge, 2010).

[27]R. Raussendorf and H. J. Briegel, "A One-Way Quantum Computer", Phys. Rev. Lett. **86**, 5188–5191 (2001).

[28]D. Gottesman, "Class of quantum error-correcting codes saturating the quantum Hamming bound", Phys. Rev. A **54**, 1862–1868 (1996).

[29]D. E. Gottesman, "Stabilizer Codes and Quantum Error Correction", PhD thesis (California Institute of Technology, 1997).

[30]S. Aaronson and D. Gottesman, "Improved simulation of stabilizer circuits", Phys. Rev. A **70**, 052328 (2004).

[31]M. Van Den Nest, "Simulating quantum computers with probabilistic methods", Quantum Info. Comput. **11**, 784–812 (2011).

[32]K. Fujii, *Quantum Computation with Topological Codes: From Qubit to Topological Fault-Tolerance*, Vol. 8, SpringerBriefs in Mathematical Physics (Springer Singapore, Singapore, 2015).

[33]D. A. Lidar and T. A. Brun, eds., *Quantum Error Correction* (Cambridge, 2013).

[34]S. Bravyi, *Lagrangian representation for fermionic linear optics*, (Sept. 20, 2004) arXiv:quant-ph/0404180.

[35]S. Bravyi, M. Suchara, and A. Vargo, "Efficient algorithms for maximum likelihood decoding in the surface code", Phys. Rev. A **90**, 032326 (2014).

[36]J. Helsen, S. Nezami, M. Reagor, and M. Walter, *Matchgate benchmarking: Scalable benchmarking of a continuous family of many-qubit gates*, (Nov. 25, 2020) arXiv:2011.13048.

[37]H. Pashayan, J. J. Wallman, and S. D. Bartlett, "Estimating Outcome Probabilities of Quantum Circuits Using Quasiprobabilities", Phys. Rev. Lett. **115**, 070501 (2015).

[38]M. Howard and E. Campbell, "Application of a Resource Theory for Magic States to Fault-Tolerant Quantum Computing", Phys. Rev. Lett. **118**, 090501 (2017).

[39]J. R. Seddon and E. T. Campbell, "Quantifying magic for multi-qubit operations", Proc. R. Soc. A **475**, 20190251 (2019).

[40]P. Rall, D. Liang, J. Cook, and W. Kretschmer, "Simulation of qubit quantum circuits via Pauli propagation", Phys. Rev. A **99**, 062337 (2019).

[41]J. R. Seddon, B. Regula, H. Pashayan, Y. Ouyang, and E. T. Campbell, "Quantifying Quantum Speedups: Improved Classical Simulation From Tighter Magic Monotones", PRX Quantum **2**, 010345 (2021).

[42]C. Gardiner and P. Zoller, *Quantum Noise: A Handbook of Markovian and Non-Markovian Quantum Stochastic Methods with Applications to Quantum Optics*, 3rd. (Springer-Verlag, Berlin, 2004).

[43]W. Hoeffding, "Probability Inequalities for Sums of Bounded Random Variables", J. Am. Stat. Assoc. **58**, 13–30 (1963), JSTOR: 2282952.

[44]A. Heimendahl, M. Heinrich, and D. Gross, *The axiomatic and the operational approaches to resource theories of magic do not coincide*, (Nov. 27, 2020) arXiv:2011.11651.

[45]E. T. Campbell, "Catalysis and activation of magic states in fault-tolerant architectures", Phys. Rev. A **83**, 032317 (2011).

[46]F. Arute, K. Arya, R. Babbush, D. Bacon, J. C. Bardin, R. Barends, S. Boixo, M. Broughton, B. B. Buckley, D. A. Buell, B. Burkett, N. Bushnell, Y. Chen, Z. Chen, B. Chiaro, R. Collins, W. Courtney, S. Demura, A. Dunsworth, D. Eppens, E. Farhi, A. Fowler, B. Foxen, C. Gidney, M. Giustina, R. Graff, S. Habegger, M. P. Harrigan, A. Ho, S. Hong, T. Huang, W. J. Huggins, L. Ioffe, S. V. Isakov, E. Jeffrey, Z. Jiang, C. Jones, D. Kafri, K. Kechedzhi, J. Kelly, S. Kim, P. V. Klimov, A. Korotkov, F. Kostritsa, D. Landhuis, P. Laptev, M. Lindmark, E. Lucero, O. Martin, J. M. Martinis, J. R. McClean, M. McEwen, A. Megrant, X. Mi, M. Mohseni, W. Mruczkiewicz, J. Mutus, O. Naaman, M. Neeley, C. Neill, H. Neven, M. Y. Niu, T. E. O'Brien, E. Ostby, A. Petukhov, H. Putterman, C. Quintana, P. Roushan, N. C. Rubin, D. Sank, K. J. Satzinger, V. Smelyanskiy, D. Strain, K. J. Sung, M. Szalay, T. Y. Takeshita, A. Vainsencher, T. White, N. Wiebe, Z. J. Yao, P. Yeh, and A. Zalcman, "Hartree-Fock on a superconducting qubit quantum computer", Science **369**, 1084–1089 (2020).

[47]C. Neill, P. Roushan, K. Kechedzhi, S. Boixo, S. V. Isakov, V. Smelyanskiy, A. Megrant, B. Chiaro, A. Dunsworth, K. Arya, R. Barends, B. Burkett, Y. Chen, Z. Chen, A. Fowler, B. Foxen, M. Giustina, R. Graff, E. Jeffrey, T. Huang, J. Kelly, P. Klimov, E. Lucero, J. Mutus, M. Neeley, C. Quintana, D. Sank, A. Vainsencher, J. Wenner, T. C. White, H. Neven, and J. M. Martinis, "A blueprint for demonstrating quantum supremacy with superconducting qubits", Science **360**, 195–199 (2018).

[48]A. Kandala, K. Temme, A. D. Córcoles, A. Mezzacapo, J. M. Chow, and J. M. Gambetta, "Error mitigation extends the computational reach of a noisy quantum processor", Nature **567**, 491 (2019).

[49]P. Jurcevic, A. Javadi-Abhari, L. S. Bishop, I. Lauer, D. F. Bogorin, M. Brink, L. Capelluto, O. Günlük, T. Itoko, N. Kanazawa, A. Kandala, G. A. Keefe, K. Krsulich, W. Landers, E. P. Lewandowski, D. T. McClure, G. Nannicini, A. Narasgond, H. M. Nayfeh, E. Pritchett, M. B. Rothwell, S. Srinivasan, N. Sundaresan, C. Wang, K. X. Wei, C. J. Wood, J.-B. Yau, E. J. Zhang, O. E. Dial, J. M. Chow, and J. M. Gambetta, "Demonstration of quantum volume 64 on a superconducting quantum computing system", Quantum Sci. Technol. **6**, 025020 (2021).

[50]E. Pednault, J. A. Gunnels, G. Nannicini, L. Horesh, and R. Wisnieff, *Leveraging Secondary Storage to Simulate Deep 54-qubit Sycamore Circuits*, (Oct. 21, 2019) arXiv:1910.09534.

[51]C. Huang, F. Zhang, M. Newman, J. Cai, X. Gao, Z. Tian, J. Wu, H. Xu, H. Yu, B. Yuan, M. Szegedy, Y. Shi, and J. Chen, *Classical Simulation of Quantum Supremacy Circuits*, (May 14, 2020) arXiv:2005.06787.

[52]A. Agrawal, R. Verschueren, S. Diamond, and S. Boyd, "A rewriting system for convex optimization problems", J. Control. Decis. **5**, 42–60 (2018).

[53]S. Diamond and S. Boyd, "CVXPY: A Python-Embedded Modeling Language for Convex Optimization", J. Mach. Learn. Res. **17**, 5 (2016).

[54]D. Gross, "Hudson's theorem for finite-dimensional quantum systems", J. Math. Phys. **47**, 122107 (2006).

[55]M. Heinrich and D. Gross, "Robustness of Magic and Symmetries of the Stabiliser Polytope", Quantum **3**, 132 (2019).

[56]S. Bravyi and D. Gosset, "Improved Classical Simulation of Quantum Circuits Dominated by Clifford Gates", Phys. Rev. Lett. **116**, 250501 (2016).

[57]S. Bravyi, G. Smith, and J. A. Smolin, "Trading Classical and Quantum Computational Resources", Phys. Rev. X **6**, 021043 (2016).

[58]K. Mitarai, Y. Suzuki, W. Mizukami, Y. O. Nakagawa, and K. Fujii, *Quadratic Clifford expansion for efficient benchmarking and initialization of variational quantum algorithms*, (Dec. 14, 2020) arXiv:2011.09927.

[59]R. S. Bennink, E. M. Ferragut, T. S. Humble, J. A. Laska, J. J. Nutaro, M. G. Pleszkoch, and R. C. Pooser, "Unbiased simulation of near-Clifford quantum circuits", Phys. Rev. A **95**, 012301 (2017).

[60]D. Stahlke, "Quantum interference as a resource for quantum speedup", Phys. Rev. A **90**, 022302 (2014).

[61]S. Hakkaku and K. Fujii, "Comparative Study of Sampling-Based Simulation Costs of Noisy Quantum Circuits", Phys. Rev. Applied **15**, 064027 (2021).

[62]K. Mitarai and K. Fujii, "Overhead for simulating a non-local channel with local channels by quasiprobability sampling", Quantum **5**, 388 (2021).

[63]A. Kitaev, "Fault-tolerant quantum computation by anyons", Ann. Phys. **303**, 2–30 (2003).

[64]R. Babbush, C. Gidney, D. W. Berry, N. Wiebe, J. McClean, A. Paler, A. Fowler, and H. Neven, "Encoding Electronic Spectra in Quantum Circuits with Linear T Complexity", Phys. Rev. X **8**, 041015 (2018).

[65]A. Kandala, A. Mezzacapo, K. Temme, M. Takita, M. Brink, J. M. Chow, and J. M. Gambetta, "Hardware-efficient variational quantum eigensolver for small molecules and quantum magnets", Nature **549**, 242–246 (2017).

[66]Y. Matsuzawa and Y. Kurashige, *A Jastrow-type decomposition in quantum chemistry for low-depth quantum circuits*, (Sept. 26, 2019) arXiv:1909.12410.

[67]R. Wiersema, C. Zhou, Y. de Sereville, J. F. Carrasquilla, Y. B. Kim, and H. Yuen, "Exploring Entanglement and Optimization within the Hamiltonian Variational Ansatz", PRX Quantum **1**, 020319 (2020).

[68]Y. Li and S. C. Benjamin, "Efficient Variational Quantum Simulator Incorporating Active Error Minimization", Phys. Rev. X **7**, 021050 (2017).

[69]K. Heya, K. M. Nakanishi, K. Mitarai, and K. Fujii, *Subspace Variational Quantum Simulator*, (Apr. 17, 2019) arXiv:1904.08566.

[70]C. Hempel, C. Maier, J. Romero, J. McClean, T. Monz, H. Shen, P. Jurcevic, B. P. Lanyon, P. Love, R. Babbush, A. Aspuru-Guzik, R. Blatt, and C. F. Roos, "Quantum Chemistry Calculations on a Trapped-Ion Quantum Simulator", Phys. Rev. X **8**, 031022 (2018).

[71]Y. Nam, J.-S. Chen, N. C. Pisenti, K. Wright, C. Delaney, D. Maslov, K. R. Brown, S. Allen, J. M. Amini, J. Apisdorf, K. M. Beck, A. Blinov, V. Chaplin, M. Chmielewski, C. Collins, S. Debnath, K. M. Hudek, A. M. Ducore, M. Keesan, S. M. Kreikemeier, J. Mizrahi, P. Solomon, M. Williams, J. D. Wong-Campos, D. Moehring, C. Monroe, and J. Kim, "Ground-state energy estimation of the water molecule on a trapped-ion quantum computer", npj Quantum Inf **6**, 1–6 (2020).

[72]I. D. Kivlichan, C. Gidney, D. W. Berry, N. Wiebe, J. McClean, W. Sun, Z. Jiang, N. Rubin, A. Fowler, A. Aspuru-Guzik, H. Neven, and R. Babbush, "Improved Fault-Tolerant Quantum Simulation of Condensed-Phase Correlated Electrons via Trotterization", Quantum **4**, 296 (2020).

[73]M. Motta, E. Ye, J. R. McClean, Z. Li, A. J. Minnich, R. Babbush, and G. K.-L. Chan, "Low rank representations for quantum simulation of electronic structure", npj Quantum Inf **7**, 1–7 (2021).

[74]E. Knill, *Fermionic Linear Optics and Matchgates*, (Aug. 8, 2001) arXiv:quant-ph/0108033.

[75]B. M. Terhal and D. P. DiVincenzo, "Classical simulation of noninteracting-fermion quantum circuits", Phys. Rev. A **65**, 032325 (2002).

[76]R. Jozsa and A. Miyake, "Matchgates and classical simulation of quantum circuits", Proc. R. Soc. A **464**, 3089–3106 (2008).

[77]H. R. Grimsley, S. E. Economou, E. Barnes, and N. J. Mayhall, "An adaptive variational algorithm for exact molecular simulations on a quantum computer", Nat. Commun. **10**, 1–9 (2019).

[78]D. Wecker, M. B. Hastings, and M. Troyer, "Progress towards practical quantum variational algorithms", Phys. Rev. A **92**, 042303 (2015).

[79]S. Hakkaku, Y. Tashima, K. Mitarai, W. Mizukami, and K. Fujii, *Quantifying Fermionic Nonlinearity of Quantum Circuits*, (Dec. 13, 2021) arXiv:2111.14599.

[80]J. Lee, W. J. Huggins, M. Head-Gordon, and K. B. Whaley, "Generalized Unitary Coupled Cluster Wave functions for Quantum Computation", J. Chem. Theory Comput. **15**, 311–324 (2019).

[81]K. Mitarai and K. Fujii, "Constructing a virtual two-qubit gate by sampling single-qubit operations", New J. Phys. **23**, 023021 (2021).

[82]J. Hachmann, W. Cardoen, and G. K.-L. Chan, "Multireference correlation in long molecules with the quadratic scaling density matrix renormalization group", J. Chem. Phys. **125**, 144101 (2006).

[83]W. A. Al-Saidi, S. Zhang, and H. Krakauer, "Bond breaking with auxiliary-field quantum Monte Carlo", J. Chem. Phys. **127**, 144101 (2007).

[84]T. Tsuchimochi and G. E. Scuseria, "Strong correlations via constrained-pairing mean-field theory", J. Chem. Phys. **131**, 121102 (2009).

[85]A. V. Sinitskiy, L. Greenman, and D. A. Mazziotti, "Strong correlation in hydrogen chains and lattices using the variational two-electron reduced density matrix method", J. Chem. Phys. **133**, 014104 (2010).

[86]D. A. Mazziotti, "Large-Scale Semidefinite Programming for Many-Electron Quantum Mechanics", Phys. Rev. Lett. **106**, 083001 (2011).

[87]N. Lin, C. A. Marianetti, A. J. Millis, and D. R. Reichman, "Dynamical Mean-Field Theory for Quantum Chemistry", Phys. Rev. Lett. **106**, 096402 (2011).

[88]L. Stella, C. Attaccalite, S. Sorella, and A. Rubio, "Strong electronic correlation in the hydrogen chain: A variational Monte Carlo study", Phys. Rev. B **84**, 245117 (2011).

[89]M. Motta, D. M. Ceperley, G. K.-L. Chan, J. A. Gomez, E. Gull, S. Guo, C. A. Jiménez-Hoyos, T. N. Lan, J. Li, F. Ma, A. J. Millis, N. V. Prokof'ev, U. Ray, G. E. Scuseria, S. Sorella, E. M. Stoudenmire, Q. Sun, I. S. Tupitsyn, S. R. White, D. Zgid, and S. Zhang, "Towards the Solution of the Many-Electron Problem in Real Materials: Equation of State of the Hydrogen Chain with State-of-the-Art Many-Body Methods", Phys. Rev. X **7**, 031059 (2017).

[90]M. Motta, C. Genovese, F. Ma, Z.-H. Cui, R. Sawaya, G. K.-L. Chan, N. Chepiga, P. Helms, C. Jiménez-Hoyos, A. J. Millis, U. Ray, E. Ronca, H. Shi, S. Sorella, E. M. Stoudenmire, S. R. White, and S. Zhang, "Ground-State Properties of the Hydrogen Chain: Dimerization, Insulator-to-Metal Transition, and Magnetic Phases", Phys. Rev. X **10**, 031058 (2020).

[91]J. R. McClean, N. C. Rubin, K. J. Sung, I. D. Kivlichan, X. Bonet-Monroig, Y. Cao, C. Dai, E. S. Fried, C. Gidney, B. Gimby, P. Gokhale, T. Häner, T. Hardikar, V. Havlíček, O. Higgott, C. Huang, J. Izaac, Z. Jiang, X. Liu, S. McArdle, M. Neeley, T. O'Brien, B. O'Gorman, I. Ozfidan, M. D. Radin, J. Romero, N. P. D. Sawaya, B. Senjean, K. Setia, S. Sim, D. S. Steiger, M. Steudtner, Q. Sun, W. Sun, D. Wang, F. Zhang, and R. Babbush, "OpenFermion: the electronic structure package for quantum computers", Quantum Sci. Technol. **5**, 034014 (2020).

[92]Q. Sun, T. C. Berkelbach, N. S. Blunt, G. H. Booth, S. Guo, Z. Li, J. Liu, J. D. McClain, E. R. Sayfutyarova, S. Sharma, S. Wouters, and G. K.-L. Chan, "PySCF: the Python-based simulations of chemistry framework", WIREs Comput. Mol. Sci. **8**, e1340 (2018).

[93]Q. Sun, X. Zhang, S. Banerjee, P. Bao, M. Barbry, N. S. Blunt, N. A. Bogdanov, G. H. Booth, J. Chen, Z.-H. Cui, J. J. Eriksen, Y. Gao, S. Guo, J. Hermann, M. R. Hermes, K. Koh, P. Koval, S. Lehtola, Z. Li, J. Liu, N. Mardirossian, J. D. McClain, M. Motta, B. Mussard, H. Q. Pham, A. Pulkin, W. Purwanto, P. J. Robinson, E. Ronca, E. Sayfutyarova, M. Scheurer, H. F. Schurkus, J. E. T. Smith, C. Sun, S.-N. Sun, S. Upadhyay, L. K. Wagner, X. Wang, A. White, J. D. Whitfield, M. J. Williamson, S. Wouters, J. Yang, J. M. Yu, T. Zhu, T. C. Berkelbach, S. Sharma, A. Sokolov, and G. K.-L. Chan, "Recent developments in the PySCF program package", J. Chem. Phys. **153**, 024109 (2020).

[94]W. Kutzelnigg, "Quantum chemistry in Fock space. I. The universal wave and energy operators", J. Chem. Phys. **77**, 3081–3097 (1982).

[95]W. Kutzelnigg and S. Koch, "Quantum chemistry in Fock space. II. Effective Hamiltonians in Fock space", J. Chem. Phys. **79**, 4315–4335 (1983).

[96]W. Kutzelnigg, "Quantum chemistry in Fock space. IV. The treatment of permutational symmetry. Spin-free diagrams with symmetrized vertices", J. Chem. Phys. **82**, 4166–4186 (1985).

[97]R. J. Bartlett, S. A. Kucharski, and J. Noga, "Alternative coupled-cluster ansätze II. The unitary coupled-cluster method", Chem. Phys. Lett. **155**, 133–140 (1989).

[98] W. Kutzelnigg, "Error analysis and improvements of coupled-cluster theory", Theoret. Chim. Acta **80**, 349–386 (1991).

[99] A. G. Taube and R. J. Bartlett, "New perspectives on unitary coupled-cluster theory", Int. J. Quantum Chem. **106**, 3393–3401 (2006).

[100] Y. Suzuki, Y. Kawase, Y. Masumura, Y. Hiraga, M. Nakadai, J. Chen, K. M. Nakanishi, K. Mitarai, R. Imai, S. Tamiya, T. Yamamoto, T. Yan, T. Kawakubo, Y. O. Nakagawa, Y. Ibe, Y. Zhang, H. Yamashita, H. Yoshimura, A. Hayashi, and K. Fujii, *Qulacs: a fast and versatile quantum circuit simulator for research purpose*, (Aug. 17, 2021) arXiv:2011.13524.

[101] B. Cooper and P. J. Knowles, "Benchmark studies of variational, unitary and extended coupled cluster methods", J. Chem. Phys. **133**, 234102 (2010).

[102] F. A. Evangelista, "Alternative single-reference coupled cluster approaches for multireference problems: The simpler, the better", J. Chem. Phys. **134**, 224102 (2011).

[103] T. J. Lee and P. R. Taylor, "A diagnostic for determining the quality of single-reference electron correlation methods", Int. J. Quantum Chem. **36**, 199–207 (1989).

[104] C. L. Janssen and I. M. Nielsen, "New diagnostics for coupled-cluster and Møller–Plesset perturbation theory", Chem. Phys. Lett. **290**, 423–430 (1998).

[105] I. M. B. Nielsen and C. L. Janssen, "Double-substitution-based diagnostics for coupled-cluster and Møller–Plesset perturbation theory", Chem. Phys. Lett. **310**, 568–576 (1999).

[106] M. L. Leininger, I. M. B. Nielsen, T. D. Crawford, and C. L. Janssen, "A new diagnostic for open-shell coupled-cluster theory", Chem. Phys. Lett. **328**, 431–436 (2000).

[107] T. J. Lee, "Comparison of the T1 and D1 diagnostics for electronic structure theory: a new definition for the open-shell D1 diagnostic", Chem. Phys. Lett. **372**, 362–367 (2003).

[108] U. R. Fogueri, S. Kozuch, A. Karton, and J. M. L. Martin, "A simple DFT-based diagnostic for nondynamical correlation", Theor. Chem. Acc. **132**, 1291 (2012).

[109] M. Hebenstreit, R. Jozsa, B. Kraus, S. Strelchuk, and M. Yoganathan, "All Pure Fermionic Non-Gaussian States Are Magic States for Matchgate Computations", Phys. Rev. Lett. **123**, 080503 (2019).

[110] K. Temme, S. Bravyi, and J. M. Gambetta, "Error Mitigation for Short-Depth Quantum Circuits", Phys. Rev. Lett. **119**, 180509 (2017).

[111] Y. Suzuki, S. Endo, K. Fujii, and Y. Tokunaga, *Quantum error mitigation as a universal error-minimization technique: applications from NISQ to FTQC eras*, (Oct. 18, 2021) arXiv:2010.03887.

[112] M. Lostaglio and A. Ciani, "Error Mitigation and Quantum-Assisted Simulation in the Error Corrected Regime", Phys. Rev. Lett. **127**, 200506 (2021).